



Wrocław University
of Science and Technology

DOCTORAL THESIS

**Impact of ferromagnetic nanoparticles on
heat transfer process in nanofluids**

Author:

Robert MULKA

Supervisor:

Bartosz ZAJĄCZKOWSKI,
PhD, DSc, Assoc. Prof.

Co-supervisor:

Matthias H. BUSCHMANN,
PD Dr.-Ing. habil.

Field of science: Engineering and technology

Dyscyplina: Environmental engineering, mining and energy

Keywords: Heat transfer, laminar flow, mixed convection, ferronanofluid,
magnetic field

Wrocław, 2025

Acknowledgements

I would like to express my gratitude to my supervisor, Bartosz Zajączkowski, PhD, DSc, Assoc. Prof., for his invaluable mentorship and meritorical guidance throughout my doctoral journey. His insightful advice, encouragement, and support have been instrumental in shaping this thesis. I am equally indebted to my second supervisor, PD Dr.-Ing. habil. Matthias H. Buschmann, for his exceptional mentorship, constructive feedback, hosting me at Institut für Luft- und Kältetechnik gemeinnützige GmbH (ILK) in Dresden and generous support during my research.

I gratefully acknowledge the COST organization for providing the IG15119-48452 STSM grant, entitled "Investigation on the phenomena behind the ferronano fluid impact on the convective heat transfer," and the IG15119-48747 STSM grant, entitled "Investigation on the effect of the magnetic field imposition on the ferronano fluid droplet." Both grants were conducted under the framework of the COST NANOConVEX CIG project and hosted by PD Dr.-Ing. habil. Matthias H. Buschmann at ILK Dresden. The support provided by these grants allowed me to perform the experiments described in the section "Magnetic field interaction with ferronano fluid droplet" of this thesis.

I would also like to thank the National Science Centre, Poland, for funding my research through grant number 2021/41/N/ST8/02120. This grant facilitated the main experiments of the dissertation that form the foundation of the chapters "Ferronano fluid horizontal flow" and "Effect of inclination on heat transfer".

Contents

Acknowledgements	i
1 Introduction	1
1.1 Heat transfer	1
1.1.1 Conduction	1
1.1.2 Thermal radiation	2
1.1.3 Convection	2
1.2 Convective heat transfer in heat exchangers	3
1.2.1 Methods of convective heat transfer improvement	3
1.2.2 Emerge of ferronanofluids	6
2 Nanofluids	8
2.1 Nanofluids	8
2.1.1 Base fluids	8
2.1.2 Additives	9
2.1.3 Nanoparticles	10
2.1.4 Ferronanoparticles	10
2.1.5 Nanofluids for heat transfer enhancement	11
2.2 Nanofluids in heat transfer applications	12
2.2.1 Cooling Towers	13
2.2.2 Phase-change devices	15
2.2.3 Waste heat utilization	18
2.2.4 Techno-economic basis	20
2.2.5 Other applications	23
2.2.6 Stability and longevity	23
2.2.7 Summary of nanofluid applications	24
3 Convective heat transfer employing ferronanofluids	26
3.1 Laminar flow with ferronanofluids	27
3.1.1 Flow under a static magnetic field	29
3.1.2 Flow under an alternating magnetic field	37
3.2 Turbulent flow with ferronanofluids	41
3.3 Mixed convection in nanofluids	42
3.4 Literature review summary	47

4	Dissertation theses and objectives of the work	49
4.1	Dissertation theses	49
4.2	Objectives of the work	50
4.3	Structure of the dissertation	50
5	Characterization of selected ferronanofluid	52
5.1	Characterization of thermophysical properties	52
5.1.1	Viscosity	53
5.1.2	Specific heat capacity	55
5.1.3	Thermal conductivity	56
5.1.4	Density	59
5.2	Contact angle under a magnetic field	60
5.2.1	Contact angle	60
5.2.2	Experimental setup and procedure	61
5.2.3	Distribution of the magnetic field	63
5.2.4	Determination of the contact angle for ferronanofluid	64
5.2.5	Magnetic field effect on a ferronanofluid droplet	65
5.3	Magnetic field influence on ferronanoparticles	67
5.3.1	Orientation of cracks in dried deposit	67
5.3.2	Magnetic field effect on stress balance	70
5.4	Chapter Summary	72
6	Ferronanofluid horizontal flow	73
6.1	Experimental setup description	73
6.2	Magnetic field distribution	76
6.3	Heat transfer calculations	76
6.4	Mixed convection	79
6.5	Impact of a static magnet located above the tube	80
6.6	Impact of a static magnet located under the tube	82
6.7	Effect of flow conditions on heat transfer	84
6.8	Chapter summary	87
7	Effect of inclination on heat transfer	89
7.1	Experimental setup and methods	89
7.2	Mixed convection in inclined flow	91
7.3	Magnetic field effect on inclined flow heat transfer	94
7.4	Chapter summary	99
8	Conclusions	100
	Bibliography	105

Nomenclature

Symbols

Symbol	Description	Unit
A	Radiating surface area	m^2
A_r, A_m	Area under the power curve for reference and test materials	$W\ kg^{-1}$
B	Magnetic flux density	T
Bo	Bond number	-
Bo_m	Magnetic Bond number	-
CA	Contact angle	$^\circ$
$CA_{0,MF}$	Contact angle under magnetic field	$^\circ$
C_p	Specific heat capacity	$J\ kg^{-1}\ K^{-1}$
C_{pr}, C_{pm}	Specific heat capacity of reference and test materials	$J\ kg^{-1}\ K^{-1}$
d	Diameter of the test section tube	m
d_p	Average particle size	m
D	Molecular diffusion coefficient	$m^2\ s^{-1}$
f	Frequency	Hz
$F_{0,P}$	Sum of forces	N
$F_{0,P,MF}$	Sum of forces including magnetic force	N
Gr	Grashof number	-
Gz	Graetz number	-
h	Convective heat transfer coefficient	$W\ m^{-2}\ K^{-1}$
H	Magnetic field strength	$A\ m^{-1}$
k	Thermal conductivity	$W\ m^{-1}\ K^{-1}$
l	Length	m
m	Mass flow	$kg\ s^{-1}$
m_r, m_m	Mass of the reference and test materials	kg
Mn	Magnetic number	-
$MnRe$	Magnetic to viscous force ratio	-
Nu	Nusselt number	-
$Nu_{\%}$	Nusselt number change in horizontal flow	-
Nu_{inf}	Nusselt number in inclined flow under magnetic field	-
Nu_{mf}	Nusselt number in ferronanofluid flow under magnetic field	-
Pr	Prandtl number	-
q	Heat flux	$W\ m^{-2}$
Q_r, Q_m	Heat supplied to the reference and test materials	W
r	Radius	m

Re	Reynolds number	-
t_1, t_2	Start and end times of measurement	s
T	Temperature	°C
T_1, T_2	Absolute temperatures of radiator one and two	K
v_f	Volume fraction of particles	-
V	Volume	m ³
x	Distance from the test section inlet	m
x^+	Dimensionless axial distance	-
β	Heating rate	K s ⁻¹
χ	Volumetric susceptibility of ferronanofluid	-
μ	Dynamic viscosity	Pa s
μ_0	Vacuum permeability	N A ⁻²
σ	Stefan-Boltzmann constant	W m ⁻² K ⁻⁴
σ_{lv}	Surface tension between liquid and gas phases	N m ⁻¹
σ_{sl}	Surface tension between solid and liquid phases	N m ⁻¹
σ_{sv}	Surface tension between solid and gas phases	N m ⁻¹

Subscripts	Description
0	initial state
base	reference condition without magnetic field
bf	base fluid
dr	droplet-related property
fl	fluid
i	at thermocouple position, ranging from 1 to 9
in	inner
m	test material
mf	condition with magnetic field presence
out	outer
p	particle
s	surface
tc	thermocouple
wall	wall

Chapter 1

Introduction

1.1 Heat transfer

Heat transfer is a fundamental process that governs energy exchange in natural and engineered systems. It plays a critical role in diverse fields ranging from industrial processes and energy systems to biological systems and environmental applications. Understanding the principles of heat transfer is essential for designing efficient thermal systems, improving energy utilization, and addressing challenges related to thermal management.

Heat transfer refers to the movement of energy driven by a temperature gradient. The study of heat transfer not only provides insights into physical processes but also serves as the foundation for advanced technologies, including heat exchangers, refrigeration systems, and thermal insulation materials. There are three basic mechanisms by which heat is transported: conduction, convection, and radiation.

1.1.1 Conduction

Conduction is a process of heat transfer within one body between parts of different temperatures or between bodies that are in contact and have different temperatures. In gases and liquids, the transfer occurs due to molecules' motion and random collisions with other molecules of lower energy. In solids, the ability to conduct heat can be orders of magnitude higher, especially for electric conductors. In addition to lattice vibrations, free electron movement serves as the primary mechanism for heat conduction in solids. One-dimensional heat conduction is described by the following equation:

$$q = -k \frac{dT}{dx} \quad (1.1)$$

where k is the thermal conductivity, $\frac{dT}{dx}$ the temperature change over a distance.

The efficiency of conduction depends on the material's thermal conductivity, which quantifies its ability to transfer heat. Metals, such as copper and aluminum, are excellent conductors due to their high density of free electrons, whereas materials like wood and rubber are insulators with very low thermal conductivity. Understanding this material property is essential for selecting appropriate materials in thermal applications.

1.1.2 Thermal radiation

Thermal radiation is the emission of electromagnetic waves from all objects with a temperature above absolute zero. Particles within objects with thermal energy are in motion, causing interactions resulting in the acceleration of protons and electrons. The acceleration or deceleration of charged particles generates electromagnetic radiation. Thermal radiation transfers energy without requiring a material medium and is most effective in a vacuum, where the absence of particles prevents absorption or reflection. The heat radiation between two ideal radiators is described by the equation:

$$q = \sigma A (T_1^4 - T_2^4) \quad (1.2)$$

where σ is the Stefan-Boltzmann constant, A a radiating surface area, T_1 the absolute temperature of the first radiator, T_2 the absolute temperature of the second radiator.

Radiative heat transfer is governed by surface properties, such as emissivity and absorptivity, which determine the ability of a material to emit or absorb radiation. Blackbody radiation serves as an idealized reference, where a perfect emitter absorbs and emits radiation at all wavelengths. Real surfaces deviate from this behavior, and their performance is characterized using emissivity coefficients. This property is critical in applications such as thermal insulation, solar energy harvesting, and spacecraft thermal control systems.

1.1.3 Convection

Convection represents a distinct mode of heat transfer, differing from conduction and radiation. Here, internal energy is transported by fluid motion, while the basis of heat transfer is heat conduction in a fluid. Convective heat transfer occurs when a moving fluid exchanges heat with a surface. It can be categorized into two types:

- Free (or natural) convection: driven by buoyancy forces caused by density differences due to temperature variations.
- Forced convection: induced by external means, such as pumps or fans.

Convective heat transfer from a surface to a flowing fluid is defined by the equation:

$$q = h(T_s - T_{fl}) \quad (1.3)$$

where h is a convective heat transfer coefficient, T_s surface temperature, T_{fl} fluid temperature.

Convection plays a crucial role in various natural and engineered systems, from atmospheric heat exchange to industrial cooling processes. In forced convection, where the fluid is actively moved, the heat transfer coefficient increases due to the higher fluid velocity and enhanced mixing, resulting in improved thermal performance. In free convection, the heat transfer is passive and depends largely on buoyancy-driven flow. The effectiveness of convection also depends on whether the flow is laminar

or turbulent, with turbulent flow leading to higher heat transfer due to fluid mixing. Understanding these dynamics is key to optimizing heat exchange systems, from designing heat exchangers to managing temperature regulation in various engineering applications.

1.2 Convective heat transfer in heat exchangers

Convective heat exchangers are instruments engineered to transfer thermal energy between diverse media. The devices are widely employed across numerous industrial sectors, including HVAC, process engineering, power generation, and mining. Their broad range of applications underscores the critical role these devices play. Enhancing the performance of convective heat exchangers offers several advantages, including compact designs, improved process control, and lower operating costs. These improvements ultimately benefit the end user through lower prices of final goods and a reduced carbon footprint. Consequently, an examination of the underlying physics governing convective heat exchangers is crucial to identify methods that optimize their efficiency.

The performance of a convective heat exchanger is described by a convective heat transfer coefficient. The coefficient is influenced by the geometry of a heat exchanger, including the shape of the heat transfer surface and the presence of turbulence-inducing elements, thermophysical properties of the working fluid, and flow-related parameters. Consequently, examining convective heat transfer under diverse operating conditions provides insights allowing for enhancing the device. The need to improve the convective heat transfer coefficient has brought together many researchers seeking optimal solutions, pushing the efficiency of heat exchangers, thus reaching the limit of what is technically possible.

1.2.1 Methods of convective heat transfer improvement

Heat transfer enhancement can be achieved through two distinct methods: active and passive. The active method involves the application of external energy to enhance the heat transfer process. Several techniques are available to achieve active heat transfer enhancement [1]:

- Incorporation of mechanical aids: bases on mixing the fluid using mechanical elements or by rotating surface. It includes approaches such as stirring and surface scraping, commonly used in process heat exchangers handling viscous liquids. The method also involves the utilization of rotating tubes, cylinders, plates etc.
- Surface and fluid vibration: focuses on vibrating exchanger or fluid. Properly selected surface vibration parameters lead to improved heat transfer, just as in the case of liquid vibration. Because of the difficulties of heat exchanger vibration caused by its size, fluid vibration is more popular.

- Exposure to external fields: involves the application of electric or magnetic fields to induce mixing in the fluid near the heat exchange surface. The method includes electromagnetic pumping of gravity driven flows, exposure of the fluid flow to a magnetic field, and the application of a voltage to the heat exchanging surface.
- Gas injection: bases on mixing of the medium by a gas injection. Heat transfer intensification is performed by injecting gas through a porous surface. In convective heat exchangers bubbles cause liquid mixing as in nucleate boiling.
- Fluid suction: relies on fluid suction through a porous heated surface. The method is less popular than gas injection due to problematic application in heat exchangers.

Passive methods do not require extra energy to enhance heat transfer, making them a preferable approach to improving heat exchanger performance over active methods. By eliminating the need for additional energy, the focus shifts to optimizing the design of components that influence the convective heat transfer process. The methods classifying to this category [1]:

- Surface treatment: bases on adjusting the surface with a suitable finish or coating. Surface condition affects strongly nucleate and pool boiling. Surface treatment enhancing wettability considerably increase pool-boiling critical heat flux.
- Surface roughening: focuses on the production of rough surfaces, unlike methods classified as surface treatment, the roughness scale affects single-phase flows. The method is one of the first considered to enhance heat transfer in forced convection and provides the expected gains. In free convection, the method is not as effective, due to the low velocity of the medium.
- Surface extension: relies on increasing heat exchange area and cause flow disturbances.
- Insertion of enhancement devices: involves placement of obstacles that disrupt the flow along the heat exchange surface. The fluid flow near the surface is changed by inserts such as metallic meshes, static mixers and elements of various shapes such as rings, disks etc.
- Insertion of swirl-flow devices: bases on inserting devices that generate vortexes. Such components include inlet vortex generators, twisted tapes, and axial core inserts with screw-like windings.
- Tube coiling: relies on shaping the tubes in the form of coils that allow secondary flow.
- Incorporation of surface-tension structures: uses wicks or groves to improve liquid flow, especially in phase change applications.

- Introduction of additives: employs the addition of a solid, liquid or gas phase substance to the fluid.

Selecting an appropriate method for enhancing convective heat transfer is linked to the limitations imposed by the specific heat exchanger application. In addition, investment and operating cost, as well as operational reliability and safety considerations, play an important role [1]. For example, increasing the heat exchange surface will increase the heat transfer, but will be associated with a higher investment and operating cost and will increase the weight and size of the device. These consequences often prevent the use of this method in compact applications such as electronics. The effort of researchers to develop the efficiency of heat exchangers for many of the methods mentioned has reached a barrier that cannot be surpassed in terms of cost-effectiveness, despite the initial ease of implementation. The passive method gains more and more significance since provides great potential in development. A significant research focus in recent years has been on surpassing the performance limitations of commonly used heat transfer liquids (e.g., water, ethanol, glycols). The introduction of particles into the base fluid to enhance its physicochemical properties is gaining interest. The classic approach of introducing solid particles is dominant, but other solutions are also investigated, such as the use of encapsulated phase-change materials. Initially, researchers attempted to create suspensions with solid micro-particles, but failed to meet expectations due to poor stability, flow channel clogging, and higher pump power requirements. Meanwhile, many hydraulic issues were resolved with suspensions of particles smaller than 100 nm. These fluids are commonly referred to as nanofluids.

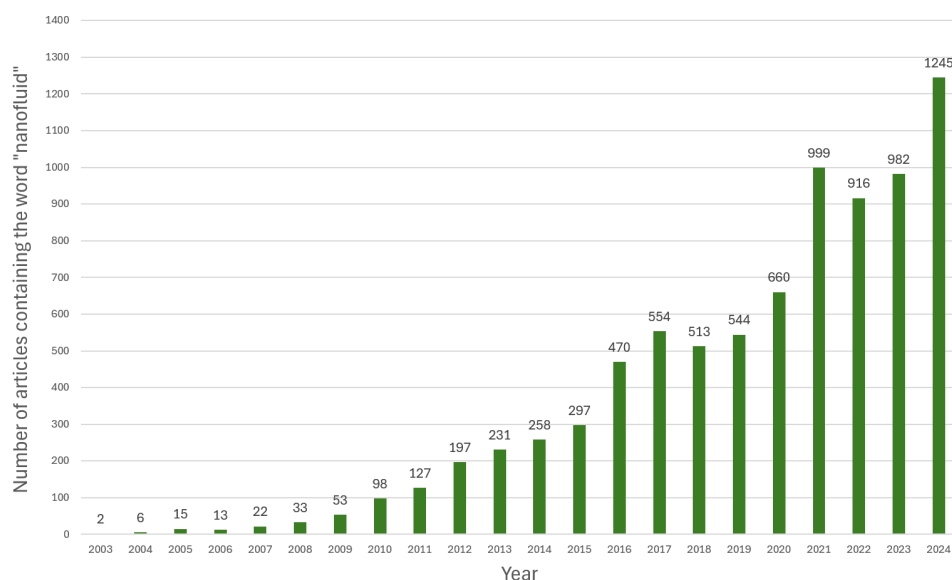


FIGURE 1.1: A graph showing the number of articles containing the word “nanofluid” in recent years [2]. Data are narrowed to International Journal of Heat and Mass transfer, Applied Thermal Engineering, International Communications in Heat and Mass Transfer, Case Studies in Thermal Engineering, International Journal of Thermal Sciences. Date of preparation 23.10.2024.

Nanofluids consist of a base fluid (such as water, glycols, refrigerants, or oils), and a dispersed solid phase of nanometer-sized particles. Since their introduction by Choi and Eastman [3], nanofluids have attracted increasing attention due to their properties that promise the development of high performance heat transfer fluids [4–6]. Fig. 1.1 illustrates the increasing number of articles that include the word ‘nanofluid’ in selected journals dedicated to the topic of heat transfer. Drawn by the prospect of improved thermal efficiency, research groups in Poland [7–9] and globally [4–6, 10–13] have explored nanofluids, examining their characteristics and the unique challenges presented by nanoparticle-enhanced mediums [14, 15]. The COST Action Nanouptake (<https://www.cost.eu/actions/CA15119>) was one of the most coordinated research initiatives, with 25 countries collaborating to advance nanofluids, generating a substantial amount of data [14, 16–19]. Scientists have highlighted various reasons for the improved heat transfer processes when using nanofluids, such as the increased apparent thermal conductivity from the presence of solid nanoparticles, Brownian motion, liquid layering, and particle aggregation [6]. The reason for the occurrence of several mechanisms is to be found in the diversity of nanofluids, caused, for example, by nanoparticle material, shape and size distribution, or used additives.

A notable example within a nanofluids group is ferronanofluids (or ferrofluids). Ferronanofluids contain ferromagnetic nanoparticles that are made of magnetic materials, typically iron-based compounds like magnetite Fe_3O_4 or maghemite Fe_2O_3 . The increased interest in ferronanofluids stems from their responsiveness to a magnetic field. This unique characteristic unlocks a possibility to enable an actively controllable heat transfer. The use of ferronanofluid and a magnetic field combines both methods of heat transfer improvement, passive and active. The first research on ferrofluids dates back to the 1930s, when Elmore [20] conducted studies on the magnetisation of suspensions containing Fe_3O_4 particles. Nearly forty years later, Papell [21] patented suspension containing magnetic particles sized between 0.06 and 0.24 micrometers. Shortly thereafter, Papell and Faber [22] explained connections between magnetic induction, magnetic gradient, particle concentration, and body forces. These studies formed the basis for researchers in the following years in undertaking the application of ferronanofluids and a magnetic field in heat transfer.

1.2.2 Emerge of ferronanofluids

The growing interest in nanomaterials and nanofluids in recent years has accelerated research into the applications of ferronanofluids. Still, the scientific focus on ferronanofluids remains lower compared to the range of studies on other types of nanofluids. Existing literature focuses on the convective heat transfer employing ferronanofluids does not clearly conclude whether their application is beneficial. The magnetic susceptibility of ferronanoparticles opens a possibility of controlled and precise regulation of heat transfer. Local adjustment of magnetic field parameters could be used for spot modifications of heat transfer characteristics. Such a solution can be applied to heat exchangers that have to provide precise temperature control or

have to operate in a scheduled mode. An important aspect to consider is the inclined flow, which is inherent in real-world applications. Changes in the flow direction relative to gravity impact heat transfer parameters. Consequently, for the optimal design of systems utilizing nanofluids, it is essential to consider the effects of flow inclination. The application of ferronanofluids and magnetic field introduces the possibility of improving heat transfer conditions in inclined flow. In addition to the areas mentioned, there are applications indirectly related to heat transfer that can benefit from ferronanofluids. One such instance is in electrical equipment, where a magnetic field is generated during the regular device operation. For example, electrically insulating liquids with dispersed ferronanoparticles can enhance electrical performance and diminish thermal stress in the equipment.

Despite the promising results presented of Papell and Faber [22], it is not confirmed that applying a magnetic field to a ferronanofluid flow always enhances heat transfer. Recent studies suggest that the improvement results from a complex interaction of several forces — including inertial, viscous, magnetic, and gravitational forces — which determine the flow dynamics. A summary by Buschmann [23] discussed experimental findings from 18 studies on magnetically influenced ferronanofluid flow and pointed out three required actions to complement the state of knowledge: an investigation of the governing equations to find the relevant parameter space, development of numerical models that include specific mechanisms suited to a magnetically affected ferronanofluid flow, and experiments designed to test the switchability of heat transfer. Addressing these issues and drawing meaningful conclusions require numerous experiments and validation studies. The primary focus of this dissertation is the investigation of the force balance affecting ferronanofluid flow in a magnetic field and its impact on heat transfer. To achieve this, research hypotheses are formulated and will be experimentally tested, addressing the need to perform tests on ferronanofluids to determine their heat transfer switch potential.

Chapter 2

Nanofluids

2.1 Nanofluids

Nanofluids in their basic form consist of two components: a liquid and dispersed nano-sized particles. Choi and Eastman introduced the term "nanofluid" in 1995 in a theoretical study on the improvement of a fluid thermal conductivity through the inclusion of nanoparticles [3]. Nanofluids, compared to suspensions with mili- and micro-sized particles, provide enhanced thermal conductivity, improved suspension stability, reduced surface erosion, and lower pressure drop. These unique properties make nanofluids a highly attractive medium for advanced thermal management systems. The growing interest in nanofluids is driven by their potential to enhance the efficiency of heat transfer processes, constrained by the thermophysical properties of conventional working fluids.

2.1.1 Base fluids

Nanofluids are based on standard working fluids such as water, oils, glycols, alcohols, or synthetic refrigerants. Liquids typically exhibit much lower thermal conductivity than solid materials, such as metals or metal oxides. This parameter limits the inability of the liquids to transfer heat. Tabs. 2.1 and 2.2 contain thermal conductivities of example liquids and solids. The values for solid materials are in some cases several orders of magnitude higher. This shows the potential of the dispersed solid phase to increase the average thermal conductivity of a working fluid.

Liquid	Thermal conductivity, $W m^{-1} K^{-1}$	Temp., $^{\circ}C$	Ref.
Acetone	0.161	25	[24]
Engine Oil	0.145	27	[4]
Ethanol	0.254	25	[24]
Ethylene glycol	0.253	27	[4]
Water	0.606	25	[24]

TABLE 2.1: Thermal conductivity of liquids.

Solid	Thermal conductivity at 27°C, W m ⁻¹ K ⁻¹	Ref.
Aluminum	237	[24]
Al ₂ O ₃	40	[4]
Carbon nanotubes	3000	[4]
Copper	401	[24]
Fe ₃ O ₄	4	[25]
Gold	317	[24]
Iron	147	[24]
Silver	429	[24]
SiO ₂	1.38	[26]
TiO ₂	8.5	[27]

TABLE 2.2: Thermal conductivity of solid materials.

Viscosity of the base fluid is another important property in heat transfer applications. The parameter describes fluid's resistance to flow. Liquids with higher viscosity require more energy to transport, reducing the overall efficiency of the system. For this reason, low-viscosity liquids are preferred for flow applications. Tab. 2.3 presents the viscosities of chosen base fluids.

Liquid	Dynamic viscosity at 25°C, mPa·s	Ref.
Acetone	0.306	[24]
Ethanol	1.074	[24]
Ethylene glycol	17	[28]
Example lubricating oil	130	[28]
Water	0.89	[24]

TABLE 2.3: Dynamic viscosity of liquids.

2.1.2 Additives

Additives in nanofluids are used to stabilize the dispersion of nanoparticles and prevent aggregation due to van der Waals forces, which lead to sedimentation and degrade the fluid's thermal conductivity over time. These additives, typically referred to as stabilizers or dispersants, maintain the homogeneity of the nanofluid by improving the interaction between the nanoparticles and the base fluid. Fluid stability is important for maintaining uniform thermal and physical properties of nanofluids and ensures their long-term stability, a crucial factor for industrial applications.

Common stabilizers used in nanofluids include surfactants (e.g., cetyltrimethylammonium bromide, CTAB) and polymers (e.g., polyvinylpyrrolidone, PVP). Surfactants are substances made up of two groups: a hydrophobic (lyophobic) group and a hydrophilic (lyophilic) group. Because of the structure, surfactants tend to accumulate on the interfacial surface. In the case of water, the hydrophilic part will remain in the liquid part and the hydrophobic part outside it. For this reason, they show surface tension-reducing properties. Polymers are substances that consist of large molecules

built by connected monomers. Their addition results in increase of water viscosity, dependent on the additive concentration and molecular weight of the polymer.

2.1.3 Nanoparticles

Nanoparticles are defined as solid objects with dimensions ranging between 1 and 100 nanometers [29]. Nanoparticles are made from materials such as metals (e.g. Au, Ag, Cu, Fe), oxides (e.g. TiO_2 , CuO , SiO_2 , Al_2O_3 , Fe_3O_4), carbon-based nanoparticles (e.g. graphene oxide, nanotubes, nanohorns, diamond). The method of production influences nanoparticle quality, including size, shape, and distribution. Tailoring these characteristics enables nanofluids to achieve desired performance in specific applications. Methods of producing nanoparticles are divided into chemical and physical [4]. Examples of chemical methods:

- Chemical vapor deposition - a technique where a gas is deposited onto a surface due to a high-temperature chemical reaction.
- Chemical precipitation - a method in which ions in solution containing a stabilizer are reduced to a metallic form.

Physical methods include:

- Inert-gas condensation - a method that involves evaporating a material under low pressure, then transporting it with the assistance of an inert gas to a cooled surface, where it condenses.
- Mechanical grinding - a technique that involves the mechanical processing of the material, typically in ball mills, where it is crushed and ground to the desired size.

The possibility to engineer a nanofluid through the appropriate selection of nanoparticles allows to benefit from their extraordinary properties in specific applications. This flexibility sparked an idea of using ferronanoparticles as a dispersed phase. Although this approach is counterintuitive, given the desire to use a material with the highest possible thermal conductivity, such as graphene, copper or aluminum, ferronanoparticles can be influenced by a magnetic field, thus affecting heat and mass transfer.

2.1.4 Ferronanoparticles

Ferronanoparticles exhibit superparamagnetic form of magnetism [30]. In this type of magnetism, a magnetic field can align the electron spins parallel to the field, causing attraction. In the absence of a magnetic field, Brownian motion causes the particles to lose their magnetization. This unique magnetic responsiveness enables ferronanoparticles to enhance heat and mass transfer under controlled conditions. In comparison to natural diamagnetic and paramagnetic fluids, ferronanofluids

are characterized by a $10^4 - 10^6$ higher magnetic susceptibility, which results in meaningful magnetic force values [31].

Ferromagnetic nanoparticles are most often made of magnetite, hematite, cobalt, and ferrites [32]. The two most commonly employed methods to produce nanoparticles are ball-milling and the chemical precipitation method [31]. The chemical precipitation method is preferred due to the uniform size of particles it produces. This method involves the interaction between iron salt solutions and concentrated alkali. The formed magnetite sediment, in combination with a surfactant and a base fluid, forms ferronanofluid. The quality of the outcoming nanoparticles has an impact on their magnetic parameters (their size, shape, and crystal structure).

The possibility to manipulate ferronanoparticles, and consequently ferronanofluids, using an external magnetic field has gathered interest in heat transfer applications. An important feature is their demagnetization upon exiting the region influenced by a magnetic field, enabling spot interactions without impacting other areas of the system.

three potential mechanisms enhancing heat transfer in laminar flow caused by magnetic field are indicated [23]:

- Chain aggregates formation,
- Secondary motions,
- Dune like structures formation.

The occurrence of each of these mechanisms is a result of the force balance acting on the flow.

2.1.5 Nanofluids for heat transfer enhancement

Heat transfer fluids benefit from the inclusion of nanoparticles due to the significantly higher thermal conductivity of the solid phase. Increased average thermal conductivity of a working medium by the presence of a solid phase appears not to be the only cause for extraordinary performance of nanofluids. Various mechanisms contribute to the enhanced thermal performance, though their relative significance remains a topic of debate. The most explored are:

- Brownian motion - random movement of solid particles, resulting in collisions and heat transfer between them, leading to an increase in the average thermal conductivity of the medium.
- Liquid layering - formation of an ordered layer of liquid around the solid particles, leading to an increase in the phonon mean free path, and, consequently, to an increase in the volume of the liquid with higher thermal conductivity.
- Nanoparticle aggregation - formation of chain aggregates with high thermal conductivity, enabling more efficient heat transport in the medium.

Sergis and Hardalupas [33] presented a statistical analysis of papers related to the use of nanofluids in heat transfer processes. The results show that in about 33% of the works, the increase in heat transfer was attributed to Brownian motion, 22% to liquid layering, aggregation alone was indicated in 1% of the articles, but 10% of them attributed the improvement in Brownian motion and aggregation simultaneously. However, there is no shortage of papers that deny each of these mechanisms. Nie et al. [34] presented a theoretical analysis of the contribution of Brownian motion to the enhancement of thermal conductivity and indicated that the effect is negligibly small. The authors provided a similar analysis for liquid layering. The ordered structure of the liquid around the nanoparticles that allows for an increase in thermal conductivity is so small that its contribution is insufficient. Hong et al. [35] investigated the effect of Fe nanoparticles aggregation. The results indicate that the cessation of agent sonication leads to a gradual agglomeration of nanoparticles and a consequent reduction in the thermal conductivity of the fluid. Given the contradictory voices in the discussion, it is not possible to unequivocally state which specific mechanism is responsible. General conclusions on this matter are still under discussion and remain an open question.

Nanofluids hold significant potential for phase-change heat transfer applications. In addition to the mechanisms previously discussed, nanoparticles can also impact device operation. For instance, nanoparticles can deposit on the heated surface, as a result of the bubble nucleation. The created nanoparticle layer facilitates capillary wicking [36], which helps in decreasing the wall superheat by improving liquid flow. The deposition of nanoparticles on the evaporator wall has been documented in thermosyphon heat exchanger experiments [9, 19, 37]. The occurrence of these mechanisms is strongly dependent on the material of the nanoparticles, and the long-term stability of the layers formed remains uncertain and is an ongoing area of research [14].

Employing nanofluids necessitates weighing their potential advantages against possible drawbacks. A prevalent concern is that the enhanced viscosity of nanofluids requires additional energy for medium transfer. From a broader, operational perspective, the utilization of nanofluids faces several challenges that include long-term stability concerns, corrosion and erosion of system components, and the absence of specific regulations to facilitate and accelerate their widespread use.

The next section presents the current status of work being undertaken, focusing on the implementation of nanofluids in heat transfer applications, and others potentially benefiting from nanofluids' unique properties. This is followed by an overview of the barriers associated with the industrial use of nanofluids.

2.2 Nanofluids in heat transfer applications

The application of nanofluids in industrial heating and cooling systems has garnered significant attention in recent years, driven by their potential to significantly enhance

efficiency and performance [38]. Nanofluids, with their superior thermal conductivity and unique properties, offer the possibility of improving heat transfer rates in a wide range of applications, making them an attractive alternative to conventional liquids. Despite their numerous benefits, the use of nanofluids is not without its limitations. Issues such as high production costs, potential environmental impact of nanoparticles, and the need for rigorous testing and standardization remain significant challenges that need to be addressed. This chapter examines the utilization of nanofluids in various industrial heating and cooling systems, shedding light on the advantages and challenges associated with their use.

2.2.1 Cooling Towers

Many industrial-scale processes produce substantial amounts of heat that must be continuously dissipated to maintain efficient operation. Cooling towers are extensively utilized to discharge excess heat loads from various sources, including electric power generation units, thermal and nuclear power plants, chemical and petroleum industries, as well as refrigeration and air conditioning systems. The efficiency of wet cooling towers (WCTs) is typically influenced by several factors, including air and water flow rates, water temperature, and the type of packing used [39]. As a result, many researchers have studied how these parameters affect the performance of the cooling tower. Despite the better thermal properties of nanofluids, the number of studies on their use is limited (Tab. 2.4).

Askari et al. [40] performed experimental research to examine the effects of multi-walled carbon nanotubes (MWCNT) and nanoporous graphene nanoparticles on the thermal performance and water usage of a wet cooling tower (WCT). The results indicated that the thermal conductivity of nanofluids increased by 16% for nanoporous graphene and 20% for MWCNT nanofluids compared to the base fluid. As a result, using either nanofluid can lower water consumption in WCTs. Additionally, the authors found that the rise in viscosity for both nanofluids (at 20°C: MWCNT: 1.12, 1.16, 1.25 cP; nanoporous graphene: 1.15, 1.27, 1.31 cP at 0.1, 0.3, and 0.5 wt% concentrations, respectively) is minimal for industrial use.

Imani-Mofrad et al. [41] developed a method to standardize ambient conditions during various WCT experiments using a small-scale lab setup with a fill column height of 0.4 m. They investigated the impact of four nanofluids (ZnO/Water, SiO₂/Water, Al₂O₃/Water, and Graphene/Water at concentrations between 0.02 and 0.08 wt%) on the heat transfer performance of a cross-flow WCT. Their results indicated that introducing nanoparticles into pure water improved the effectiveness, cooling tower performance, and volumetric heat transfer coefficient.

TABLE 2.4: Investigations on the nanofluid use in wet cooling towers.

Nanofluid	Base fluid	Concentration(s)	Stabilizers	Application	Study type	Source
MWCNT, Nanoporous graphene	Water	0.1, 0.3, 0.5 wt%	Gum Arabic, Tween80, CTAB, Triton x100, Terpolymer	Wet cooling tower	Lab setup	[40]
MWCNT, MWCNT-COOH, MWCNT-OH	Water	0.02, 0.04, 0.06, 0.08, 0.1 wt%	Present /none / none	Wet cooling tower	Lab setup	[42]
MgO, TiO ₂	Water	0.1, 0.5, 1.0 wt%	-	Wet cooling tower	Lab setup	[43]
Al ₂ O ₃ , Graphene, SiO ₂ , ZnO	Water	0.02, 0.05, 0.08 wt%	Gum Arabic	Wet cooling tower	Lab setup	[41]
ZnO	Water	0.02, 0.04, 0.06, 0.08, 0.1 wt%	Cetyl Trimethyl Ammonium Bromide	Wet cooling tower	Lab setup	[44]
Al ₂ O ₃	Water	0.1, 0.3, 0.5, 0.8 and 1 wt%	PEG400, Tween80, SDBS, glycerin, Tween 20	Wet cooling tower	Lab setup	[45]

Xie et al. [45] investigated the impact of aluminum oxide nanoparticles incorporated into spray water on the heat and mass transfer performance of a closed WCT. Their findings indicated that the thermal conductivity, viscosity, and density of aluminum oxide nanofluids increased with higher mass fractions. Importantly, the nanofluid concentration of 0.5 wt% yielded the optimal heat and mass transfer performance, resulting in a 19% improvement in cooling efficiency.

Elsaid [43] carried out experiments to improve the efficiency of a WCT within central air-conditioning system under different operating conditions. Employing MgO and TiO₂ nanoparticles, he explored the effects of different parameters including nanoparticle concentration ratio, sprayer angle, type of filling, and the spacing of filling sheets. The findings indicated that the optimal system performance was achieved with a 1% MgO/water nanofluid, using PVC fill with 12 mm sheet spacing and a spray angle of 90°.

Bakhtiyar et al. [42] explored the use of MWCNT/H₂O, MWCNT-COOH/H₂O, and MWCNT-OH/H₂O nanofluids in a cross-flow cooling tower. They found that the efficiency of the cooling tower was positively influenced, showing enhancements of 6.17%, 15.85%, and 11.1%, respectively (at 0.1 wt%), relative to pure water. The researchers mentioned the risk of nanoparticle agglomeration in highly concentrated nanofluids, which can cause clogging in the system. The concentration of nanofluids considered in the study was limited to not cause such problems.

Rahmati [44] conducted an experimental study on the performance of a WCT using ZnO/water nanofluid at concentrations of 0.02, 0.04, 0.06, 0.08, and 0.1 wt% across three different packing configurations. Results demonstrated that incorporating nanofluids enhanced the cooling tower's performance, with efficiency improving as nanoparticle concentration increased. The greatest cooling efficiency was achieved with ZnO nanofluid in the densest packing configuration. Additionally, the benefit of higher packing density was more significant when the nanofluid was utilized.

2.2.2 Phase-change devices

Despite the acknowledged potential for enhancing heat transfer in phase-change systems using nanofluids, including thermosyphons and heat pipes [23], the investigation into condensation and evaporation processes in the presence of nanoparticles continues to be an active area of research (Tab. 2.5). For example, nanoparticle deposition on the evaporator surface and the impact on device efficiency requires further study [19, 37]. Although there is a considerable amount of experimental research on nanofluid evaporation, the study of condensation is notably less thorough, with a greater focus on theoretical models and simulations [46].

TABLE 2.5: Investigations on the nanofluid use in phase change devices.

Nanofluid	Base fluid	Concentration(s)	Stabilizers	Application	Study type	Source
Au	Water	2.88×10^{-4} vol. %	-	Thermosyphon	Lab setup	[37]
TiO ₂	Water	0.1, 0.2, 0.3, 0.4 vol. %	-	Thermosyphon	Lab setup	[37]
Cu	Water	0.13 wt%	-	Pool boiling	Lab setup	[47]
Al ₂ O ₃	Water	0.1, 0.5 vol. %	-	Evaporator	Lab setup	[48]
SiO ₂	Water	2 vol. %	KOH	Thermosyphon	Lab setup	[19]
CuO	Water	3.5, 5, 10, 20 wt%	none	Cooling electrical components	Real application	[49]

Buschmann and Franzke [37] examined the effects of using nanofluids containing titanium dioxide at different concentrations (0.1, 0.2, 0.3, and 0.4 vol.%) and gold (2.88×10^{-4} vol.%) in a thermosyphon heat exchanger. Their results indicated that employing TiO₂ nanofluid led to a maximum reduction in the thermal resistance of the device by 24%, with the most effective concentration being between 0.2–0.3 vol.%. Outside this range, the impact diminished or even turned negative. The reduction was attributed to a layer of deposited nanoparticles on the evaporator surface. The study also examined the aging effect of these layers. At concentrations of 0.3 and 0.4 vol.%, repeated tests showed a substantial increase in thermal resistance compared to the initial measurements, indicating a rapid aging of the formed layer.

Doretti et al. [47] examined the influence of using a water-based Cu nanofluid (0.13 wt%) in pool boiling on thermal performance. The experimental setup ensured the deposition of nanoparticles on the surface by applying heat and operating the device for 30 minutes. The observed heat transfer coefficients were 15–34% greater than those recorded for pure water. SEM images taken post-experiment showed a compact and uniform layer of deposited nanoparticles with some damaged areas, potentially caused by the cleaning process.

Fu et al. [48] investigated the evaporation of water-based Al₂O₃ nanofluid (0.1, 0.5 vol.%) from a micro-grooved heat exchanger surface. They found that using a nanofluid with a 0.5 vol.% concentration increased heat transfer performance by 44.6% compared to water. Moreover, their results indicated that applying nanofluid to the smooth surface of the evaporator did not improve heat transfer, highlighting the potential for leveraging nanofluid advantages through suitable heat exchanger design.

Kujawska et al. [19] examined the performance of a thermosyphon using a water-based silica nanofluid (2 vol.%). Their findings indicated a decrease of the device thermal resistance at heat source temperatures between 35–50 °C when compared to water. Moreover, the use of nanofluid mitigated the occurrence of geysier boiling regimes, which are detrimental to both the thermal performance and mechanical durability of the device. The study also observed nanoparticle deposition on the evaporator surface, as shown by reduced thermal resistance under similar working conditions. SEM images revealed a built-up layer that cracked during sampling and transport, suggesting fragility and raising concerns about long-term stability.

Handling high heat fluxes poses considerable difficulties, especially in environments with limited space or additional temperature constraints, such as in electronics. The rising power requirements in the computing field, with server processors and graphics units reaching power values of 400 W [50] and 450 W [51] respectively. Combining that with application in advanced systems like satellites and military systems [52], places supreme demands on cooling solutions. The present methods employ heat pipes relying on phase-change mechanisms, which are effective in addressing these needs. The improvement of their efficiency is crucial for developing

more compact heat exchangers or enhancing the power dissipation capabilities. Utilizing nanofluids as substitutes for the currently used working fluids provides such an opportunity.

Roger Riehl [49] explored the use of CuO nanofluid in thermal management systems for pulsating heat pipes designed for cooling surveillance equipment. Incorporating nanofluid into a single-phase cooling loop resulted in a 12% improvement in the heat transfer coefficient compared to water at a temperature of 55°C and a 20% nanoparticle mass fraction. This benefit came with a 34% increase in pressure drop. Despite the high concentration of nanoparticles and their deposition in the liquid reservoir, prolonged testing showed no significant change in performance, suggesting the nanoparticles stayed well-dispersed in the base fluid. Using nanofluids with a 3.5% mass concentration in heat pipe operations significantly lowered the heat source temperature from 118°C to 83°C under a 50 W heat load, which is crucial for effective electronic cooling. The study underlined the importance of ensuring chemical compatibility between the nanoparticles, heat pipe material, base fluid, and surfactant to avoid the formation of non-condensable gases that could diminish device performance. Additionally, the purity of these materials, as well as the geometry and size distribution of nanoparticles, were identified as essential factors impacting overall performance. In another research, Riehl and Murshed [53] investigated the longevity of heat pipes filled with nanofluid. They discovered the problem of non-condensable gas release caused by nanoparticles during device operation, which leads to reduced performance over time due to a decrease in effective heat transfer surface area. Their findings highlighted the necessity of examining the release rate of non-condensable gases based on the chemical compatibility between the device material, base fluid, nanoparticles, and surfactant.

2.2.3 Waste heat utilization

The utilization of waste heat has immense potential to reduce global primary energy consumption. Firth et al. [54] conducted an analysis indicating that waste heat in 2030 will range from 51.5% in a scenario maintaining policies as of mid-2016 to 23% in a scenario transitioning entirely to renewable energy sources for electricity generation. Consequently, irrespective of the chosen scenario, waste heat remains a valuable resource offering environmental and economic profits. Researchers are exploring the potential of using nanofluids for heat recovery in a variety of applications due to the increased efficiency of the process, or the possibility of enabling it for low temperature heat sources (Tab. 2.6).

TABLE 2.6: Investigations on the nanofluid use in waste recovery systems.

Nanofluid	Base fluid	Concentration(s)	Stabilizers	Application	Study type	Source
MIL101	R245fa	0.7 wt %	-	ORC	Simulation	[55]
ZnO	EG/Water (50/50)	0.006-0.08 vol. %	-	Thermoelectric generator	Simulation	[56]
Cu	EG	1, 2, 3, 4, 5, 6 %	-	Thermoelectric	Simulation	[57]
Al ₂ O ₃ , CuO, Fe ₃ O ₄ , SiO ₂	R152a, R245fa, R125, R1234fy	5, 10, 20 vol. %	-	PV/T ORC	Simulation	[58]
Fe ₃ O ₄ , SiO ₂	Water	0.5 wt %	none / gum arabic	PV/TE	Lab setup	[59]

Cavazzini et al. [55] introduced a numerical model evaluating the influence of using R245fa nanofluid, which includes metal-organic heat carrier nanoparticles, on the efficiency of an Organic Rankine Cycle (ORC). Their study suggests the possibility of improving cycle efficiency, especially for low-temperature heat sources. The authors emphasize the necessity for further optimization of both the nanofluid properties and cycle operating conditions to precisely determine the benefits of nanofluid use in the ORC.

Sami [58] examined the performance of an ORC cycle employing a PV/T collector with nanofluid solutions based on Al_2O_3 , CuO , Fe_3O_4 , and SiO_2 . The findings indicate a potential 17% boost in system efficiency when CuO nanofluid is used instead of water.

Soltani et al. [59] experimentally assessed a photovoltaic thermoelectric system utilizing five different cooling methods for thermoelectric modules, including natural and forced convection with air, water, and SiO_2 and Fe_3O_4 (0.5 wt%) water-based nanofluids. Water cooling notably amplified power production by 47.7% compared to air cooling, while nanofluid usage led to an average increase of 5.7% over water cooling. Improved cooling not only enhanced thermoelectric module performance but also lowered PV module temperatures, thus raised its efficiency.

Karana and Sahoo [56] explored the potential application of nanofluids in a thermoelectric generator (TEG) system to recover waste heat from exhaust gases. By analyzing ZnO and SiO_2 nanofluids based on an EG-W (50/50) mixture on the cooling side of the TEG, they noted an 11.80% enhancement in power generation with SiO_2 nanofluid and an 9.86% increase with ZnO nanofluid, maintaining the same TEG surface area.

Li et al. [57] performed a comparable study, evaluating the performance of Cu-ethylene glycol nanofluid and ethylene glycol-water as coolants in a thermoelectric automotive waste recovery system. Their results indicated that the use of nanofluid reduced the temperature of the cold side of the thermoelectric module, leading to a higher power output.

2.2.4 Techno-economic basis

The integration of nanofluids into industrial applications necessitates a comprehensive assessment of their impact on heat transfer parameters alongside increased investment and operating costs compared to conventional fluids. Despite their ability to enhance heat transfer, the dispersed nanoparticles often elevate the medium's viscosity, resulting in heightened pressure drop and increased energy consumption [60]. Moreover, operational challenges stemming from nanoparticle agglomeration and deposition in the system further compound operational costs [49]. Addressing these challenges requires additional design considerations and ensuring the quality and purity of both installation and nanofluid materials. That results in increased

investment costs. These additional considerations do not negate the potential overall cost reduction and ancillary benefits, such as decreased energy consumption and consequent CO₂ emissions (Tab. 2.7).

Liu et al. [61] performed a techno-economic evaluation of Al₂O₃ and CuO nanofluids (0.5, 1, 2%) in propylene glycol/water (60/40 vol.) based nanofluids in horizontal ground exchangers for heat pumps. Their results showed that using nanofluids significantly raised the liquid exit temperature of the heat exchanger, with stable COP values at specific concentrations appropriate for large-scale use. Nonetheless, the authors identified issues like nanoparticle deposition, especially problematic in ground heat exchangers. Despite these challenges, the low maintenance and operational costs combined with high heat transfer efficiency led to favorable CO₂ emission outcomes.

Kode et al. [62] conducted a techno-economic study of LiCl liquid desiccant with multiwalled carbon nanotube additive in an atmospheric water generation system. They found that the addition of 0.5 vol.% nanoparticles reduced water generation costs by about 7.5%, underlying the economic advantages of nanoparticle integration.

Mehrpooya et al. [63] investigated the use of different nanofluids in shell and tube heat exchangers within a combined heat and power system (CHP) and a solar-driven organic Rankine cycle (ORC). Their findings revealed notable cost savings, particularly with Ag/water nanofluid.

Taheri and Zahedi [64] conducted a techno-economic assessment of a quadruple hybrid system for water and biofuel production combining solar, hydro, biomass, and geothermal energy sources. Utilizing GO/CuO nanofluid increased water production efficiency by 14% and lowered production costs compared to base thermal oil. However, the use of nanofluids requires higher initial capital investment.

TABLE 2.7: Investigations on the nanofluid use considering techno-economic analysis.

Nanofluid	Base fluid	Concentration(s)	Stabilizers	Application	Study type	Source
MWCNT	LiCl	0.1, 0.2, 0.3, 0.4, 0.5 vol. %	-	Atmospheric water generation system	Simulation	[62]
Al ₂ O ₃ , CuO	PG / Water (60/40)	0.5, 1, 2%	Sodium dodecyl sulfate	HP ground heat exchanger	Properties investigation / simulation	[61]
Ag, Al ₂ O ₃ , Cu, TiO ₂	Water	0.5 - 4 vol. %	-	ORC	Simulation	[63]
GO/CuO	Oil based fluid	0.3 - 0.6 wt%	-	Parabolic trough collector	Lab setup	[64]

2.2.5 Other applications

Nanoparticles dispersed in a medium have the potential to improve heat transfer characteristics, slowing down the aging process of insulating materials. Additionally, employment of nanofluids could improve insulation properties such as breakdown voltage, streamer propagation, and partial discharge, which are critical for an electrical transformer performance. Ferronanofluids, which are particularly affected by magnetic field gradients, show improved convective heat transfer around transformer components, making them a promising option. Despite the recent findings suggesting lower failure rates of transformers, further investigation is necessary to develop comprehensive guidelines for nanofluid production techniques and optimal parameters, with a special focus on nanoparticle agglomeration.

Beheshti et al. [65] examined the thermophysical properties of nanofluids with multi-walled carbon nanotubes (0.001 and 0.01 wt%) in transformer oil and assessed heat transfer under conditions similar to real. The application of nanofluids enhanced both free and forced convection heat transfer but also resulted in a reduced flash point temperature. The presence of solid particles in the transformer oil led to a decrease in breakdown voltage, restricting its suitability to transformers with a nominal voltage under 72.5 kV. The research suggests utilizing a lower concentration (0.001 wt%) of the nanofluid to improve heat transfer attributes without a significant decrease in breakdown voltage noted with the higher concentration (0.01 wt%).

Rajnak et al. [66] examined the application of $Mn_0 \cdot 6 Zn_0 \cdot 4 Fe_2O_4$ ferronanofluid in an innovative gas-to-liquid transformer oil, noting temperature reductions of 2.2 K in the core and 2.1 K in the winding. High concentrations of ferronanoparticles caused temperature increase, attributed to the constraints in thermomagnetic and natural convection due to increased density, viscosity, magnetization, and magnetic susceptibility. This highlights the critical need to match working fluid parameters with the transformer's specifications and operating conditions.

Kurimsky et al. [67] examined the insulating characteristics of magnetite ferronanofluids at different volume concentrations (0%, 0.0005%, 0.001%, and 0.002%) in both mineral oil (MO) and gas-to-liquid oil. They observed that the breakdown voltage increased for high concentration of ferronanoparticles in both oils, with MO-based fluids exhibiting an average of 10.8% greater breakdown voltage than those based on GTL. This discrepancy is likely due to the higher viscosity of MO, which limits the movement of charged particles, possibly accounting for its better performance in partial discharge tests compared to GTL.

2.2.6 Stability and longevity

Agglomeration poses a significant challenge in nanofluid applications, despite few studies reporting issues [41, 68–70], which can cause reduced performance or installation complications. Although most research stresses the importance of stable nanofluids, there is a lack of studies on the state of nanofluids or installations after

experimentation. For example, Cacua et al. [71] discussed this matter in a review on nanofluid stability in heat pipes, pointing out the limited research on the effects of stabilizing additives and long-term cyclic operation. The performance of heat pipes may degrade over time due to nanoparticle accumulation on the evaporator surface, necessitating more research across various parameters. These results highlight the need for careful implementation of nanofluids in phase-change exchangers, particularly regarding long-term efficiency.

Erosion and corrosion pose major challenges in nanofluid applications, as emphasized by several referenced studies ([65, 72]). Sharif et al. [73] visually examined heat exchanger surfaces to find sedimentation and corrosion spots. These problems are crucial in industrial environments and must not be overlooked. For example, Braut et al. [70] explored the erosion of plastic, copper, and rubber due to jet-impingement with a water-based nanofluid containing 1.33 wt% TiO₂ over 334 hours. The findings indicated a reduction in copper surface mass at a rate of $-282 \text{ g year}^{-1} \text{ mm}^{-2}$. Investigations using SEM and EDX uncovered crater-like formations with nanoparticle build-up and corrosion signs. Further surface roughness analysis showed a notable increase. Additionally, after 150 hours of testing, clumped particles were found in the tank, causing a decrease in both nanoparticle concentration and size distribution in the nanofluid. These results highlight the critical need to address erosion and corrosion in nanofluid applications.

Regulations and safety concerns surrounding nanofluids are highlighted in the article by Lourenço et al. [74], where the authors emphasize the ambiguity in current regulatory frameworks for classifying nanofluids. This ambiguity poses challenges in clearly identifying their environmental and human health impacts. The authors argue that establishing clear regulations would not only enhance public trust but also facilitate the industry's adoption of nanotechnology. To address these concerns, the authors propose an investigation involving a solar heat collector utilizing a natural, melanin nanofluid, known for its non-toxic properties. The study demonstrated that melanin nanofluid could enhance the efficiency of the collector, surpassing the performance of a TiO₂ nanofluid. This research underscores the importance of regulatory clarity and the potential of safer nanofluid alternatives in advancing nanotechnology applications.

2.2.7 Summary of nanofluid applications

Nanofluids have emerged as a promising solution for enhancing heat transfer in various industrial applications, including cooling systems, phase-change devices, and waste heat recovery. Their superior thermal properties contribute to improved efficiency, yet several challenges limit their widespread use. Increased viscosity leads to higher energy consumption, while long-term stability concerns—such as nanoparticle agglomeration and sedimentation—reduce performance over time. Additionally, erosion, corrosion, high production costs, and environmental concerns further complicate their large-scale adoption.

In cooling towers, nanofluids consistently enhance thermal conductivity and cooling efficiency. Studies report up to a 20% improvement with multi-walled carbon nanotube (MWCNT) nanofluids, while ZnO and graphene-based fluids optimize both efficiency and water usage. However, issues like nanoparticle agglomeration pose risks of clogging, particularly in densely packed systems, emphasizing the need for precise concentration control.

For phase-change devices such as thermosyphons and heat pipes, nanofluids improve heat transfer rates and reduce thermal resistance. Nanoparticles can form a layer on the evaporator surface that enhances performance initially, but long-term durability remains uncertain due to potential aging effects. Additionally, chemical interactions of nanofluids with heat exchanger materials may generate non-condensable gases, reducing system efficiency.

In waste heat recovery, nanofluids have demonstrated potential in thermoelectric generators and organic Rankine cycles (ORC). For instance, CuO nanofluids have been shown to increase heat transfer coefficients by 12%. Despite these benefits, economic feasibility remains a challenge due to the high production costs of nanoparticles and concerns over their environmental impact.

Key challenges still hinder large-scale implementation. Stability issues, particularly nanoparticle aggregation, can compromise long-term reliability. Environmental and health risks remain underexplored, with limited regulatory frameworks addressing nanoparticle dispersal. Finally, the high cost of production and the need for specialized systems restrict broader industrial adoption.

Chapter 3

Convective heat transfer employing ferronanofluids

Ferromagnetic nanoparticles enhance heat transfer through size-induced phenomena, such as Brownian motion and liquid layering. However, their relatively low thermal conductivity has received less attention compared to graphene- or copper-based nanoparticles. Research on highly efficient working fluids has primarily focused on enhancing their average thermal conductivity through the incorporation of high-thermal-conductivity nanoparticles. This approach has faced limitations due to high viscosity and stability issues in highly concentrated nanofluids, prompting renewed interest in ferronanofluids, which can be influenced by magnetic fields. Magnetic susceptibility of ferronanoparticles introduces a promising research area: leveraging magnetic field interactions to modify heat and mass transfer. While the effects of viscosity and inertia can be explained using appropriate similarity numbers, the inclusion of ferromagnetic nanoparticles interacting with a magnetic field introduces additional complexities to the heat transfer process.

The responsiveness of ferronanofluids to magnetic fields suggests potential for controlling heat and mass transfer. It is hypothesized that modulating the strength and direction of a magnetic field can amplify or diminish transfer effects as needed. The degree of influence hinges on the relative magnitude of the imposed magnetic force compared to the inertial and viscous forces affecting the flow. The potential for fluid control can be utilized in thermally developing flows, where free convection is affected by a magnetic field.

The analysis of this flow conditions requires considering gravity's role in defining buoyancy forces. Thus, essential differences will be displayed in horizontal and inclined flows with mixed convection (combination of forced and free convection). The interaction of a magnetic field with a ferronanofluid can be used to change the balance between the forces in the flow, and thus to regulate heat transfer and correct the changes resulting from flow inclination.

The following sections present a literature review of heat and mass transfer processes in ferronanofluid flows under the influence of static and alternating magnetic fields in both laminar and turbulent flows. That is followed by a state of the art analysis of mixed convection in conventional fluids and nanofluids.

3.1 Laminar flow with ferronanofluids

Research on the laminar flows of ferronanofluids under a magnetic field provides inconclusive evidence regarding its effect on heat transfer. Some works provide evidence of its positive effect on the heat transfer process [75–98], while there is also a group of papers showing the opposite [76, 93, 99–101]. Each case requires analyzing the magnetic field distribution to determine the forces affecting the flow and their effects. Taking into account the contribution of inertial forces, some investigations present the amplification effect of the magnetic field-induced impact due to an increase in Reynolds number [75, 77, 89, 90, 101, 102], or variable in the studied range [76, 79, 84, 92]. There are also works that present a decreasing importance of a magnetic field with an increase in the contribution of inertial forces [80–83, 85, 91, 93, 95, 100].

In a critical review, Buschmann [23] explored ferronanofluid laminar and turbulent flows under the influence of a magnetic field. There are three main mechanisms that result in improved heat transfer parameters in the laminar flow of ferronanofluids under the influence of a radially directed magnetic field (Fig. 3.1):

- chain aggregation,
- secondary motions,
- ferronanoparticle wall accumulation.

The occurrence of a specific phenomenon depends on the interplay of inertial, viscosity, gravity, and magnetic forces as presented in Fig. 3.2. The author highlighted three directions to advance the state of the art in the magnetically affected flow of ferromagnetic nanofluids:

- analysis of the governing equations to identify the relevant parameter space,
- development of numerical schemes incorporating the specific mechanisms relevant to magnetically affected ferronanofluid flow,
- investigation of the switch ability of heat transfer.

To address these and to draw meaningful conclusions, it is necessary to conduct many experiments and validation studies.

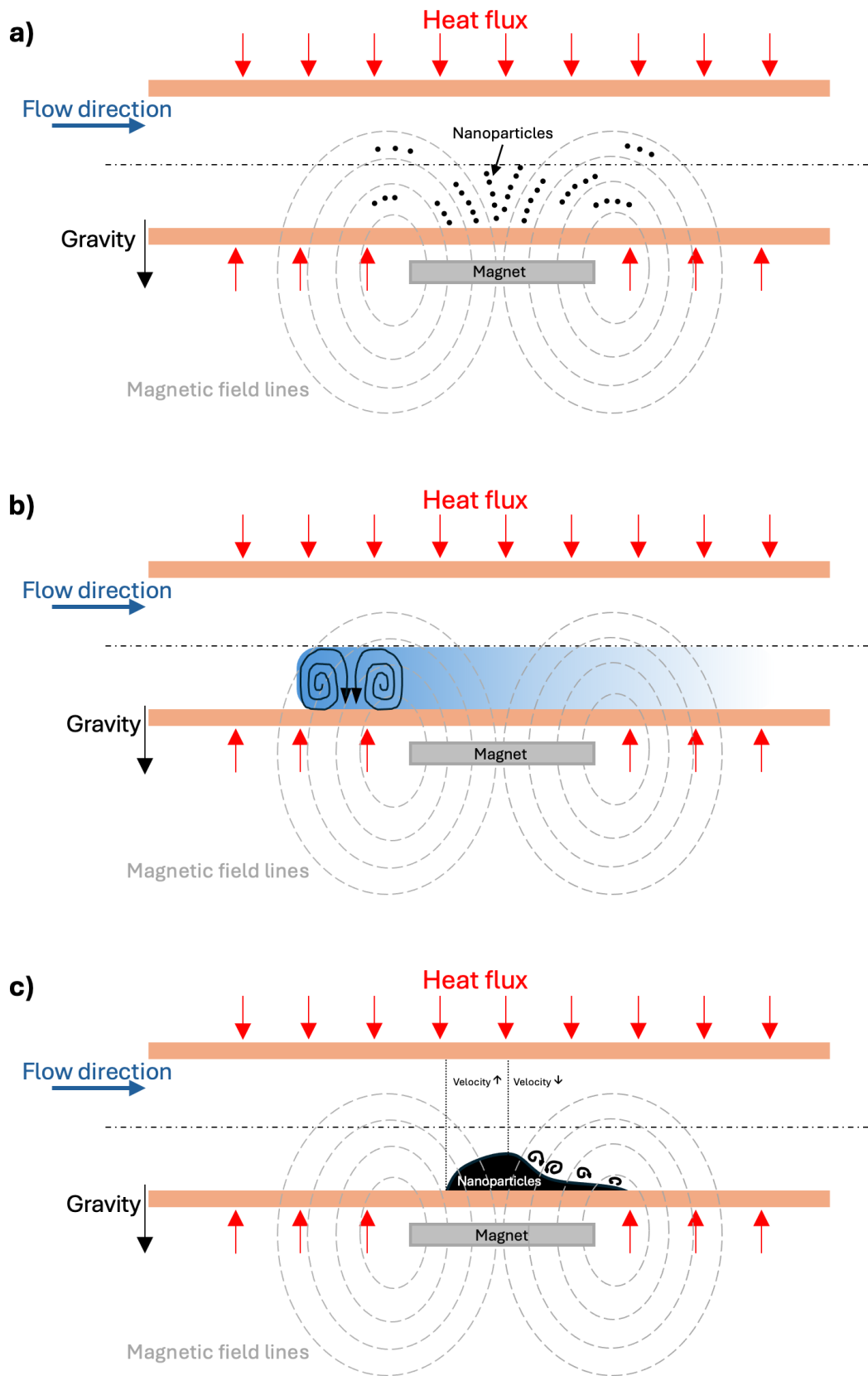


FIGURE 3.1: Mechanisms responsible for heat transfer enhancement in ferronanofluid laminar flow under radial magnetic field. Sketch a) presents chain formation, b) secondary motions, c) wall accumulation. Prepared based on [23].

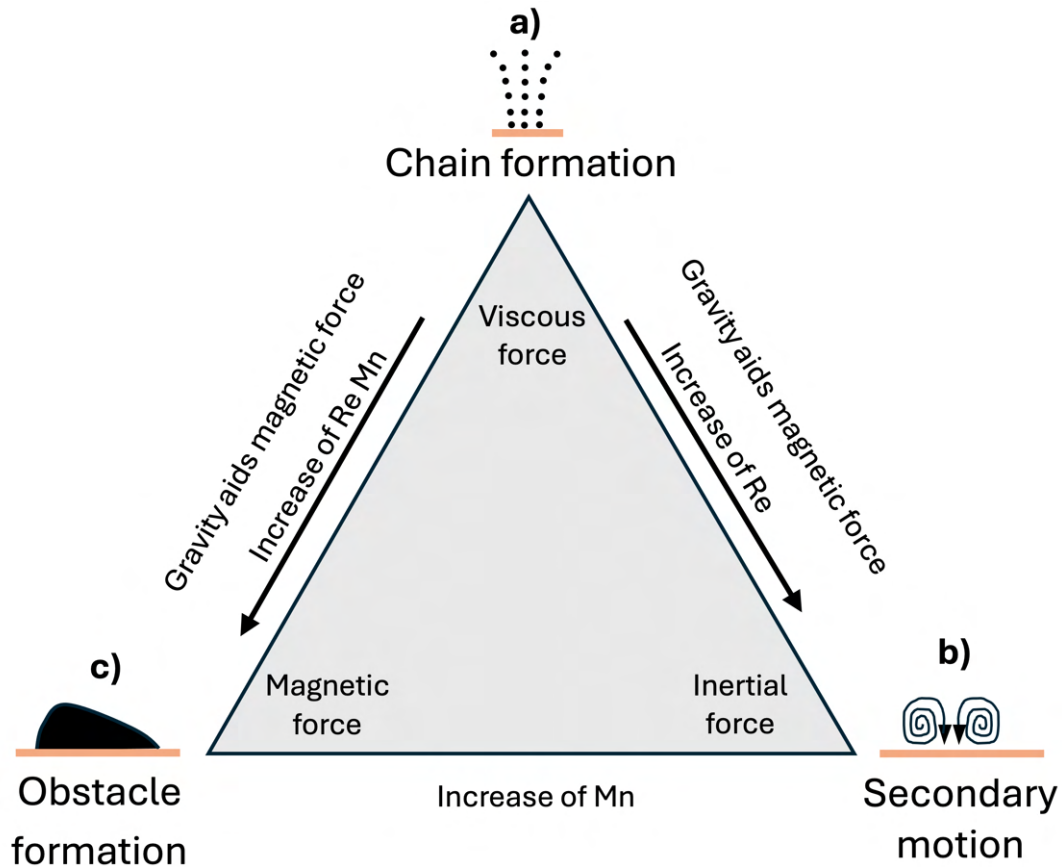


FIGURE 3.2: Interplay of inertial, viscosity, gravity, and magnetic forces in ferronanofluid laminar flow under radial magnetic field. Prepared based on [23].

3.1.1 Flow under a static magnetic field

This section outlines the state of the art concerning laminar ferrofluid flow in the presence of a static magnetic field. Tab. 3.1 summarizes the literature review, while The following paragraphs detail information extracted from the studies on the force balance influencing the flow and the main cause of the heat transfer change identified by the authors.

Azizian et al. [75] examined the impact of permanent magnets on the laminar flow of Fe_3O_4 ferronanofluid. Their investigation employed permanent magnets to generate a magnetic field perpendicular to the ferronanofluid flow. Findings revealed that heat transfer enhancement is dependent on magnetic field strength, gradient and Reynolds number. The authors attributed these results to spot aggregation and migration of ferronanoparticles.

Hammodi et al. [77] investigated Fe_3O_4 glycol-based ferronanofluid heat transfer in laminar flow conditions ($Re = 100, 250, 450, 750$) under a magnetic field generated by coils. It was found that heat transfer was enhanced with increase of particle concentration and Reynolds number.

TABLE 3.1: Summary of studies on static magnetic field effect on heat transfer in ferronanofluids

Magnetic field source	Ferromagnetic particles	Basefluid	Reynolds number	Type of experiment	Device	Magnetic field effect on heat transfer	Source
NdFeB N42	Fe ₃ O ₄	Water	451–868	Experimental setup	Tube	Heat transfer coefficient increased up to 300%	[75]
NdFeB	Fe ₃ O ₄	Water	120–480	Experimental setup	Tube	Nusselt number may change depending on several factors	[76]
Electromagnet	Fe ₃ O ₄	EG	100–750	Experimental setup	Tube	Nusselt number increased depending on Reynolds number and particle concentration	[77]
Electromagnet	Fe ₃ O ₄ , MCNT	Water	60–540	Experimental setup	Tube	Local Nusselt number increased by 30.2%	[78]
NdFeB N42	Fe ₃ O ₄	Water	391–805	Experimental setup	Tube	Averaged Nusselt number enhancement up to 361%	[79]
Electromagnet	Fe ₃ O ₄	Water	100–1000	Numerical	Tube	Nusselt number increased up to 8%	[80]
Electromagnet	Fe ₃ O ₄ , Fe ₃ O ₄ /CNT	Water	548–2190	Experimental setup	Tube	Heat transfer enhancement up to 20.5%	[81]
NdFeB N50	Fe ₃ O ₄	Water	580–820	Experimental setup	Tube	Local heat transfer coefficient increased up to 48.9%	[82]

Magnetic field source	Ferromagnetic particles	Basefluid	Reynolds number	Type of experiment	Device	Magnetic field effect on heat transfer	Source
NdFeB	Fe_3O_4 , $\text{Fe}_3\text{O}_4/\text{Cu}$	Water	1131–2102	Experimental setup and numerical	Tube	Overall heat transfer shifted up to 5% (positively or negatively) depending on a magnet position	[83]
Electromagnet	Fe_3O_4	Water	480–2000	Experimental setup	Tube	Maximum Nusselt number enhancement of 16.2% for experimental and 11.6% for numerical experiments	[89]
NdFeB N40	Fe_3O_4 , CoFe_2O_4	Water	200–1000	Experimental setup	Tube	Local Nusselt number increased up to 35.9%	[84]
Magnet (not specified)	Fe_3O_4 , MWCNT- Fe_3O_4 , $\text{Fe}_3\text{O}_4@\text{MWCNT}$	Water, EG	800–2200	Experimental setup	Tube	Cooling performance enhanced up to 10%	[85]
NdFeB	Not disclosed	Water	66	Experimental setup and numerical	Tube	Convective heat transfer coefficient increased up to 32.84%	[86]
Electromagnet	Fe_3O_4	Water	400–1200	Experimental setup	Tube	Heat transfer enhancement up to 23%	[87]
Electromagnet	Fe_3O_4	Water	Not disclosed, laminar	Experimental setup	Tube	Heat transfer enhancement up to 18.9%	[88]
Electromagnet	Fe_3O_4	Water	1200–7500	Experimental setup	Tube	Heat transfer enhancement	[98]

Magnetic field source	Ferromagnetic particles	Basefluid	Reynolds number	Type of experiment	Device	Magnetic field effect on heat transfer	Source
Electromagnet	Fe_3O_4	Water	670–1700	Experimental setup	Tube	Heat transfer deterioration	[99]
Electromagnet	Fe_3O_4	Water	465–1660	Experimental setup	Tube	Heat transfer deterioration	[100]
Electromagnet	Fe_3O_4	Water	50–400	Experimental setup	Tube	Heat transfer deterioration	[93]
Magnet (not specified)	Fe_3O_4	Water	80–1350	Experimental setup	Tube	Heat transfer deterioration	[101]
Electromagnet	Fe_3O_4	Water	1400–5000	Experimental setup and numerical	Tube	Both positive and negative effects possible along the tube	[92]
NdFeB	Fe_3O_4	Water	1400–5000	Experimental setup	Tube	Average heat transfer coefficient increased up to 1.55 times	[96]
NdFeB	Fe_3O_4	Water	2900–9820	Experimental setup	Tube	Nusselt number enhancement up to 46%	[97]

Asfer et al. [76] evaluated the heat transfer performance of a ferronanofluid under laminar flow conditions ($Re = 120\text{--}480$), subjected to a perpendicular magnetic field generated by permanent magnets. Their findings indicated that heat transfer can both increase and decrease depending on the ratio of magnetic to inertia forces and the interaction mechanism between magnetic fields and ferronanofluid. The study provided insights on ferronanoparticle chain formation and wall aggregation as potential mechanisms for heat transfer enhancement (Figs. 3.3, and 3.4).

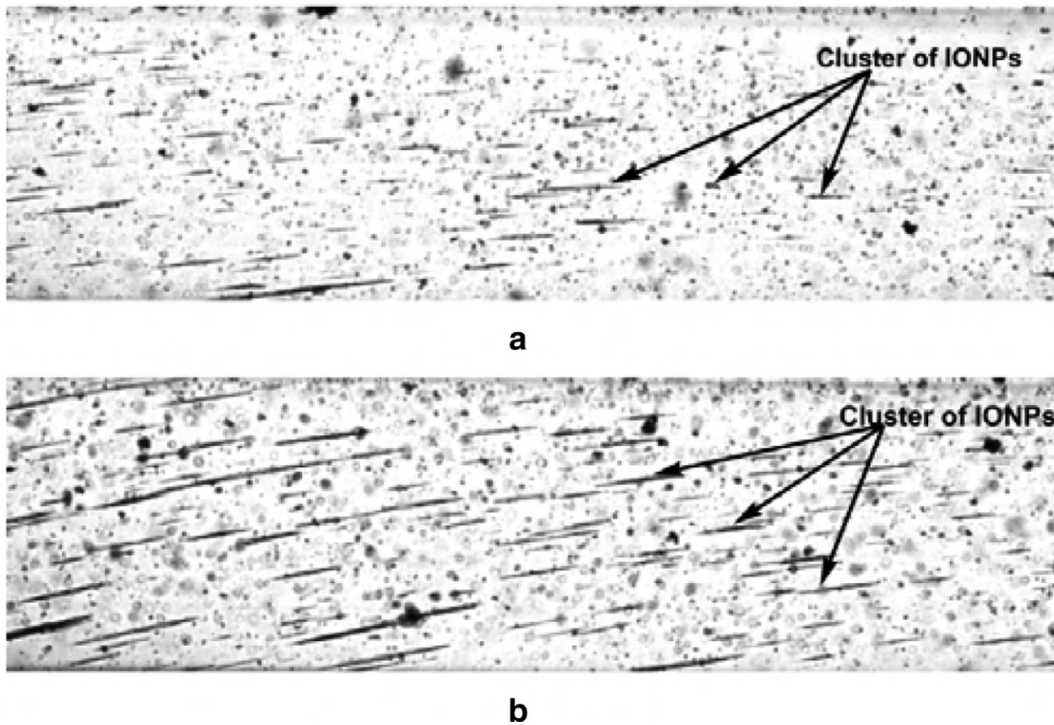


FIGURE 3.3: Chain clusters of iron oxide nanoparticles (IONPs) under the influence of a magnetic field. Image a) for $B = 0.1$ T, b) for $B = 0.2$ T [103].

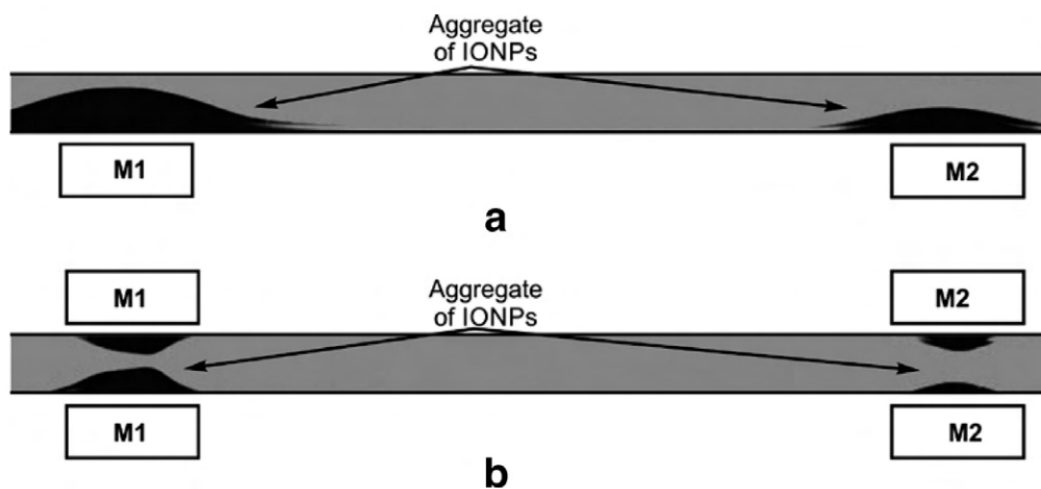


FIGURE 3.4: Wall aggregation of nanoparticles under the influence of a magnetic field. M1 and M2 represents magnets location [103].

Shi et al. [78] explored the heat transfer performance of MCNT (a nanocomposite containing carbon nanotubes and Fe_3O_4 nanoparticles) nanofluid, across Reynolds number ranging from 60 to 540. The authors examined the influence of a magnetic field generated by rotatable electromagnets, with magnetic field densities spanning from 0 to 800 G. Their findings revealed that with a controllable magnetic field, modulated by intensity and distribution, local heat transfer can be increased up to 30%.

Wang et al. [79] conducted experimental investigations on the performance of Fe_3O_4 ferronanofluid under a magnetic field generated by static ring magnets within laminar flow conditions, with Reynolds number ranging from 391 to 805. Their study revealed that each investigated magnet configuration resulted in enhanced heat transfer, dependent on Reynolds number. Proper adjustment of magnet positioning can lead to over a 3.5-fold improvement in the averaged Nusselt number along the test section for $Re = 805$.

Dahmani et al. [80] performed numerical simulations on the heat transfer performance of Fe_3O_4 ferronanofluid in laminar flow across Reynolds numbers of 100, 500, and 1000, under a nonuniform magnetic field generated by an electric current through a wire ($Mn = 0-1.13 \cdot 10^5$). It was noted that as the ratio of inertia forces increased, the impact of the magnetic field became negligible. The maximal enhancement in Nusselt number of 8% was achieved for $Re = 100$, attributed to the fluid flow pattern fluctuations.

Yarahmadi et al. [93] investigated the impact of a static, perpendicular-to-flow, coil-generated magnetic field, on the heat transfer performance of Fe_3O_4 ferronanofluid under laminar flow conditions with Reynolds numbers ranging from 465 to 1660. Their findings indicated that a constant magnetic field led solely to deterioration of heat transfer across the entire range of Reynolds number investigated, with the effect diminishing as inertia force contribution increased.

Shahsavari et al. [81] conducted experiments to assess the heat transfer characteristics in laminar flow ($Re = 548 - 2190$) of hybrid nanofluid incorporating Fe_3O_4 ferronanoparticles under the influence of a constant magnetic field (ranging from 0 to 700 G) generated by electromagnets. Their findings revealed that heat transfer enhancement increased with nanoparticle concentration and magnetic field strength. However, an increase in inertia force contribution resulted in a decrease in the magnetic field's effect on heat transfer. These results contradicted those obtained by Shahsavari [81], despite using the same test rig and magnetic configurations. Shahsavari et al. attributed heat transfer deterioration to the higher concentration of nanoparticles in the study by Yarahmadi et al.

Zonouzi et al. [82] examined the influence of quadrupole magnetic fields generated by permanent magnets on the heat transfer performance of Fe_3O_4 ferronanofluid in vertical laminar flow ($Re = 580, 710, 820$). The authors reported a heat transfer enhancement dependent on the magnets' location, which decreased with increasing Reynolds number.

Rudl et al. [83] investigated the effect of static magnets on the heat transfer performance of Fe_3O_4 ferronanofluid in laminar flow with mixed convection ($Re = 126, 236, 1224$). Their findings indicated that the orientation of magnets affected heat transfer. Magnet placement above the tube resulted in heat transfer deterioration, while under the tube led to enhancement. The effect is attributed to the magnetic field effect on the mass transfer in mixed convection. The impact of the magnetic field diminished as the Reynolds number increased.

Gürdal et al. [89] experimentally and numerically studied the heat transfer performance of Fe_3O_4 and hybrid ferronanofluids in laminar flow ($Re = 1131\text{--}2102$) through a dimpled tube under a magnetic field (ranging from 0 to 0.3 T) generated by coils. It was found that the highest magnetic field strength had a positive impact on the Nusselt number of 16.2% for Fe_3O_4 ferronanofluid and 15.9% for hybrid ferronanofluid flowing in a smooth tube, with the Nusselt number exhibiting an almost linear increase with Reynolds number. The authors attribute the increase in the Nusselt number to the increased vorticity and velocity of ferronanofluid flow when a magnetic field is applied.

Sun et al. [84] investigated the heat transfer and flow characteristics of Fe_3O_4 ferronanofluid in laminar flow ($Re = 480\text{--}2,000$) under the influence of a magnetic field generated by permanent magnets in various configurations. For an uniform magnetic field, the maximum local Nusselt number enhancement was observed for the highest magnetic field density and ferronanoparticle concentration and the lowest Reynolds number investigated. The authors attributed this enhancement to the formation of chain structures of ferronanoparticles. In the case of a nonuniform magnetic field, the maximum local Nusselt number was noted at $Re = 1080$. In this case, the cause is seen in the accumulation of ferronanoparticles at the tube wall causing thermal boundary layer reduction due to the higher fluid velocity in this zone. Additionally, the authors investigated a configuration of magnets acting against each other and alternately arranged side by side with reverse polarity. They found that the former provided the highest heat transfer enhancement due to the high magnetic field gradient and ferronanoparticle agglomeration at the tube wall.

Dinarvand et al. [85] investigated the heat transfer performance of CoFe_2O_4 and Fe_3O_4 ferronanofluids in laminar flow ($Re = 200\text{--}1000$) under the influence of a uniform magnetic field generated by permanent magnets facing each other (0, 400, 600 G). The results indicate that the magnetic field impact on heat transfer is positive for both fluids and increases with increasing magnetic field intensity. The authors noted that the effect gradually decreased as the fluid speed increased, with the highest change in Nusselt number occurring at $Re = 400$.

Mohammadfam and Zeinali Heris [86] investigated the heat transfer performance of Fe_3O_4 , MWCNT- Fe_3O_4 (doped), and $\text{Fe}_3\text{O}_4\text{@MWCNT}$ (hybrid) ferronanofluids in laminar flow ($Re = 800, 2200$) under a magnetic field ($B = 0, 200, 400$ G) generated by permanent magnets arranged in pairs along the tube on both sides. It was

found that the magnetic field enhanced heat transfer for every of examined ferro-nanofluid, with the enhancement increasing with nanoparticle concentration, except for MWCNT-Fe₃O₄, where 0.1 wt.% concentration provided the highest performance.

Shyam et al. [87] Investigated heat transfer performance of ferrofluid containing iron nanoparticles in laminar flow ($Re = 66$) under the influence of magnetic field generated by electromagnets ($B = 0, 700, 1000$ G). It was found that the heat transfer enhancement increases with increasing magnetic field density and for 1000 G reaches 23% compared to the case of magnetic field absence. Based on thermograms, the authors see the effect as a cause of nanoparticle accumulation on the wall and generation of secondary flows that allow to influence the thermal boundary layer. Additionally, bright field imaging showed the presence of chain structures at the deposit edges.

Goharkhah et al. [88] investigated the impact of a constant magnetic field generated by four electromagnets in a staggered configuration ($B = 0, 300, 500$ G) on a heat transfer of a Fe₃O₄ ferro-nanofluid in a laminar flow ($Re = 400-1200$). The authors indicated that the magnetic field enhances heat transfer and its contribution is rising with the increase of a magnetic field density. The cause is seen in the accumulation of ferro-nanoparticles at the wall, providing an increase in local thermal conductivity.

Lajvardi et al. [98] explored the heat transfer characteristics of Fe₃O₄ ferro-nanofluid laminar flow under the influence of a perpendicular magnetic field generated by coils ($B = 0-1200$ G). The authors observed that dispersed Fe₃O₄ nanoparticles failed to enhance heat transfer in comparison to water. However, the presence of a magnetic field led to an enhancement in convective heat transfer. This effect was attributed to the altered thermophysical properties of the ferro-nanofluid under the magnetic field's influence.

Sha et al. [99] conducted an investigation of Fe₃O₄ water-based ferro-nanofluid laminar flow under a constant magnetic field generated by coils. Their study covered the Reynolds number range 1200–2100 and magnetic field density range of 0–300 G. Results indicated a deterioration in ferro-nanofluid performance increasing with magnetic field strength, with optimal heat transfer parameters for no magnetic field condition.

Dibaei and Kargarsharifabad [100] studied the laminar flow of Fe₃O₄ ferro-nanofluid at Reynolds number ranging from 670 to 1700 under the influence of a constant magnetic field generated by U-shaped coils. Their research demonstrated that a magnetic field oriented perpendicular to the direction of flow hindered heat transfer compared to cases without magnetic field presence. This effect intensified with higher ferro-nanoparticle concentration and diminished with increasing inertia force contribution.

Hatami et al. [101] investigated heat transfer in Fe₃O₄-based ferro-nanofluid laminar flow under a magnetic field generated by a static magnet. It was found that the magnetic field can only lead to a decrease in heat transfer, which increased with the ratio of electromagnetic to viscous forces in the flow. The deterioration increased with increasing inertia force contribution.

3.1.2 Flow under an alternating magnetic field

This section presents the state of the art regarding laminar ferronanofluid flow in the presence of an alternating magnetic field. Tab. 3.2 presents the summary of the provided literature review. The following paragraphs contain extracted information from provided studies, focusing on the force balance acting on the flow, the effect of the wave shape and its frequency, and the mechanism responsible for changing the heat transfer parameters.

Dibaei and Kargarsharifabad [100], in the already mentioned study on the constant magnetic field, investigated the effect of an alternating magnetic field. In this case, an improvement in heat transfer parameters was observed, which was most pronounced for the lowest Reynolds numbers and the highest concentration of nanoparticles. The frequency of the magnetic field had a little effect on the heat transfer parameters.

Gürdal et al. [90] in another study investigated the effect of an alternating magnetic field generated by coils (frequency = 5 Hz, sinusoidal, triangular, and square waves, $B = 0.16$ T) on the heat transfer performance of Fe_3O_4 ferronanofluid laminar flow ($Re = 1131$ – 2102) in smooth and dimpled tubes. The results showed that the average Nusselt number can be increased by 46.5% for square wave and dimpled tube configurations compared to the case without magnetic field presence. Similarly, for a smooth tube employing ferrofluid, this increase was 44.0%. Moreover, heat transfer enhancement was increasing with Reynolds number.

Tekir et al. [91] explored the effect of an alternating magnetic field (sinusoidal, square, and triangular wave types, 0.3 T) on the heat transfer of Fe_3O_4 -Cu and Fe_3O_4 ferronanofluids in a laminar tube flow ($Re = 1100$ – 2300). It was found that the highest impact on heat transfer occurred at high concentrations of nanoparticles and low Reynolds number. It was observed that the effect was dependent on the wave frequency, with square and triangular wave types achieving maximum enhancement at $f = 15$ Hz, while sinusoidal waves achieved it at $f = 5$ Hz. The authors attributed the heat transfer enhancement to the periodic movement of nanoparticles reducing the thermal boundary layer.

Yarahmadi et al. [93] in the study involving a static magnetic field also explored the effect of an oscillating magnetic field ($f = 10, 20, 50$ Hz). Conversely to the constant magnetic field, the alternating field had a positive effect on heat transfer. The authors provide the details about the optimal configuration of the magnets and indicate that the maximum heat transfer enhancement by 19.8% was achieved for the lowest Re number investigated and highest frequency of a magnetic field. The cause of this effect is seen in the disruption of the thermal boundary layer.

TABLE 3.2: Summary of studies on alternating magnetic field effect on heat transfer in ferronanofluids

Magnetic field source	Ferromagnetic particles	Basefluid	Reynolds number	Type of experiment	Device	Magnetic field effect on heat transfer	Source
Electromagnet	Fe ₃ O ₄	Water	670–1700	Experimental setup	Tube	Heat transfer enhancement	[100]
Electromagnet	Fe ₃ O ₄	Water	1131–2102	Experimental setup	Tube	Heat transfer enhancement up to 46.45%	[90]
Electromagnet	Fe ₃ O ₄ -Cu	Water	1100–2300	Experimental setup	Tube	Heat transfer enhancement up to 15.3%	[91]
Electromagnet	Not disclosed	Water	66	Experimental setup and numerical	Tube	Heat transfer enhancement up to 39%	[87]
Electromagnet	Fe ₃ O ₄ , Fe ₃ O ₄ /CNT	Water	548–2190	Experimental setup	Tube	Heat transfer enhancement up to 7.4%	[81]
Electromagnet	Fe ₃ O ₄	Water	400–1200	Experimental setup	Tube	Heat transfer enhancement up to 31.4%	[88]
Electromagnet	Fe ₃ O ₄	Water	80–1350	Experimental setup	Tube	Average heat transfer enhancement up to 27.6%	[92]
Electromagnet	Fe ₃ O ₄	Water	465–1660	Experimental setup	Tube	Local convective heat transfer coefficient increased up to 19.8%	[93]

Magnetic field source	Ferromagnetic particles	Basefluid	Reynolds number	Type of experiment	Device	Magnetic field effect on heat transfer	Source
Electromagnet	Fe_3O_4	Water	1176–1634	Experimental setup and numerical	Tube	Local convective heat transfer coefficient increase	[102]
Electromagnet	Fe_3O_4	Water	8000–13000	Experimental setup	Tube	Nusselt number enhancement	[94]
Electromagnet	Fe_3O_4	Water	944–8413	Experimental setup	Tube	Convective heat transfer coefficient increase	[95]

Shyam et al. [87] in the same article exploring the effects of constant magnetic field, investigated the effect of alternating magnetic field ($f = 0.1$ Hz, 1 Hz, 5 Hz). It was found that the highest heat transfer enhancement of 39% was achieved for the lowest magnetic field frequency. For the $f = 5$ Hz, Nusselt number approached those obtained for a constant magnetic field. The phenomena behind the heat transfer enhancement were the same as for a constant magnetic field, nanoparticle accumulation on the wall caused the secondary flows that disturbed the thermal boundary layer. The authors attributed the mutual relationship of magnetic perturbation time scale and advective time scale as the reason for achieving the highest improvement in heat transfer for the lowest frequency of magnetic field. With near values, the accumulated particles can break away from the wall after the magnetic field is turned off. Therefore, as the frequency increases, this process is hindered, and the heat transfer efficiency approaches the parameters obtained for a constant magnetic field.

Shahsavari et al. [81] in their study on the effect of a constant magnetic field also investigated the effect of an alternating magnetic field ($f = 10, 20, 50$ Hz) on the ferronanofluid flow. The effect of using an alternating magnetic field for $Re = 548$ was also positive, but lower than that of a constant magnetic field for both ferronanofluids used. Increased frequency led to a decrease of this impact.

Goharkhah et al. [88] in the same study on a constant magnetic field examined the effect of an alternating magnetic field with a frequency of 5 Hz on the heat transfer. The results indicate that the periodically alternating magnetic field can further increase the heat transfer parameters. Besides the accumulation of nanoparticles at the wall, the authors attributed the cause of increased heat transfer to the periodic release of nanoparticles from this region causing disturbances in the thermal boundary layer.

Ghofrani et al. [92] conducted an experimental investigation on the influence of an alternating magnetic field ($B = 0.02$ T, $f = 5, 50$ Hz) on the heat transfer characteristics of Fe_3O_4 laminar flow ($Re = 80-1350$). The study revealed that a constant magnetic field led to either a deterioration or a slight enhancement of heat transfer when compared to the flow in the absence of a magnetic field. The increased pressure drop was identified as a potential reason for this observation. Conversely, for an alternating magnetic field, the increase in average heat transfer reached up to 27.6% for the lowest Reynolds number of 80 and a frequency of 50 Hz. The impact of a magnetic field on heat transfer initially decreased at a Reynolds number of 260, but then increased as the Reynolds number further increased. Additionally, it was demonstrated that higher frequencies of a magnetic field resulted in a greater enhancement. This difference diminished as the contribution of inertia forces increased.

Dibaei et al. [102] conducted a numerical and experimental investigation on the influence of an alternating magnetic field, produced by electromagnets ($B = 0.07$ T, $f = 10, 20, 50$ Hz), on the laminar flow of Fe_3O_4 ferronanofluid ($Re = 1176, 1634$). The study revealed that the heat transfer coefficient exhibited an increase with the frequency of the magnetic field. The enhanced heat transfer performance was

attributed to the accumulation of nanoparticles at the tube wall and the disturbance of the thermal boundary layer. The authors observed that heat transfer increased with the Reynolds number and attributed it to a strengthened Brownian motion.

3.2 Turbulent flow with ferronanofluids

The number of studies on the ferronanofluid turbulent flow is much smaller than for laminar flow. This makes determining the impact of the magnetic field on heat transfer even more complicated. The article [95] on the effect of an alternating magnetic field on the turbulent flow of ferronanofluid appeared relatively recently. One article [99] indicates a negative effect of the magnetic field on heat transfer, while the others confirm the possibility of improvement [94–97]. Due to ambiguous results and the limited number of papers, drawing clear conclusions is difficult. The summary of provided studies is presented in the Tabs. 3.1 and 3.2.

Guzei et al. [96] conducted a study on the effect of magnetic field generated by a permanent magnet on Fe_3O_4 ferronanofluid turbulent flow. The results indicate that the employed magnetic field improved the average heat transfer coefficient for every flow rate investigated. The study provides an insight into nanoparticle behavior. It was shown that the magnetic field can cause ferronanoparticle aggregation at the tube wall in the turbulent flow.

Karamallah et al. [97] examined the impact of constant magnetic field generated by multiple permanent magnets on the Fe_3O_4 ferrofluid turbulent flow ($Re = 2900$ – 9820). It was found that heat transfer enhancement is correlated with the increase of nanoparticle concentration and magnetic flux density.

Siricharoenpanitch et al. [94] investigated the effect of magnetic field ($0.3 \mu\text{T}$) generated by coils and pulsations on Fe_3O_4 ferronanofluid turbulent flow ($Re = 8000$ – 13000). Perpendicularly oriented magnetic field allowed the increase of Nusselt number by 14.4% and 19.0% for pulsating flow in corrugated tube for 20 Hz and 30 Hz frequencies respectively. The authors see the cause of the enhancement in ferronanoparticle migration and aggregation at the wall.

X. Zhang and Y. Zhang [95] investigated the heat transfer performance of Fe_3O_4 ferronanofluid turbulent flow ($Re = 944$ – 8413) under an alternating magnetic field generated by coils (0–90 mT, 0–100 Hz). It was found that the convective heat transfer coefficient is enhanced by employing a magnetic field and the effect is increasing with the frequency of a magnetic field. Above a concentration of 3 vol% the effect of magnetic field frequency was negligible. The increase of inertia forces in the flow caused a reduction of the magnetic field effect. The authors see the cause of enhancement in the reduction of the thermal boundary layer by the nanoparticle migration.

Sha et al. [99] in the same study investigating laminar flow mentioned in the previous section analyzed Fe_3O_4 ferronanofluid performance in a turbulent flow ($Re = 3400$ – 7500). The results were analogous to the ones obtained for laminar flow.

Convective heat transfer coefficient was reduced by employing a magnetic field by around 3% for magnetic field strength = 100 G, and 5% for 200 G.

3.3 Mixed convection in nanofluids

The flow through a heated tube causes an increase of fluid temperature near the wall. This leads to changes in the thermophysical properties of the medium, especially its density. The fact is particularly relevant in laminar flows, where there is no mass exchange between adjacent layers of the flowing fluid. Thus, heat transfer in the fluid takes place by conduction, which, in the case of hydrodynamically developed (fluid velocity profile is developed) and constant heat flux boundary condition, means that the Nusselt number tends to reach the value of 4.364. In this flow scenario, the increasing temperature difference between the fluid near the heated wall and the core of the flow causes an increase in buoyancy forces. When these forces reach a critical value, a process of fluid circulation is initiated, allowing the low-temperature mass to be transferred near the wall. This process is called mixed convection and consists of two components: forced convection and free convection. Mixed convection is identified by an increase of the Nusselt number above the expected value for the pure forced convection. This process weakens as the fluid temperature equalizes and buoyancy forces diminish, eventually returning to forced convection parameters. This phenomenon repeats in a cyclic manner.

In 1964 flow regime maps were presented by Metais and Eckert [104] (Figs. 3.5, 3.6), providing a basis for determining whether mixed convection should be considered in the chosen flow parameters. An updated version of the maps was presented by Ghajar and Tam [105] (Fig. 3.7) based on their earlier flow study under uniform wall heat flux boundary condition [106] ($Re = 280-4.9 \cdot 10^4$, $Pr = 4-158$, $Gr = 1000-2.5 \cdot 10^5$). The paper presents an equation defining the critical parameters separating mixed convection from forced convection. The authors indicated that for low Reynolds numbers for each of the investigated inlet configurations, free convection occurred at $20 < x/d_{in} < 70$ (x is the distance from the inlet to the test section, d_{in} is the inside diameter of the tube).

Rudl et al. [83] investigated the effect of a magnetic field on heat transfer in Fe_3O_4 ferronanofluid laminar flow. In the analyzed case, the focus was put on the mixed convection occurring due to an increase in buoyancy forces and the effect of ferronanoparticles interaction with a magnetic field. It was shown that secondary motions arising due to the density gradient are responsible for increased heat transfer, deviating from the solution for pure forced convection in laminar flow. The location of the studied flow (horizontal flow, $Re = 126.4$, $Gr = 603$, $GrPr = 8100$) on the flow regime maps available in the literature is inconsistent with them, as these deny the possibility of mixed convection. The study showed that heat transfer in mixed convection of ferronanofluid is controllable by a magnetic field. A magnet placed above the test tube acted on the ferronanoparticles in the direction opposite to the flow

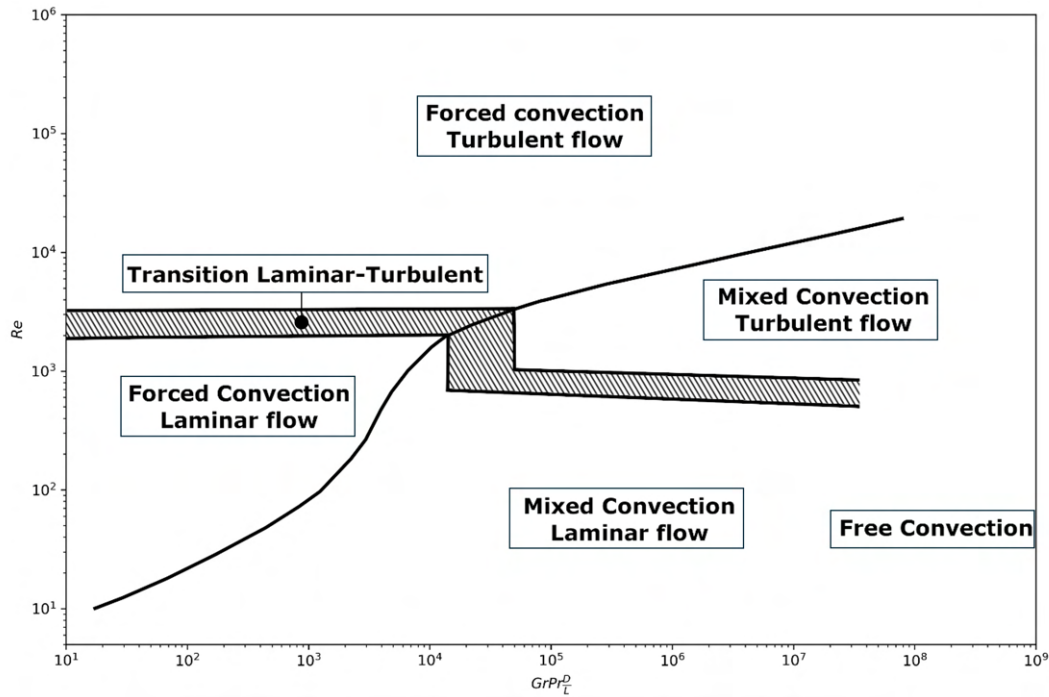


FIGURE 3.5: Flow regime map for horizontal tube flow. Based on [104].

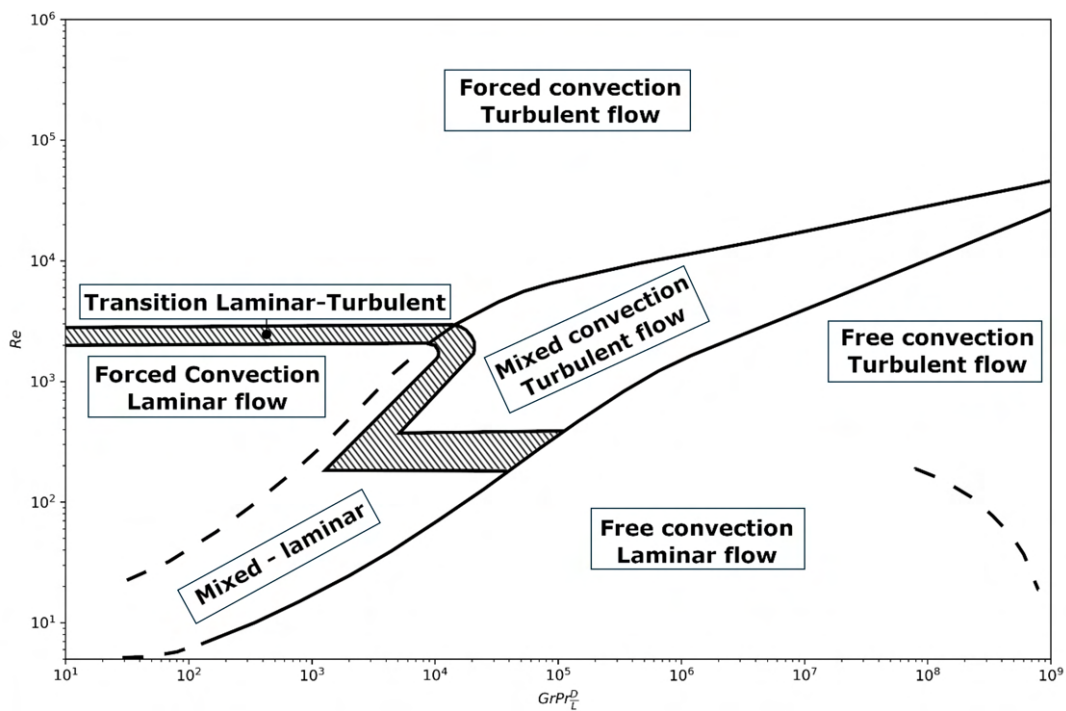


FIGURE 3.6: Flow regime map for vertical tube flow. Based on [104].

resulting from free convection, and due to viscous coupling with the surrounding fluid, it led to its weakening and reduced heat transfer. A magnet placed under the test section improved heat transfer as an effect of free convection mass transfer enhancement.

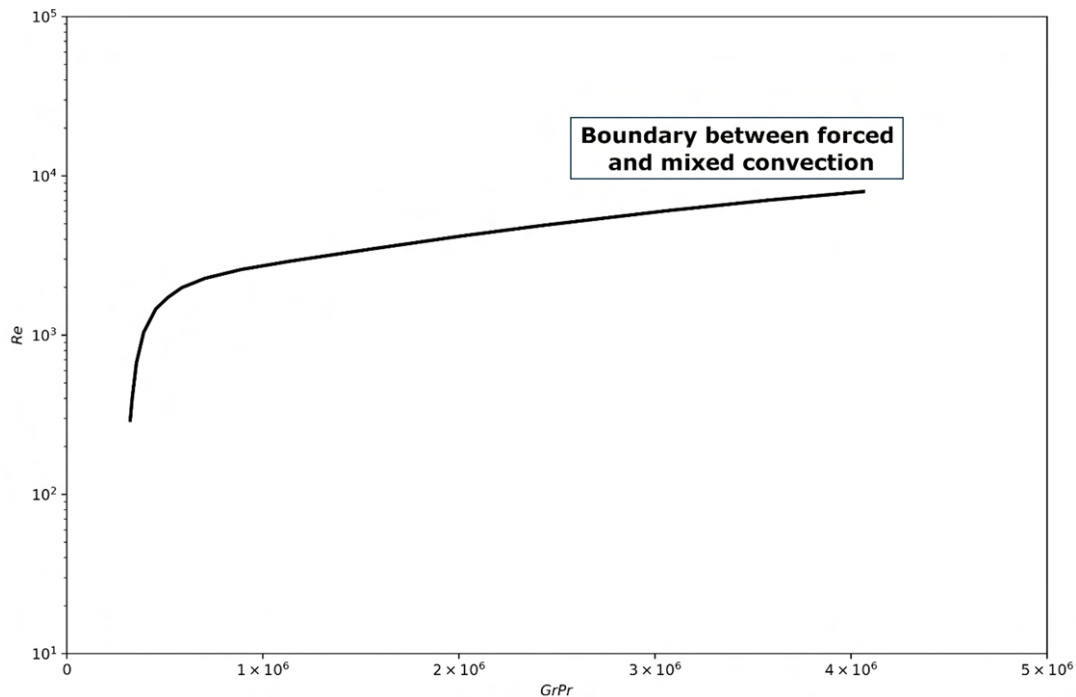


FIGURE 3.7: Flow regime map with boundary between forced and mixed convection for horizontal tube flow. Based on [105].

Colla et al. [107] investigated heat transfer of TiO_2 water-based nanofluid under laminar and mixed flow conditions. The results for pure laminar flow align with the analytical solution. As buoyancy forces emerge, heat transfer increases due to secondary motions. In the case of nanofluid, the point of departure from the analytical solution occurs later in the flow compared to water, and the heat transfer impact of mixed convection is significantly weaker. This effect is attributed to Brownian motion and thermophoresis, which lead to local fluid temperature equalization. The authors conclude that under mixed convection conditions, single-phase models are inadequate for describing these processes when nanofluids are employed.

Utomo et al. [108] conducted an experimental and theoretical investigation of heat transfer in water-based alumina and titania nanofluids under laminar flow conditions ($Re = 300$ – 1070). The authors demonstrated the possibility of mixed convection processes for both nanofluids, as evidenced by the deviation of the Nusselt number distribution along the test section from the theoretical solution for laminar flow. The study used numerical simulations to show that fluid mixing occurs due to the increasing influence of buoyancy forces. In contrast to the findings of [107], these results aligned with data obtained for water, indicating that for the investigated nanofluids, a single-phase model can be applied to determine heat transfer parameters in mixed convection.

The literature review reveals a paucity of studies addressing heat transfer in non-horizontal configurations, particularly at low Reynolds numbers, where the impact of gravity cannot be ignored due to buoyancy effects. This is also true for nanofluids. In 1958, Hallman [109] investigated forced and free laminar convection in a vertical tube.

His findings indicated that free convection enhances heat transfer in upward vertical flows and causes deterioration in downward vertical flows compared to the results derived from the analytical solution for pure forced convection, where $Nu = 4.36$.

Two comprehensive review articles by Jackson et al. [110] and Galanis and Behzadmehr [111] synthesized findings on mixed convection in vertical tubes. The main conclusion is that in laminar flow with mixed convection, heat transfer is enhanced in upward flow and diminished in downward flow. The enhancement is attributed to an increase in fluid velocity near the tube wall, induced by buoyancy forces. To maintain continuity, cooler fluid from the flow core is entrained in the opposite direction, resulting in its deceleration. Furthermore, as illustrated by Scheele and Hanratty [112] (Fig. 3.8), small disturbances may occur in upward vertical flow. Unlike in downward flow, these disturbances may remain unmeasurable due to their small amplitude.

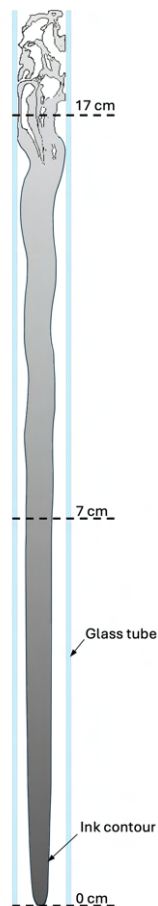


FIGURE 3.8: Dye flow pattern in upward thermodynamically developing vertical flow. Made based on [112].

Barozzi et al. [113] investigated laminar water flow through a circular duct, revealing that an increase in inclination ($0-60^\circ$, $Re = 500$) led to a reduction in the Nusselt number. The authors examined the influence of the Reynolds number on the Nusselt number in inclined flow. They found out that the reduction in Nu diminishes

as the Reynolds number increases. At $Re = 1500$, its inclination impact becomes negligible.

Everts et al. [114] conducted experimental and numerical investigations on heat transfer in upward and downward vertical flows of water within the Reynolds number range of 180 to 2300. The authors observed that in upward flow, for Reynolds numbers below 250, buoyancy forces significantly contribute to convection. This results in an increase in fluid velocity near the wall, enhancing heat transfer compared to the solution for pure forced convection. The determination of streamlines for the lowest Reynolds number investigated was not possible due to the influence of free convection effects. Consequently, mass transfer under such conditions remains inadequately explored.

Akbari et al. [115] performed numerical investigations using Al_2O_3 nanofluid in both horizontal and inclined flows. The study showed that increasing the inclination reduces the radially directed buoyancy force while increasing its axial component, thereby diminishing secondary motion. Consequently, fluid velocity near the wall increases. The authors noted that this balance adjustment resulted in the highest heat transfer coefficient at a 45° inclination.

Mirmasoumi and Behzadmehr [116] conducted a numerical analysis of the impact of nanoparticle diameter on laminar mixed convection at various inclinations. Their findings revealed that increasing the Grashof number intensifies secondary flow, but the effect is mitigated by the inclination angle. Consistent with the findings of Akbari et al. [115], the highest heat transfer coefficient was observed at a 45° inclination angle.

Ben Mansour et al. [117] conducted a numerical investigation of Al_2O_3 nanofluid heat transfer at selected tube inclinations and found that natural convection is the dominant contributor to heat transfer in the horizontal configuration. The study showed that increasing the inclination angle reduces the Nusselt number, with up to a 30% reduction in vertical flow. Furthermore, it was demonstrated that nanoparticle concentration does not affect heat transfer in vertical flow. In a subsequent experimental study, Ben Mansour et al. [118] explored heat transfer in horizontal and vertical tubes using Al_2O_3 nanofluid. Their findings confirmed a decrease in the Nusselt number with increasing flow inclination across the entire investigated Reynolds number range and supported the numerical observation that nanoparticle concentration has no impact on vertical flow heat transfer.

The studies reviewed present inconclusive evidence regarding the effect of inclination on heat transfer parameters. Numerical investigations by Akbari et al. [115] and Mirmasoumi and Behzadmehr [116] suggest that a 45° inclination yields the highest heat transfer. In contrast, findings by Ben Mansour et al. [117, 118] indicate that heat transfer decreases with increasing inclination, reaching its minimum in the vertical position. Experimental results by Barozzi et al. [113] align with these conclusions. However, in each spatial configuration, free convection driven by the temperature gradient in the fluid must be considered. Vertical upward flow is associated with

increased fluid velocity near the wall, which may lead to flow disturbances. In other configurations, the balance between increased fluid velocity and fluid mixing depends on the inclination angle.

3.4 Literature review summary

Based on the above literature review, the following summary is drawn:

- A magnetic field can influence the mass transfer process of ferronanoparticles in both laminar and turbulent flows, resulting in changes of heat transfer. Determining its effect requires consideration of the magnetic field distribution within the flow, as this governs ferronanoparticle transfer and directly impacts heat transfer.
- In laminar flows of ferronanofluids, nanoparticle chain formation, wall aggregation and secondary motion are mentioned as the main potential mechanisms that can cause a positive effect on heat transfer. **It is essential to describe all forces acting on ferronanofluid flow under the influence of a magnetic field to systematize the available experimental data.**
- The effect of the inertia, represented by the Reynolds number, on heat transfer in ferronanofluid flow under the influence of a magnetic field is ambiguous. **Further studies are required to evaluate the effect of the ratio of magnetic forces to inertial forces on heat transfer parameters.**
- The use of an alternating magnetic field to enhance heat transfer parameters in ferronanofluid flow is feasible. The primary mechanism attributed to this effect is the periodic release of ferronanoparticles from the magnetic field's influence, disrupting the thermal boundary layer. However, there is no consensus on the optimal shape of the magnetic field waveform or the effect of frequency on heat transfer parameters.
- Heat transfer in turbulent ferronanofluid flows remains underexplored. Contradictory findings exist regarding the effect of applying a magnetic field. The migration of ferronanoparticles and wall aggregation are claimed as the reason for the increase in heat transfer parameters.
- Thermally developing laminar flow may involve mixed convection driven by temperature gradients in the fluid. Existing flow regime maps in the literature are insufficient to determine the dominant flow type for ferronanofluids. **Additional experimental data are needed, particularly for low Reynolds and Grashof numbers.**
- The current understanding of inclined nanofluid flow is limited. An analysis of the heat transfer process in thermally developing laminar flow taking gravity

into account should be carried out. There is no clear consensus on how flow inclination affects heat transfer parameters. **Further experimental studies are necessary to assess the effect of ferronanofluid flow inclination and the interaction of ferronanoparticles with a magnetic field.**

The laminar hydrodynamically developed and thermally developing flow of ferronanofluid under the influence of an external magnetic field is complex due to the number of parameters affecting the process. The presence of ferronanoparticles not only changes thermophysical parameters of the fluid, but also introduces additional phenomena due to their scale. In addition, their interaction with the magnetic field triggers additional mechanisms that influence mass transfer and, consequently, heat transfer.

Due to heating of the medium in laminar flow, the temperature gradient in the fluid will impose buoyancy forces and may lead to the occurrence of mixed convection projected in heat transfer parameters. This process is gravity-dependent, and an inclined flow alters the relationship of the speed vector and gravity. The inclusion of magnetic influence on ferronanoparticles can change the transfer process in the state of mixed convection.

The literature review highlights a significant gap in understanding the interaction between magnetic fields and ferronanofluid flow, particularly in the context of mixed convection and non-horizontal flows. Therefore, it is crucial to systematize the interaction mechanisms between ferronanoparticles and magnetic fields. Conducting studies on laminar flows with mixed convection in various spatial configurations will advance the current state of research. The research presented in this dissertation aims to address these gaps.

Chapter 4

Dissertation theses and objectives of the work

4.1 Dissertation theses

Nanofluids enhance heat transfer due to their superior thermal properties compared to conventional working fluids. Increasing the average thermal conductivity of a fluid by incorporating solid particles has reached its practical limits, as further improvements are constrained by particle aggregation, increased viscosity, and stability issues. Ferronanofluids provide an additional advantage as they respond to external magnetic fields, enabling active control of both mass and heat transfer.

The force balance in magnetically influenced flows is complex and requires further investigation to fully understand the interactions among magnetic, inertial, buoyant, and viscous forces. Magnetic fields can be used to induce and control secondary flow structures in ferronanofluids, which is relevant for practical applications with varying spatial configurations. Changes in the relative orientation of gravity and flow direction directly affect mixed convection and mass transfer. A controlled magnetic field can influence mixed convection in these configurations, offering new possibilities for optimizing heat and mass transfer.

The intended research seeks to both qualitatively and quantitatively examine the interplay of forces influencing heat transfer in the flow of ferronanofluid. The hypotheses to be investigated are:

- Understanding the relationships between viscous, inertial, magnetic, and gravitational forces is crucial for assessing ferronanofluids' impact on convective heat transfer. These relationships can be described by appropriate similarity numbers that express the ratio of forces that affect the flow of ferronanofluids.
- For any ferronanofluid, certain critical value of introduced similarity number reflects the potential to affect heat transfer.
- The mutual orientation of gravity and the flow direction of ferronanofluid in various spatial configurations influences the development of secondary motions, which can either enhance or reduce heat transfer.

- The external magnetic field intensifies or suppresses secondary motions in various spatial configurations, and thus allows to actively influence heat transfer.

Currently, there is insufficient data to confirm or refute these theses. Extensive experimentation is crucial to uncover the mechanisms governing transfer processes in ferronanofluids. Addressing this gap is the primary research objective of this proposed dissertation.

4.2 Objectives of the work

To verify the theses presented, the dissertation focuses on the following research tasks:

- Characterization of the thermophysical properties of the used ferronanofluid.
- Analysis of the magnetic field interaction with the ferronanofluid droplet and the effect of a magnetic field on the ferronanoparticle arrangement.
- Investigation of heat transfer in horizontal laminar ferronanofluid flow impacted by a magnetic field.
- Analysis of the gravity impact on heat transfer in mixed convection of ferronanofluid laminar flow, along with an investigation into the applicability of magnetic field for controlling heat transfer in inclined flows.

4.3 Structure of the dissertation

The dissertation consists of seven chapters:

- The first chapter presents the motivation for exploring the scientific topic.
- The second chapter provides an introduction to the topic of nanofluids, the most important thermophysical properties of nanofluids relevant to heat transfer, and the mechanisms contributing to improved heat transfer. The chapter also includes a literature review of nanofluid applications, including studies presenting obstacles preventing large-scale implementation.
- Chapter three focuses on a literature review concerning convective heat transfer in ferronanofluids. It summarizes studies on both laminar and turbulent flows under static and alternating magnetic fields. Additionally, the chapter reviews literature on mixed convection in horizontal and inclined flows using both conventional liquids and nanofluids. The chapter concludes with a summary highlighting existing knowledge gaps.
- Chapter four presents research theses and tasks set for the thesis.

- The fifth chapter presents data on the thermophysical properties of the ferronanofluid used in the study. This is followed by an investigation on the interaction of ferronanofluid droplet and a magnetic field and analysis of the magnetic field effect on the ferronanoparticle arrangement.
- Chapter six details experiments conducted in horizontal setup. The horizontal flow investigations aim to assess the impact of magnetic field strength generated by permanent magnets placed above and below the test tube within the mixed convection zone. Additionally, it includes an analysis of the forces acting on the flow and their influence on heat transfer.
- Chapter seven summarizes the flow studies on the inclined flow. The experiments examine the impact of flow inclination on heat transfer and explores the potential of using magnets to regulate it.
- The entire work is concluded in the final, eighth chapter.

Chapter 5

Characterization of selected ferronanofluid

5.1 Characterization of thermophysical properties

Determination of heat transfer performance requires the information on thermophysical properties of the used fluid. For standard working fluids, these data are readily available in the literature. For nanofluids, obtaining accurate data can be challenging, as it may be difficult to find a fluid with parameters matching the investigated one. In addition, nanofluids of the same type may come from different production batches, which also affects their thermophysical parameters due to manufacturer production tolerances.

The ferronanofluid investigated (MSG-W10) in heat transfer experiments was acquired from FerroTec (USA) (Fig. 5.1). It contains magnetite Fe_3O_4 nanoparticles dispersed in deionised water (concentration between 2.8 and 3.5 vol.% [119]). The suspension is stabilized with an organic chemical anionic polymer.

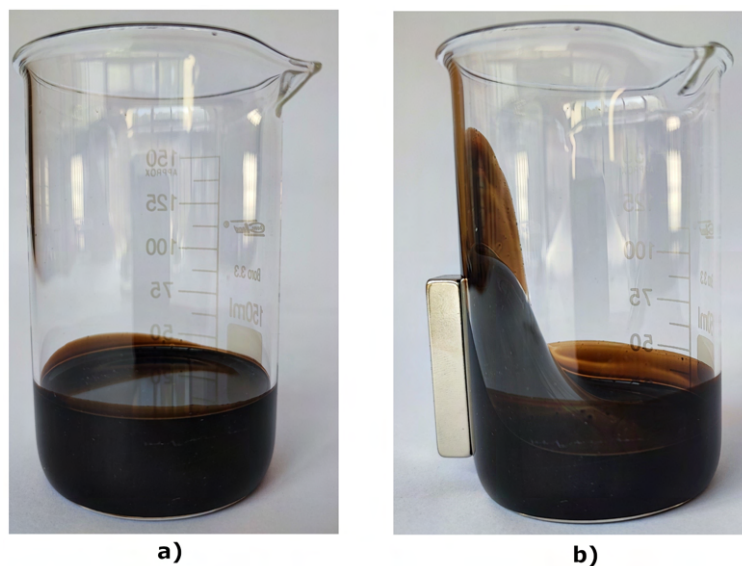


FIGURE 5.1: Photos of the MSG-W10 ferronanofluid. Image a) shows unaffected sample, image b) the influence of a magnetic field on the sample.

5.1.1 Viscosity

Viscosity quantifies a fluid's ability to transmit shear stress between adjacent layers during motion. This property plays a significant role in heat transfer processes. The viscosity of the working fluid influences linear resistance and thus the pressure drop in the flow. The parameter is crucial in determining the required pumping power. Nanofluids generally exhibit higher viscosity than their base fluids, an essential factor to consider in practical applications. The paper by Prasher et al. [120] presents an analysis of the laminar flow of nanofluids through a tube. The authors found that when relative viscosity increases fourfold compared to relative thermal conductivity, the benefits of improved heat transfer are negated.

According to the findings of the study [60], certain nanofluids demonstrate a shear rate-independent viscosity, categorizing them as Newtonian fluids, whereas others display a shear rate-dependent viscosity, categorizing them as non-Newtonian fluids.

Einstein presented a general relationship defining the viscosity of a fluid containing a dispersed solid phase [121]:

$$\mu_{nf} = \mu_{bf}(1 + 2.5\phi) \quad (5.1)$$

where μ_{bf} denotes the viscosity of the base fluid, and ϕ is the volume fraction of the dispersed particles in the fluid. This relationship is valid only for volume concentrations less than 1%. For accurate calculations of viscosity, it is essential to refer to available models and validate them with empirical studies. Parameters such as shape, size, concentration of nanoparticles, and temperature affect the viscosity value [60].

The basic viscosity measurement is performed using a capillary viscometer (Fig. 5.2), where viscosity is determined by the flow time of the fluid through capillary tubes. More advanced devices such as rheometers allowing to control shear rate are also commonly used.

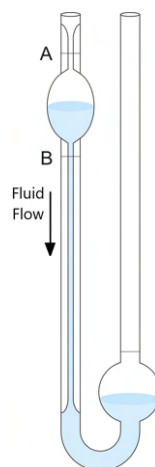


FIGURE 5.2: Schematic and the principle of operation of a capillary viscometer [122]. The liquid is drawn above mark A, and the time taken to pass from A to B is recorded for viscosity calculation.

The viscosity of the ferronano fluid used was measured using an MCR 301 rheometer (Anton Paar GmbH) in a temperature range of 15 to 60 °C under no external magnetic field influence. Temperature increments were established at 0.2 K min⁻¹ for the range of 15 to 40 °C and 0.5 K min⁻¹ for 40 to 60 °C, while maintaining a constant shear rate of 50 s⁻¹ (Fig. 5.3). These data were compared with the values for water [123], which is the base medium of the fluid under study. The results show that the test fluid values in the presented temperature range are 2.8 times for the lowest temperatures and 2.5 times higher for the highest temperatures. The black dashed line in Fig. 5.3 is a polynomial fit of the data used for the heat transfer calculations and is described by the equation:

$$\mu(T) = 0.0008T^2 - 0.105T + 4.62 \quad (5.2)$$

where T is a ferronano fluid temperature in °C.

It should also be noted that the values obtained here are 1.25 times higher for the lowest temperatures tested and 1.20 times higher for the highest temperatures than in the research presented in [83] for the same type of ferronano fluid produced by FerroTec. This leads to the conclusion that for commercial nanofluids the adequate choice is to measure thermophysical parameters rather than to rely on correlations available in the literature.

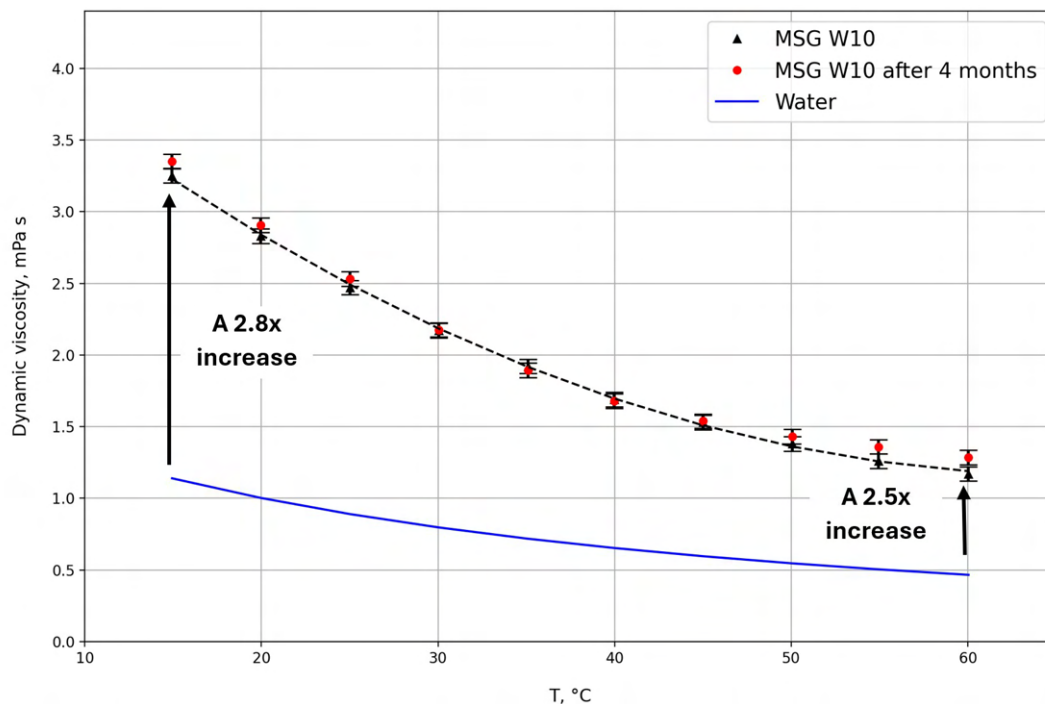


FIGURE 5.3: Dynamic viscosity of the investigated ferronano fluid (MSG-W10) and water [123] (blue line). Black triangles indicate initial values, and red dots indicate values after 4 months of ferronano fluid storage [15].

To assess the long-term stability of ferronanofluid, viscosity measurements were repeated after four months. The ferrofluid was stored in a bottle provided by the manufacturer at room temperature in a dark environment, with weekly agitation. The results, depicted in Fig. 5.3, show no significant alterations, confirming to sustained stability of the fluid over time.

5.1.2 Specific heat capacity

The parameter that defines the amount of heat required to increase the temperature of one kilogram of material by one kelvin is specific heat capacity. The value is determined using differential scanning calorimetry (DSC). This method involves measuring the difference in energy needed to raise the temperature of a test sample and a reference sample. The specific heat capacity is calculated using the following formula [124]:

$$Q = mC_p\beta \quad (5.3)$$

where Q denotes power measured by DSC, m sample mass, C_p is the specific heat capacity, and β is the heating rate. The procedure for determining specific heat capacity consists of three measurements:

- Measurement with an empty crucible, to exclude the heat flowing into it during the test.
- Measurement with a reference material, to obtain the necessary data for determining the specific heat capacity of the test material. An example of a reference material is sapphire, due to its well-known specific heat capacity as a function of temperature.
- Measurement with the test material, determining the amount of supplied heat.

Three measurement methods in differential scanning calorimetry are distinguished [124]:

- Dynamic method. The method consists of three stages. In the first stage the material is heated at a constant temperature for 10–15 minutes, in the second stage a heat flux is applied that increases the sample's temperature by 10–20 K min⁻¹. In the final stage the temperature is maintained for 10–15 minutes. The specific heat capacity of the test material is determined using the following equation:

$$C_{pm} = \frac{C_{pr}m_rQ_m}{m_mQ_r} \quad (5.4)$$

Where C_{pr} is the specific heat capacity of the reference material, m_r the mass of the reference material, Q_m the heat supplied to the material, m_m the mass of the test material, and Q_r the heat supplied to the reference material.

- Isothermal step method. The method involves gradually increasing the sample's temperature by 1–3 K. Each step is followed by an isothermal stage lasting 2–3

minutes. The specific heat capacity is calculated using the same equation as in the dynamic method.

- Area method. The method uses isothermal segments, where the sample is held at a constant temperature for a specific period before increasing the temperature stepwise by 1 K.. For each step the area under the power curve is determined. The following equations are used:

$$A_r = \frac{Q_r}{m_r} = C_{pr}\beta \quad (5.5)$$

$$A_m = \frac{Q_m}{m_m} = C_{pm}\beta \quad (5.6)$$

Where A_r and A_m are the areas under the power curve for the reference and test materials, respectively.

Specific heat capacity is calculated using the equation:

$$C_{pm} = \frac{C_{pr}A_m}{A_r} \quad (5.7)$$

The specific heat capacity of the ferronanofluid was measured using a differential scanning calorimeter (μ DSC VII, Setaram) in the range of 18 to 57°C. The results are shown in Fig. 5.4 together with the values for water, which is the base medium of the ferronanofluid. The black dashed line in Fig. 5.4 is a linear fit of the data used for the heat transfer calculations and is described by the equation:

$$C_p(T) = 0.00095T + 3.34 \quad (5.8)$$

where T is a ferronanofluid temperature in °C.

The data obtained are up to 2% smaller than the results reported for the same ferronanofluid in [83].

5.1.3 Thermal conductivity

Thermal conductivity quantifies the capability of a material to transfer heat. This heat transfer rate is represented by the thermal conductivity coefficient, k , which varies based on factors such as the state of matter, substance, density, and temperature.

The dispersion of particles in liquids is based on the idea that it can enhance the thermal conductivity of working fluids since solid materials have higher thermal conductivity than liquids. Adding milli- and micro-sized particles introduces additional complications in heat exchanger operation, like greater surface erosion and increased pumping power needs due to higher fluid viscosity. Nanofluids overcome these challenges by mitigating such issues. Additionally, heat transfer in nanofluids benefit from Brownian motion, interfacial layering and nanoparticle chain aggregation. The effect of nanoparticles on the fluid's overall thermal conductivity is influenced

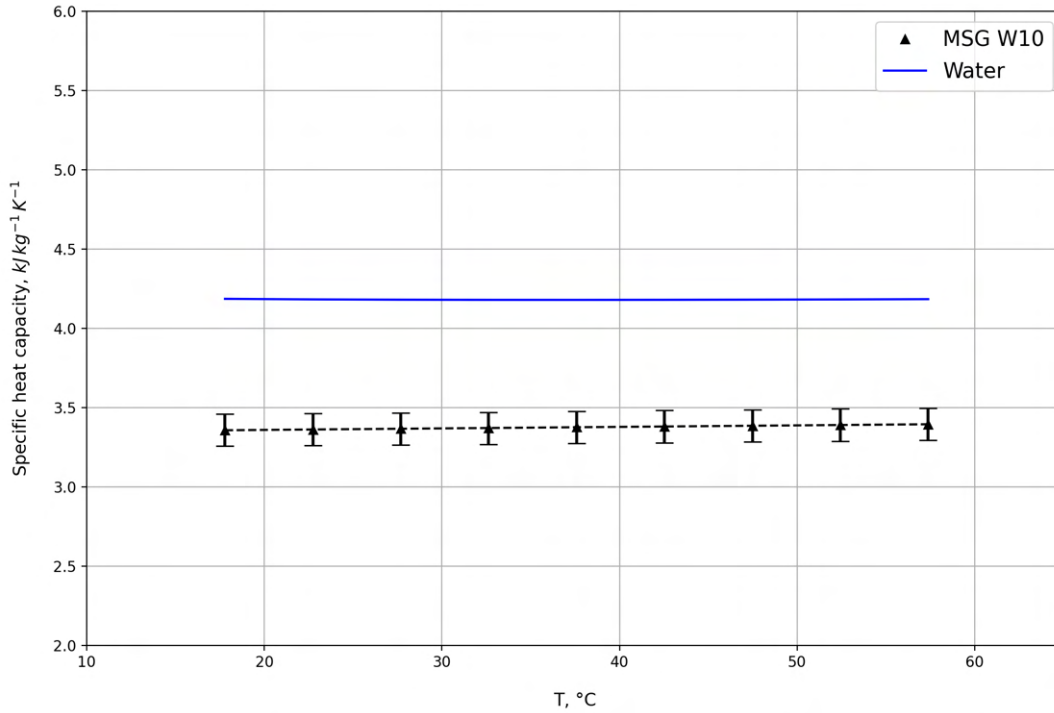


FIGURE 5.4: Specific heat capacity of the investigated ferronanofluid (MSG-W10) and water [123] (blue line). Black triangles indicate values for ferronanofluid [15].

by their specific properties, including size, shape, and material. On a broader scale, considerations within nanofluids include concentration, dispersion quality, presence of agglomerates, interactions between nanoparticles and the base fluid, pressure, and temperature. The number of parameters and the complex interactions have led to extensive research on nanofluids. These studies aim to establish a comprehensive theory of nanofluids, though some areas still remain not fully understood.

The hot wire method plays a prominent role in measuring the thermal conductivity of nanofluids (Fig. 5.5). The measurement apparatus consists of a metal wire serving as a heat source, a temperature sensor, and a container. To determine the thermal conductivity coefficient, the container is filled with the test fluid, and the wire is connected to a power source. When electric current is present, the wire acts as the heat source, following Joule's law. The surrounding fluid absorbs this heat, lowering the temperature of the wire to a specific value after the measurement time. The end temperature of the wire is used to calculate the thermal conductivity coefficient of the fluid.

The short measurement duration (2–8 seconds) minimizes the impact of natural convection within the container. Coupled with a precise measurement system, this allows for an accurate determination of the thermal conductivity coefficient. The value is calculated based on the following equation [4]:

$$k = \frac{q}{4\pi(T_2 - T_1)} \ln \frac{t_2}{t_1} \quad (5.9)$$

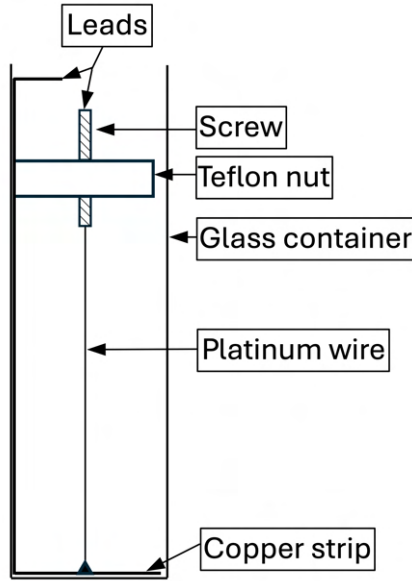


FIGURE 5.5: Design of a hot wire method device. Based on [4].

Where q represents the amount of heat generated per unit length of the wire, t_1 and t_2 are the start and end times of the measurement corresponding to temperatures T_1 and T_2 respectively.

Thermal conductivity is also measured using the ring gap method (Fig. 5.6). The apparatus consists of two parts - an outer and an inner part - forming three distinct volumes: the ring-shaped volume and two hemispherical volumes, all filled with nanofluid. From the inner part, the fluid is heated with a specified power. Heat passes through the fluid, and then reaches the outer part of the device where temperature is measured. The gap uniformity between the outer and inner parts is crucial to the accuracy of the method.

Calibration using a reference fluid with known thermal conductivity is required each time the device is assembled. In an ideal scenario, the thermal conductivity value is determined by the equation [125]:

$$k_{nf} = \frac{q}{2\pi(T_{in} - T_{out}) \left(\frac{l}{\ln\left(\frac{r_{out}}{r_{in}}\right)} + \frac{2r_{in}r_{out}}{r_{out} - r_{in}} \right)} \quad (5.10)$$

Where q is the amount of heat supplied by the heater, T_{in} the temperature of the inner thermocouple, T_{out} the temperature of the outer thermocouple, l the length of the cylindrical part, r_{out} the outer radius, and r_{in} is the inner radius.

The thermal conductivity of nanofluids is also determined using Maxwell's equation [127]:

$$k_m = \left(\frac{k_p + 2k_{fl} + 2(k_p - k_{fl})v_f}{k_p + 2k_{fl} - (k_p - k_{fl})v_f} \right) k_{fl} \quad (5.11)$$

Where k_p and k_{fl} represent the thermal conductivity of the particles and the base fluid, respectively, and v_f is the volume fraction of particles. This equation does not

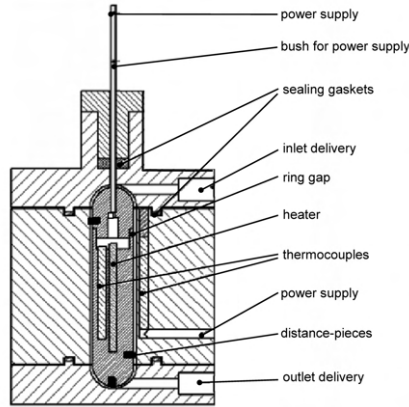


FIGURE 5.6: Design of a ring gap method device [126].

account for Brownian motion and interfacial layering, hence the results obtained will underestimate the thermal conductivity of the nanofluid.

The presented relation is better suited for larger particles. The authors in [128] noted this fact while investigating the thermal conductivity of nanofluids based on Al_2O_3 with three particle sizes: 10 nm, 100 nm, and 150 nm. The results for the smallest nanoparticles, compared to Maxwell's equation, significantly differ to their disadvantage. However, the difference for larger particles decreases (<2%). Consequently, a modification of Maxwell's equation was proposed to account for the increased heat flux relative to the base fluid, considering Brownian motion:

$$\frac{q_{eff}}{q_f} = \left(\frac{k_p + 2k_f + 2(k_p - k_f)v_f}{k_p + 2k_f - (k_p - k_f)v_f} \right) + \frac{k_p \sigma T}{k_f D \mu d_p} \left(\frac{6v_f}{\pi} \right)^{\frac{1}{3}} \quad (5.12)$$

where σ denotes the Boltzmann constant, T the temperature of the fluid, D the molecular diffusion coefficient, μ the dynamic viscosity, and d_p the average particle size.

Data on MSG-W10 ferronanofluid thermal conductivity are presented in the Fig. 5.7 and describe the ferronanofluid used by Rudl et al. [83]. Due to the similar ratio of the solid content for both nanofluids and the fact that magnetite has a low thermal conductivity relative to the base fluid, reported as $4 \text{ W m}^{-1} \text{ K}^{-1}$ at 300 K [25] and $5 \text{ W m}^{-1} \text{ K}^{-1}$ at 298 K [129], these values will be used in the heat transfer calculations in this study. The black dashed line in Fig. 5.7 is a polynomial fit of the data used for the heat transfer calculations and is described by the equation:

$$k(T) = -3.93 \cdot 10^{-6} T^2 + 0.0015T + 0.585 \quad (5.13)$$

where T is a ferronanofluid temperature in $^{\circ}\text{C}$.

5.1.4 Density

The density of the ferronanofluid was measured using a pycnometer and a Satorius MSG SD EE scale at 20°C and is 1210 kg m^{-3} .

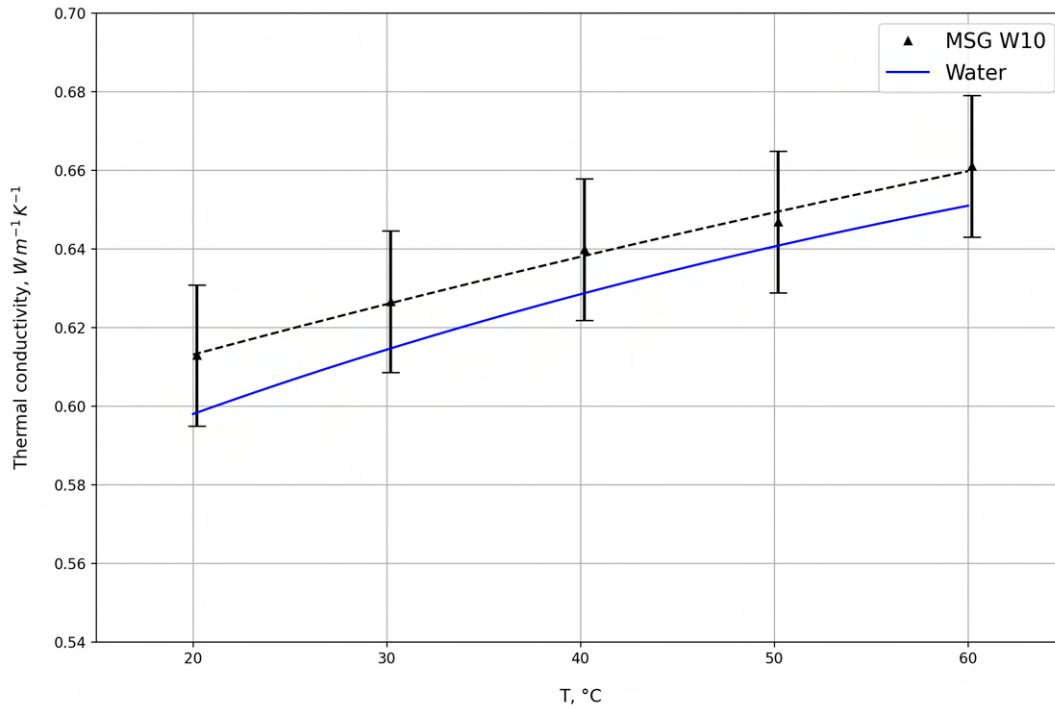


FIGURE 5.7: Thermal conductivity of the MSG-W10 ferronanofluid and water [123] (blue line). Black triangles indicate values for ferronanofluid [130].

5.2 Contact angle under a magnetic field

To determine the effect of the magnetic field on the ferronanofluid, experiments examined the droplet. The change in the contact angle of the ferronanofluid droplet under the influence of a magnetic field served as a suitable method for characterizing interactions. The contact angle was determined on copper and aluminium surfaces, materials commonly used in heat exchangers. The outcome was the relationship between magnetic field strength and the contact angle. The ferronanofluid used is the same type as in heat transfer experiments (MSG-W10), but comes from another batch, the same one used in study by Rudl et al. [83].

5.2.1 Contact angle

The contact angle is defined as the angle created where the solid, liquid, and gas phases meet. When a liquid is placed on a solid surface, it does not spread out completely but rather forms a droplet. The shape of this droplet dictates how the surface is wetted, with the contact angle at the phase boundaries being an indicator. The contact angle (CA) is illustrated in Fig. 5.8.

Its value is determined by Young's equation:

$$\theta = \arccos \left(\frac{\sigma_{sv} - \sigma_{sl}}{\sigma_{lv}} \right) \quad (5.14)$$

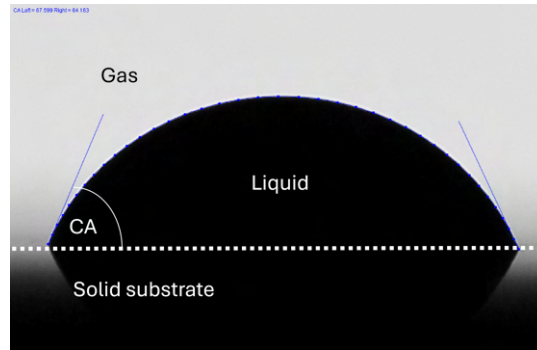


FIGURE 5.8: Example of a contact angle measurement using ImageJ program with the DropSnake plug-in [131]

Here, σ_{sv} represents the surface tension between the solid and gas phases, σ_{sl} the surface tension between the solid and liquid phases, and σ_{lv} the surface tension between the liquid and gas phases.

5.2.2 Experimental setup and procedure

Contact angle analyses were carried out with a self-developed measurement device (Fig. 5.9). The experimental setup consisted of a sample table with a substrate, an indirect light source, a light diffuser, and a digital SLR camera (Canon EOS 70D) with a macro lens. A micropipette (VWR VE-20) was used to position droplets on the substrate. A precision thermometer (Greisinger GMH 3700 series) was used to measure temperature directly above a droplet. Humidity was monitored with a ventilation meter (Velocicalc 9565).

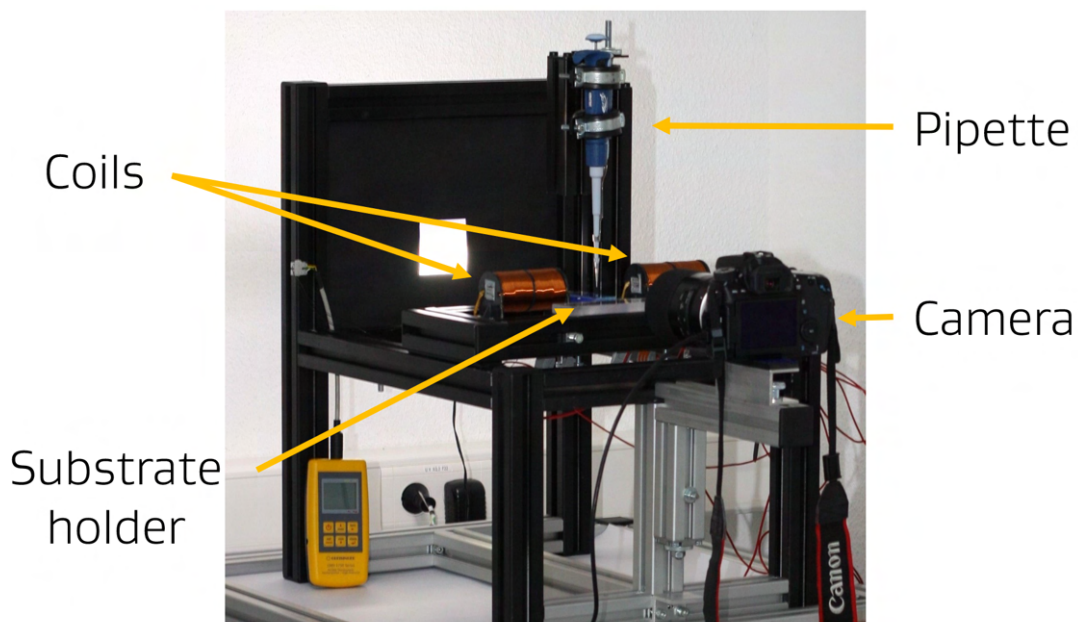


FIGURE 5.9: Experimental setup for measurement of a contact angle under magnetic field measurement [15].

The test stand was equipped with two electromagnetic coils, arranged horizontally on the same plane as the surface of a substrate. Such positioning of coils allowed for the generation of a homogeneous and horizontal magnetic field acting on a droplet. Magnetic field strength was measured with a magnetic field meter (List-Magnetik MP-1000, Germany) and controlled by adjustment of the electric current through the coils (DC power supply PeakTech 1580).

The experiments considered five values of the magnetic field strength, measured in the droplet placement position. The substrates were cleaned shortly before each experiment. Schuster et al. [132] and Hernaiz et al. [18] presented the importance of a thorough cleaning process and its influence on the results. Schuster et al. reported that the relative error without cleaning is about 15%. A proper cleaning with ethanol or acetone reduced that error to less than 8%. Hernaiz et al. indicated that remains of a cleaner or even a slight coating left by a detergent limit the contact between the liquid and the surface and affect CA measurements. In the current study, a surface cleaning process employing acetone and a lint-free towel is performed before each measurement.

Analysis of the obtained images was carried out using the ImageJ program with the DropSnake plug-in (Fig. 5.10) [131]. Contact angle determination involved defining the contour of the droplet using points and curve fitting. The valid automatic curve fitting identifying the contact angle requires a sharp image with a high contrast between the droplet and the background to allow correct identification of the contour. Despite a properly executed procedure, in some cases it was necessary to manually adjust the curve, since the contrast near the surface was lower.

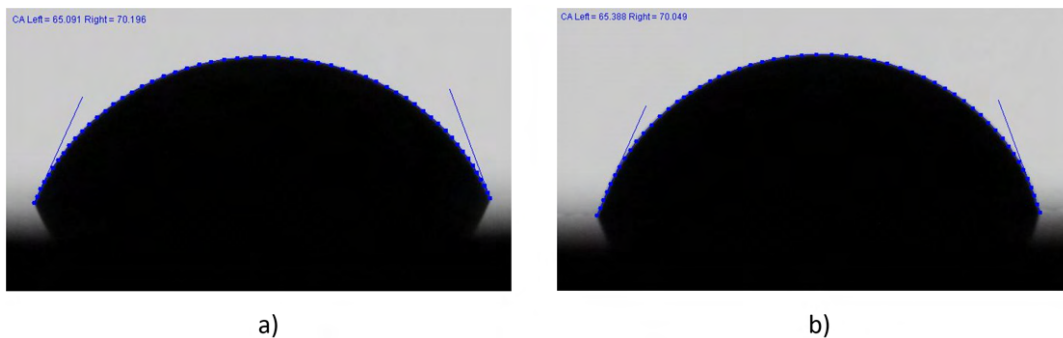


FIGURE 5.10: Image analysis performed using the DropSnake plugin. Images present ferrofluid droplet on a copper a) and aluminium b) substrate [15].

Fig. 5.11 shows the procedure of the experiments. For each analysis, a droplet with a volume of $6 \mu\text{l}$ was dropped onto the substrate. Droplets were deposited on copper or aluminium substrates, and each was subjected to one of the five magnetic field strengths.

Before the magnetic field was applied, the first image was taken to determine the initial contact angle CA_0 . Then, the second image was acquired to observe the initial effect of the lateral impulse exerted by the magnetic field on the droplet, which manifests itself in a change of the contact angle from CA_0 to $CA_{0,MF}$. The droplet

was then covered with a plastic box to ensure stable drying conditions. If the dosage was not satisfactory (e.g., the droplet is asymmetrical), the measuring process was aborted after the second image was taken and the test was repeated. Dried samples were then investigated under a microscope (Zeiss Stemi 2000-c with a camera module Zeiss Axiocam 105 Color registering images in 2560×1920 pixels resolution).

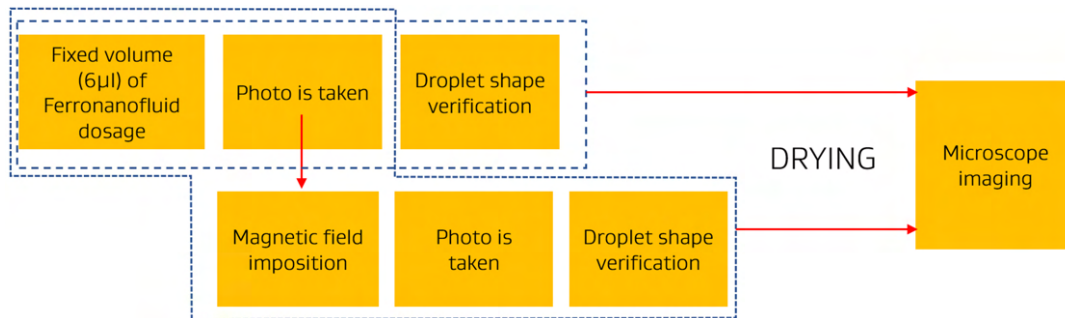


FIGURE 5.11: Algorithm of the experiments on contact angle and magnetic field impact on the drying ferronano fluid droplet [15].

5.2.3 Distribution of the magnetic field

The magnetic field distribution was numerically simulated using the FEMM application (finite element method magnetics) [133]. The numerical setup corresponded to the experimental situation. The substrate was placed between two horizontal coils with electric current. The prepared model consisted of a planar problem and was solved as such. Fig. 5.12 presents the results of the simulation. Magnetic field distribution, especially magnetic field lines, provides a basis for further inferences regarding ferronano fluid droplet dynamics.

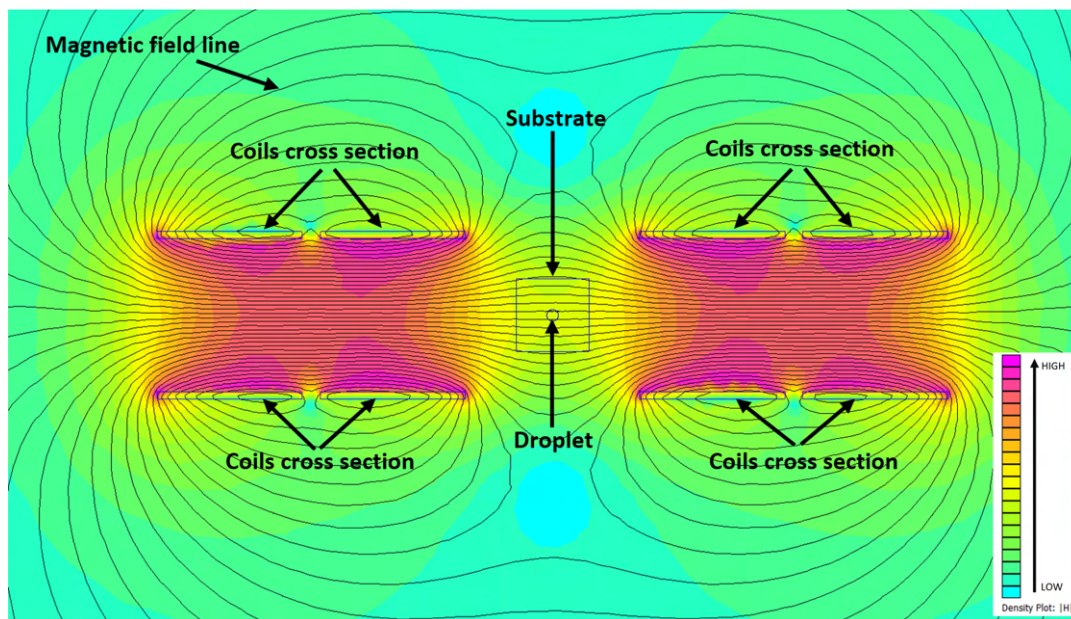


FIGURE 5.12: Results obtained with the FEMM application. The magnetic field intensity distribution is depicted by colours in the image [15].

5.2.4 Determination of the contact angle for ferronano fluid

The reference results, without the influence of a magnetic field, of the ferronano fluid contact angle are presented in Fig. 5.13. It contains the results of contact angle measurements for the six samples made for each of the surfaces used. The average contact angle on the copper substrate is $71.5 \pm 1.8^\circ$ (temperature of measurements ranging from 20.8°C to 26.3°C) and on the aluminium substrate $69.6 \pm 2.0^\circ$ (temperature of measurements ranging from 22.4°C to 28.2°C).

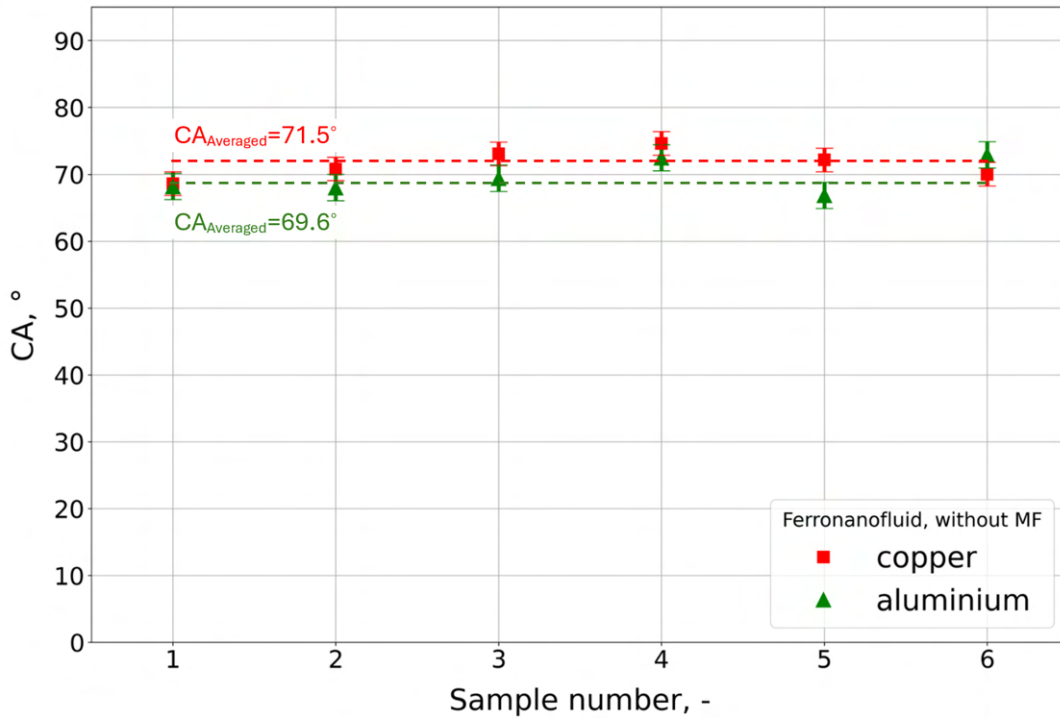


FIGURE 5.13: Contact angle of MSG-W10 ferronano fluid on copper and aluminium substrates [15].

The description of droplets includes not only geometric parameters. Forces acting on a droplet are defined by the Bond number Bo [134]. The Bond number is defined as the ratio between the gravitational force (the hydrostatic pressure) and the surface force (the capillary pressure) resulting from the surface tension. An additional magnetic force acts on the droplet as a volume force in a manner similar to gravity. To describe forces acting on a droplet under magnetic influence, the magnetic Bond number Bo_m is used [135]. The magnetic Bond number represents the ratio between the magnetic force and the surface force. It equals zero in situations without a magnetic field.

$$Bo = \frac{\rho g r_{dr}^2}{2\sigma} \quad (5.15)$$

$$Bo_m = \frac{\mu_0 \chi H_0^2 V_{dr}^{\frac{1}{3}}}{2\sigma} \quad (5.16)$$

H_0 denotes the imposed magnetic field strength and χ the ferronano fluid's volumetric susceptibility. The vacuum permeability μ_0 equals $4\pi \times 10^{-7} \text{ V s A}^{-1} \text{ m}^{-1}$. For MSG-W10, the ferronano fluid employed in this study, the susceptibility is 0.6691 and the surface tension 0.05 N m^{-1} [119].

5.2.5 Magnetic field effect on a ferronano fluid droplet

Studying the interaction of ferronano fluid droplets under the influence of a magnetic field reveals that two phases must be distinguished: initial phase and holding phase. The first, or initial phase, is dominated by the lateral momentum imposed on the droplet by switching on the magnetic field. In the second, or holding phase, the magnetic field is constant over time. Due to the rapidly changing magnetic field during the switch-on process, the first phase is very dynamic and involves significant changes in contact angle and droplet shape. The second phase is dominated by the drying process. The visible effects due to the magnetic field are rather weak. However, they are present in the final cracking pattern.

Subsequently, the effective medium theory, which treats nano fluids in an averaged approach, cannot be assumed for the drying of the suspension droplet. The drying of droplets under magnetic fields is, like any drying of suspensions, a two-phase phenomenon. Ferronano particles move due to acting forces - capillary, gravity, magnetic, etc. - independently from the basefluid. However, movement of ferronano particles is coupled with the basefluid via viscosity.

The magnetic effects on the droplet during the initial phase are described using the difference between the contact angle $CA_{0,MF}$ immediately after the magnetic field is imposed and the initial contact angle CA_0 found right after dosing the droplet on the substrate.

$$\Delta CA_0(H_0) = CA_{0,MF}(H_0) - CA_0 \quad (5.17)$$

Fig. 5.14 compares the ΔCA_0 values as a function of the magnetic field strength H and of the Bo_m for both substrates. In the absence of a magnetic field, $CA_{0,MF}(H_0)$ and CA_0 are nearly identical. An increase of H_0 increases $\Delta CA_0(H_0)$ linearly up to about 4° . No differences were found for the two substrates. For H_0 greater than about 90 A cm^{-1} , some of the ΔCA_0 values continue to follow the straight line, while others fall well below, reaching negative values.

Switching on the magnetic field causes droplet lateral deformation. Two regimes were observed:

- **De-pinning regime:** the droplet starts to flow and the contact line moves outward. The contact angle decreases and the droplet elongates.
- **Pinning-fixed regime:** the droplet deforms while maintaining the integrity of the contact line. The contact angle increases, but the droplet radius remains unchanged.

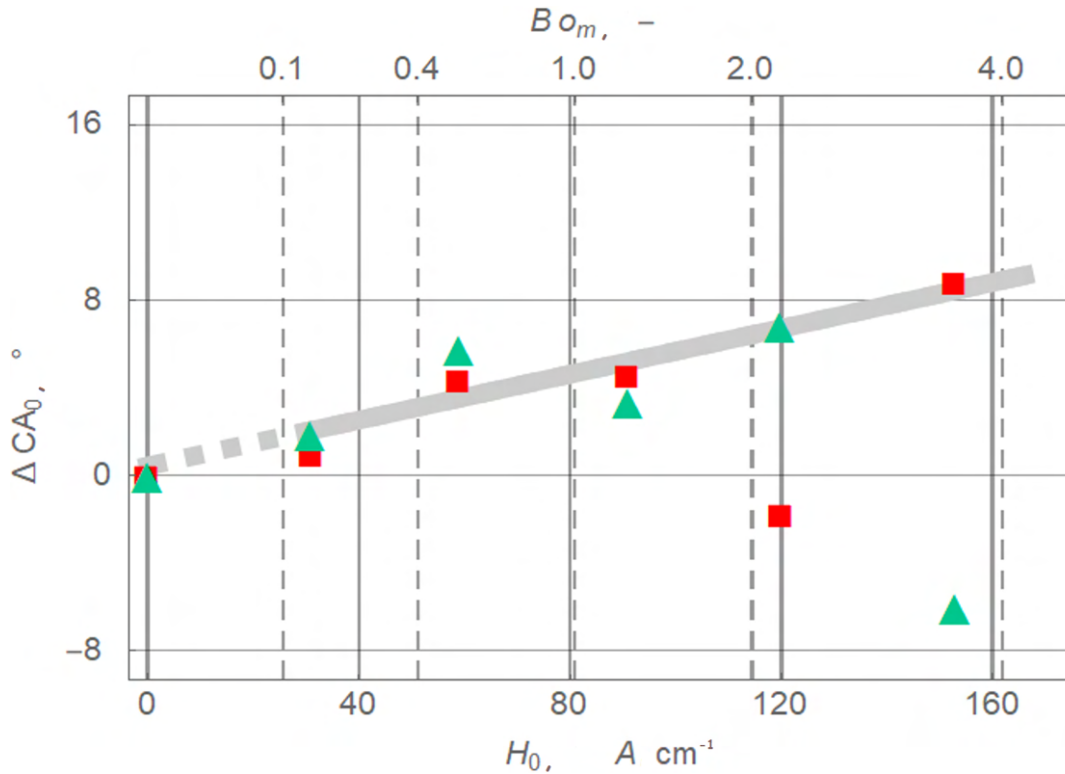


FIGURE 5.14: Effect of switching-on the magnetic field on the initial contact angle. Droplet placed on the copper (red squares) and aluminium substrate (green triangles). The full gray line indicates the linear approximation of all data of the de-pinning regime. The broken gray line is its extension to the situation without magnetic field [15].

The de-pinning regime indicates that the sum of all forces $F_{0,p}$ (friction, adhesion, line tension, etc.) that hold the droplet in place and in shape without a magnetic field is exceeded for a short time by switching on the coils. Since the magnetite particles cannot leave the droplet, they are pressed against the droplet surface and deform it. The deformation stops when a new equilibrium is reached. $F_{0,p,MF}$, which denotes the sum of all forces including the magnetic one, is then equal to zero. The resulting contact angle $CA_{0,MF}$ is smaller than CA_0 . The effect resembles a situation in which the surface had become more hydrophilic.

Similar analysis can be conducted for the pinning-fixed regime. The force associated with switching on the coils is too weak to overcome $F_{0,p}$ and thus does not move the contact line. It is strong enough only to deform the droplet surface. The contact angle $CA_{0,MF}$ achieved is larger than CA_0 . The effect is similar to making the surface more hydrophobic.

Fig. 5.15 presents characteristic cases of the two regimes. The images indicate that the shape of the droplet changes in both regimes. The transition between the two regimes does not depend only on the magnetic field. In the case of the copper substrate, the droplet flows when the magnetic field strength equals 120 A cm^{-1} , but at a value of 153 A cm^{-1} , only deformation of the droplet occurs. These observations suggest that the aforementioned critical value of $F_{0,p}$ is very sensitive to local surface conditions. Gao et al. [136] discussed similar effects and drew attention to local

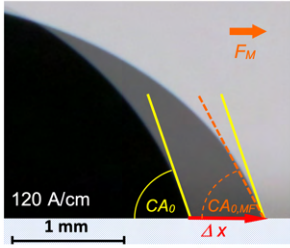
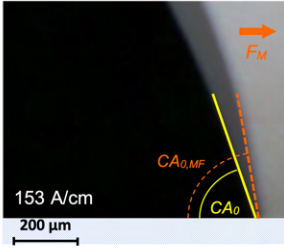
de-pinning regime	pinning-fixed regime
	
$F_{0,P} < F_{0,MF}$ $\Delta x > 0, CA_0 > CA_{0,MF}$	$F_{0,P} > F_{0,MF}$ $\Delta x = 0, CA_0 < CA_{0,MF}$

FIGURE 5.15: Change of a initial contact angle due to magnetic field. The superimposed images present the initial state without magnetic field (black) and immediately after switching on the coils (gray). The substrate is in all cases copper (dotted blue) [15].

increases of the $F_{0,P}$ during movement of the droplet related to the temporary line pinning caused by surface inhomogeneity and contamination. Therefore, a local critical value of the pinning force occurs, which, despite the increase of the magnetic force, cannot be exceeded, causing the droplet front to stop. Note that each experiment of this study is performed on a new substrate to avoid nanoparticle remainders or chemical interactions of the suspension used with it. For this reason, small differences in the surface occur from substrate to substrate.

In summary, the pinning-fixed regime prevails up to a magnetic field strength of about 90 A cm^{-1} or a magnetic Bond number of about 2.5. Above this threshold, a metastable situation exists, allowing both the pinning-fixed and de-pinning regimes.

5.3 Magnetic field influence on ferronanoparticles

Evidence that a magnetic field can affect the shape of a droplet prompted research into the cause behind it. This investigation was carried out through the analysis of dried ferronanofluid droplet deposit. The experiments focused on preparing samples of droplets dried in the presence of a magnetic field, followed by an analysis of the resulting crack patterns.

5.3.1 Orientation of cracks in dried deposit

The holding phase mentioned in section 5.2.5, with a constant magnetic field acting on a droplet, ends with the complete exsiccation of the droplet. Along with the macroscopically observable the shrinkage of the droplet volume due to evaporation, an internal transport of particles also takes place. The particles are conveyed to the droplet edge and backward to the centre of the droplet. The coffee-ring effect

is the result of the interaction of outward capillary flow and circular Marangoni convection [137]. Due to the homogeneity of the magnetic field, no direct magnetic force acts on the droplet or particles. Amin et al. [138] derived the particle size from Langevin curves for MSG-W11, a water-based ferronano fluid from FerroTech that is very similar to MSG-W10 used in this study. The size found, from 5.5 to 12.2 nm, indicates that the particles are small enough to be single-domain particles. Therefore, they should align with the magnetic field, as Pauchard et al. [139] found for maghemite particles of 10 nm size. The tendency of the cracks is to be parallel to the applied magnetic field and therefore to be parallel to the resulting magnetization of the particles (in competition with the elastic stress).

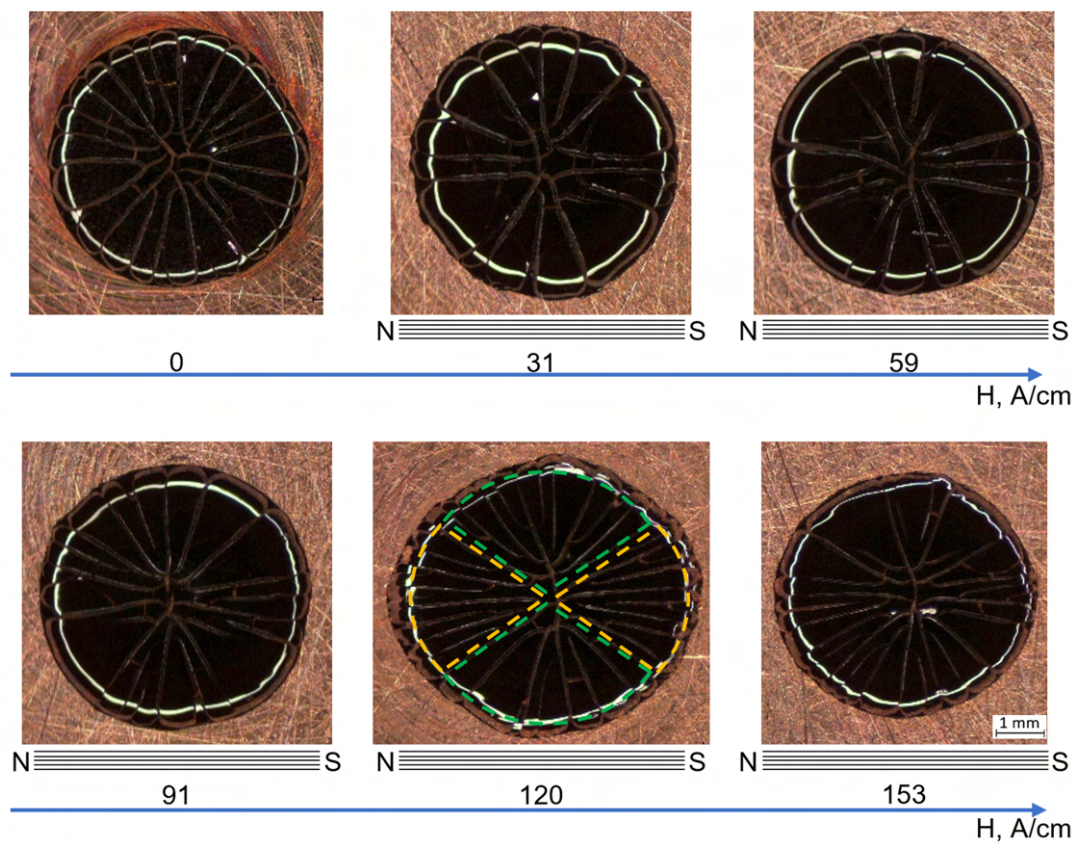


FIGURE 5.16: Magnetic field impact on the drying ferronano fluid droplets placed on the copper substrate. The coils were placed to the left and right of each sample. The image for $H_0 = 120 \text{ A cm}^{-1}$ indicates schematically the regions where elastic stress (green) and where magnetic stress (orange) dominates [15].

Fig. 5.16 shows the crack pattern of the fully desiccated droplets. The images are taken under the microscope after the drying process. The orientation of the particles during drying affects the crack pattern. A more horizontal orientation of the cracks is observed under the magnetic field. Pauchard et al. [139] showed experimentally that cracks may align in the direction of the magnetic field. This alignment is caused by an additional magnetic stress component that competes with the elastic, circumferential stress.

In Fig. 5.16, all droplets show an almost circular shape. The initial changes in the shape of the droplets, whether they change both the contact line and the contact angle (de-pinning regime) or only the contact angle (pinning-fixed regime), are stopped immediately after they occur. Exceptions are the droplets with the highest magnetic field strengths (120 and 153 A cm⁻¹). A detailed inspection of the droplet under 153 A cm⁻¹ at 300 s after the application of the magnetic field reveals that the droplet is slightly elongated (Fig. 5.17). The droplet is stretched parallel to the magnetic field by an amount of $2\Delta x$. To maintain volume continuity, the expansion of the drop causes a reduction in its height. Together with the reduction in height due to evaporation, a total reduction by Δh results. The contact angle increases from the initial value of $CA_0 = 70.0^\circ$ without the magnetic field to a contact angle of $CA_{0, MF} = 78.8^\circ$ after switching on the magnetic field, and then decreases to a value of $CA_{MF} = 73.7^\circ$ at 300 s. Note that these angles are only the values in the observation plane. An explanation for this finding is open and is therefore omitted here.

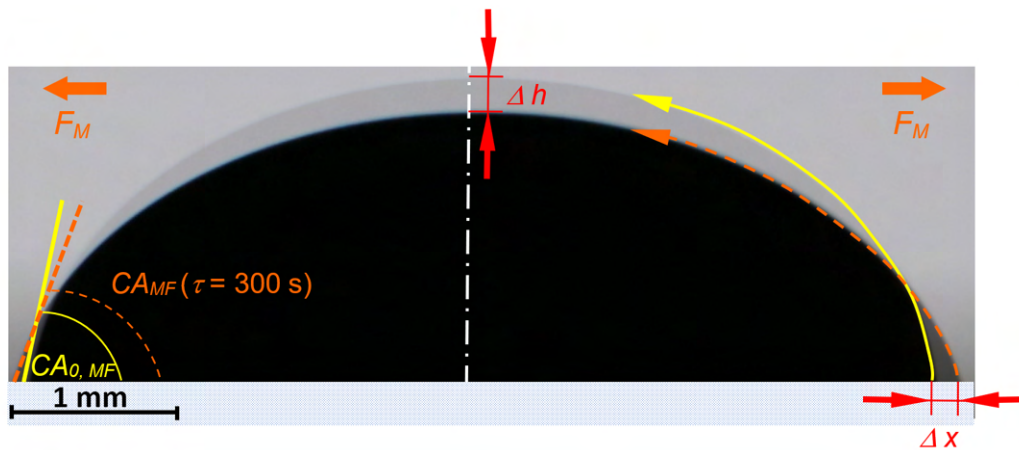


FIGURE 5.17: Evolution of the droplet on a copper substrate after 300 s. The magnetic field strength is 153 A cm⁻¹ and the magnetic Bond number 3.58. The superimposed images present the initial state (yellow full contour) and situation 300 s after switching on the magnetic field (orange broken contour). The superimposed area of the droplet appear deep black [15].

To investigate whether the crack pattern is affected by the magnetic field rather than droplet deformation, elongated droplets were prepared without applying a magnetic field. One sample was produced by tilting the substrate on which it was placed. Additionally, to exclude the possibility that the resulting crack pattern was influenced by this specific method, the second sample was prepared. In this case, the dispensed droplet was elongated using the pipette tip with which it was poured.

Fig. 5.18 shows the results of this experiment. Fig. 5.18a presents a droplet dried without a magnetic field and not manipulated. The expected radial crack pattern is present. The pattern is dominated by long pads stretched from the droplet edge toward its center and circumferential bridges (red ellipses). Some of the second generation cracks join the first generation cracks [14] and form confluences (marked with orange ellipses). Fig. 5.18b also shows a dried droplet without a magnetic field, but this time the droplet is artificially stretched by tilting the substrate. As before,

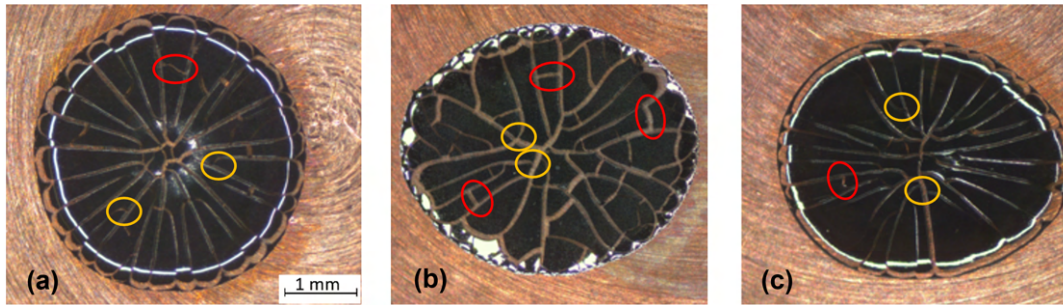


FIGURE 5.18: Comparison of crack networks. Image (a) shows the crack pattern of a droplet drying without magnetic field, image (b) of a artificially elongated droplet drying without the magnetic field and image (c) droplet elongated by a magnetic field (153 A cm^{-1}). Red ellipses indicate bridge cracks and orange ellipses confluences. [15].

most of the cracks are oriented from the rim to the center. However, the number of bridge cracks connecting adjacent radial cracks has increased. The crack pattern of the droplet elongated by the pipette tip confirmed this finding (not shown in Fig. 5.18). Fig. 5.18c shows a droplet dried under a magnetic field (153 A cm^{-1}). This time the elongation is a consequence of the magnetic field. In the vertical central region, the cracks are aligned along the stretching and thus in the direction of the magnetic field (orange frame in Fig. 5.16). In general, the magnetic field affects the shape of the resulting cracks. The cracks tend to align parallel to the magnetic field lines depicted in the Fig. 5.16.

5.3.2 Magnetic field effect on stress balance

The number of pads was analyzed to evaluate the effect of the magnetic field on the stress distribution in a drying droplet. This method is based on stress distribution and material strength analysis and is used to evaluate deposit thickness [140, 141]. It allows to determine whether the magnetic field affects the distribution of nanoparticles in the droplet, and thus the stresses arising in the drying droplet.

Fig. 5.19 shows the number of pads per droplet area. A pad is a part of the coating that is completely surrounded by cracks or the outer edge of the dried droplet. The area of the droplet is determined by assuming either circular or elliptical shape. For this purpose, the width and length of the droplet were measured. When assuming a circular droplet shape, these two parameters were averaged and treated as the radius of a corresponding circle. In the elliptical approach, the area of an ellipse was calculated from the width and the length of the droplet.

Fig. 5.19 shows that the two approaches (circular and elliptical) lead to very similar data. The eccentricity of the drop shape is thus small, but not zero. All data under magnetic influence, with exception of aluminium under magnetic field strength of 153 A cm^{-1} , lie on a straight line. The extension of this line for the case without magnetic field does not agree with the data for $H_0 = 0$. Apparently, a minimum magnetic field strength is required to order the magnetite particles and thus influence the crack pattern. The magnetic stress is proportional to the induced magnetic force

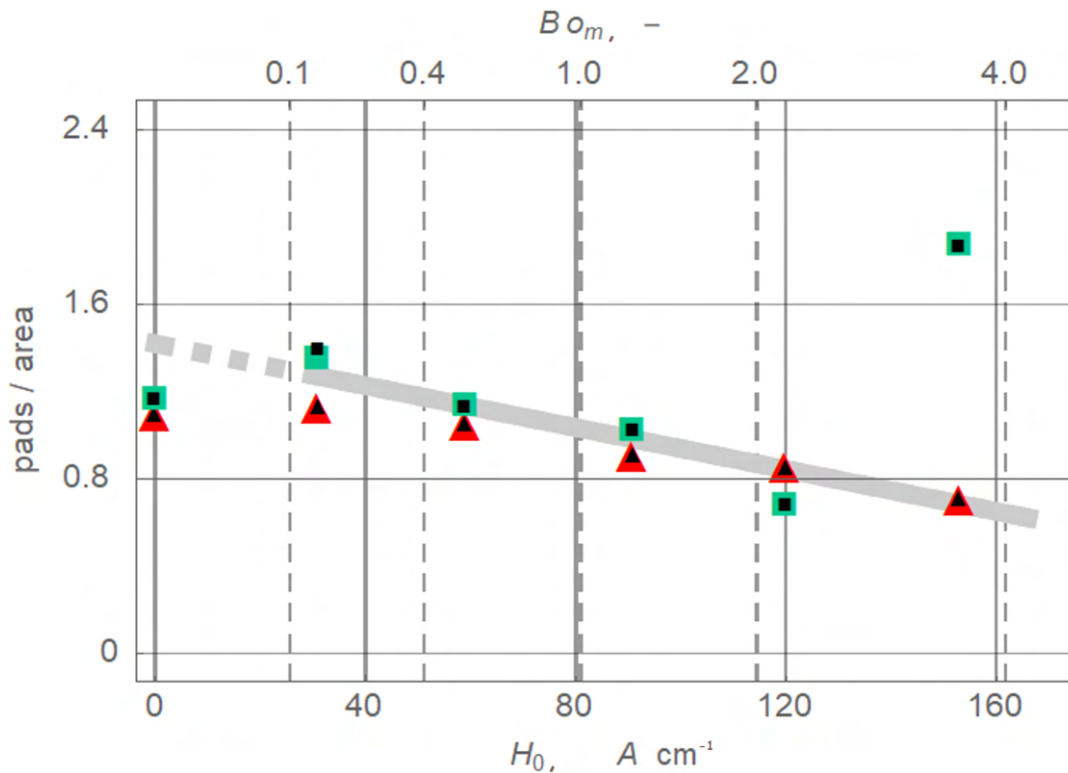


FIGURE 5.19: Number of pads per droplet area. Droplet placed on the copper (black and red triangles) and on the aluminium substrate (black and green squares). The black symbols indicate the circular and the coloured symbols the elliptical approach. The full grey line indicates the linear regression of all data magnetic influence (except aluminium 153 A cm⁻¹). The broken grey line is its extension to the situation without magnetic field [15].

due to permanent magnetization and therefore proportional to the magnetic field squared. Therefore, as long as it is much smaller than the elastic stress, it does not affect the total stress tensor.

The decrease in the number of pads per area means that the size of the pads increases with increasing magnetic field strength. As shown in Fig. 5.18, the number of bridges (marked with red ellipses) decreases under the influence of the magnetic field. Bridges - cracks in the circumferential direction - can only form if there is a sufficiently strong radial stress component. Pauchard et al. [139] indicated that the ordering of the magnetic particles increases the critical stress needed for a crack to develop. It is assumed that this effect prevents the development of bridge cracks.

The analyses presented lead to the conclusion that a magnetic field orders ferro-nanoparticles in MSG-W10 ferronano fluid in line with a magnetic field distribution. It proves that the use of a magnetic field in heat transfer experiments is justified, and the changes in heat transfer are indeed caused by the interaction of ferro-nanoparticles with the magnetic field.

5.4 Chapter Summary

- Two instantaneous regimes of a magnetic field and the ferronanofluid droplet interaction are found. Both depend on the strength of the magnetic field. For a magnetic Bond number $Bo_m < 2.5$, the pinning-fixed regime is present. Here, the contact angle increases, but the droplet radius remains unchanged. For $Bo_m > 2.5$, the droplet enters a metastable state where an additional de-pinning regime occurs. This regime is characterized by a decrease in the contact angle and a stretch of the droplet in the direction of the coils. In addition the droplet's transition from the pinning-fixed regime into the de-pinning regime over time is possible.
- The influence of the magnetic field during the drying process of the drops is reflected by the final crack pattern. In magnetic field free environments, cracks form due to elastic stresses. The application of a magnetic field introduces additional magnetic stress. The latter can order the magnetite particles and therefore lead to development of cracks that follow the direction of a magnetic field. The effect of an elongated droplet shape changes in crack alignment is negligible.
- The correlation of increasing pad size with increasing magnetic field strength is noted. The number of circumferential cracks caused by the radial stress component decreases under the magnetic field. The cause for this is seen in the ferronanoparticle ordering, which increases the critical stress required for a crack to develop.
- Further experiments regarding the magnetic field effect on the ferronanofluid droplet dynamics and deposit cracking for $Bo_m > 4$ are recommended as an extension of the investigation provided. The effect of stronger magnetic fields on the crack network is particularly interesting due to the possibility of reducing the number of cracks, unwanted in some applications.
- In case of commercial nanofluids the correct choice is to measure thermophysical parameters rather than to rely on data or correlations available in the literature.

Chapter 6

Ferronanofluid horizontal flow

The chapter examines the heat transfer performance of a ferronanofluid in laminar flow, both with and without the presence of a magnetic field. The experiments are conducted at three Reynolds number values: 109, 150, and 163. The initial section addresses heat transfer in horizontal thermally developing flow. Subsequent sections explore the change of the heat transfer through the use of a static magnet. The concluding section provides an analysis of the force balance exerted on the flow and its relationship with heat transfer employing ferronanofluid.

6.1 Experimental setup description

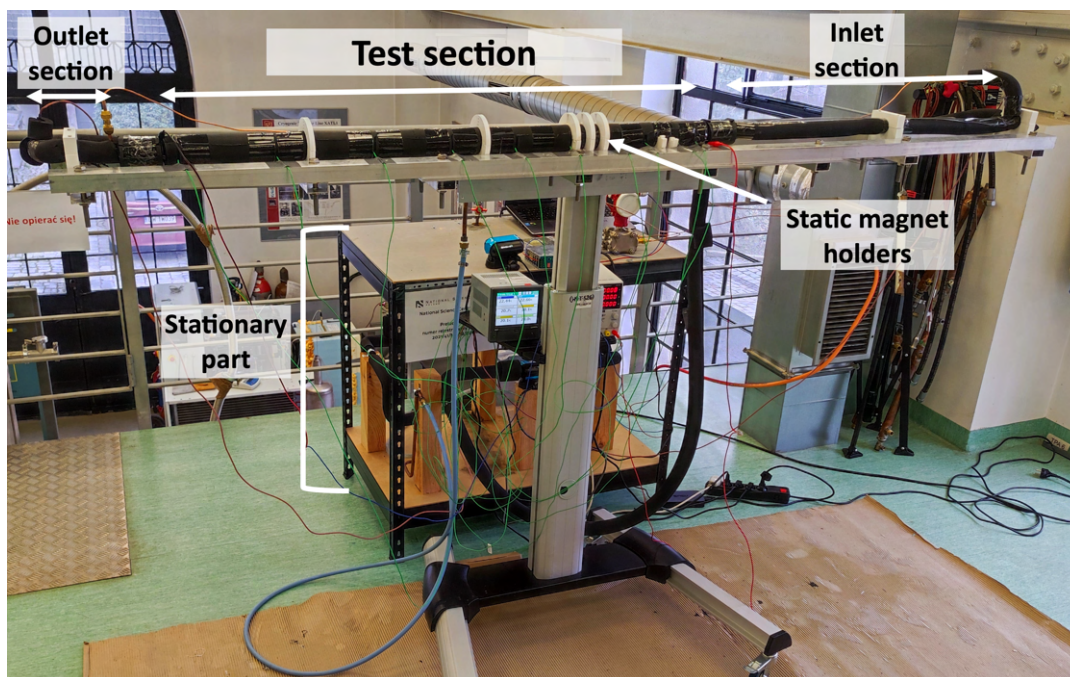


FIGURE 6.1: Photo of experimental setup for horizontal configuration [142].

The photo and schematic of the experimental setup are shown in Fig. 6.1 and Fig. 6.2. The main section consists of three separate copper tubes (99.9% Cu, $d_{in} = 6$ mm, wall thickness = 1 mm), serving as inlet, test, and outlet sections. Sections are thermally and electrically insulated from each other with Teflon sleeves. The inlet

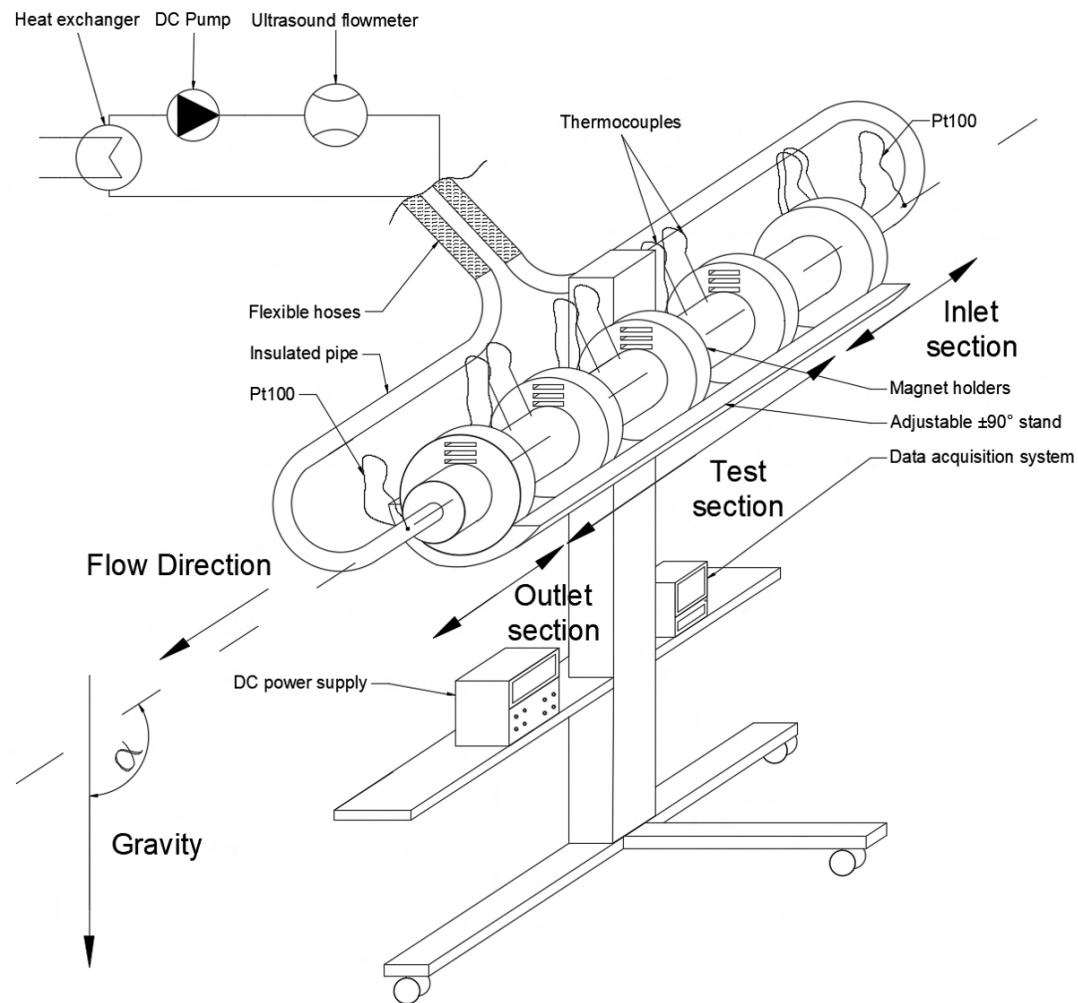


FIGURE 6.2: Experimental setup schematic.

section (900 mm) ensures that the flow entering the test section is fully developed for the investigated Reynolds number range. The main tube (1200 mm) is equipped with 9 K-type thermocouples attached with a thermally conductive adhesive at the distances of 57, 100, 185, 245, 355, 484, 625, 781, 965 mm from the inlet. The thermocouples were calibrated within the measurement range of the experiments. To ensure uniform heat flux distribution along its surface, the test tube is coiled with a resistive Teflon-coated wire with a 10-mm spacing between coils. The electrical wire is connected to a DC power supply (LongWei, LW-K3010DC). The outlet section incorporates an internal copper helicoid to provide fluid mixing and temperature equalization. The heated tube is insulated with a fiberglass tape (E-glass fiber type) and NMC Aeroflex HT insulation (19 mm, EPDM). Both the inlet and outlet sections are insulated with K-Flex ST frigo insulation (13 mm, synthetic rubber foam) and equipped with Pt100 thermoelements to measure fluid temperature. The magnets are inserted into 3D-printed holders attached to the test section. To allow for test section rotation, it is connected to the stationary part using flexible Teflon hoses (see Fig. 6.2). To dissipate the heat acquired in the test section, the fluid flows through a plate heat exchanger

TABLE 6.1: Accuracy of used measuring equipment

Device	Accuracy
Type K thermocouple	0.3 K
Pt100	0.15+0.002 t
DC power supply (LW-K3010DC)	0.3% \pm 1 digit
Flowmeter (Atrato 720)	1%
Magnetic Field meter (List-Magnetik MP-1000)	1 A cm ⁻¹

that is connected to a refrigerated thermostatic bath (PolyScience, SD7LR-20-A12E). Fluid flow is forced by a DC gear pump (ZC-A250, Hilitand). The pump is equipped with a PWM controller and the experimental setup incorporates a precision throttle to allow flow adjustment. The volume flow rate of the ferronanofluid is measured with an ultrasonic flow meter (Atrato 720). The accuracy of the measuring equipment is detailed in Table 6.1.

The used NdFeB magnets (N38) have an axial magnetization direction, parallel to their height, and dimensions of $40 \times 10 \times 1/2/4/5/8$ mm³ (Fig. 6.3). The maximum carrying capacity of each magnet is, respectively: 1.26, 2.80, 6.50, 8.37, 11.53 kg (the carrying capacity is evaluated by pulling a magnet stuck to an iron surface in the direction perpendicular to the surface). The bottom surface of the magnet placed in the holder attached to the test tube is 28 mm from its axis for both tested configurations.

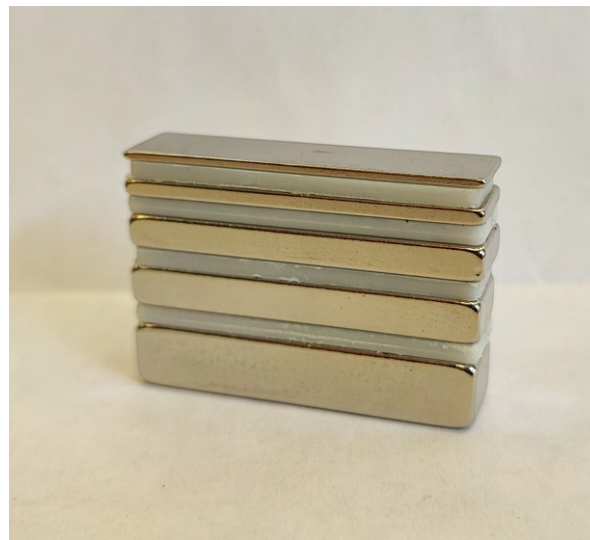


FIGURE 6.3: The N38 magnets used in the investigation.

The magnetic field affecting the flowing ferronanofluid was determined using a magnetic field strength meter (List-Magnetik MP-1000). For this purpose, a small model of the test section was made, along with all its components and magnet holders. The magnetic field meter probe was leveled and placed at the height of the centre of the tube. After each magnet was inserted, the probe was pushed in line with the axis of the tube until the maximum magnetic field strength value was recorded. The results are shown in Fig. 6.6.

To maintain the same Prandtl number at the entrance of the test section, the inlet temperature was kept constant at 15 °C. The coiled resistance wire provides a uniform heat flux of 3350 W m⁻². All investigated cases examine a horizontal flow with the magnetic field acting perpendicularly to the main flow direction. Before each series of magnetic field affected flows, a reference measurement without any magnetic presence is performed (Fig. 6.4a). Subsequently, a magnet is installed in a holder to affect the flow (Fig. 6.4b). After each measurement, the magnet is changed to another one until all are used. The procedure is performed for two magnetic field configurations: with a magnet situated above and below the test section. The acquired data is then used to determine the local Nusselt number.

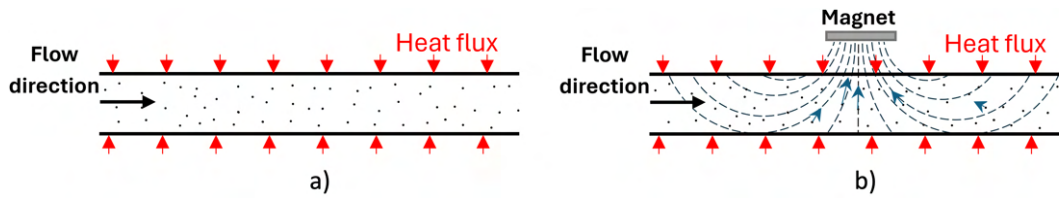


FIGURE 6.4: The procedure of the experiments. Scheme a) presents reference measurement without magnetic field presence. Scheme b) depicts the case with a permanent magnet installed. The blue arrows attached to the ferronanoparticles symbolically represent the magnetic force vector [142].

6.2 Magnetic field distribution

This section presents the numerical simulation results of the magnetic field distribution for the investigated configuration. The simulation was performed using the Ansys Electronics 2023 R2 software. Fig. 6.5a shows the geometry recreating a test section and Fig. 6.5b provides the simulation results in the form of the magnetic field distribution inside the test tube. The purpose of the numerical simulation was to extend the spot measurements of the magnetic field strength provided in Fig. 6.6. The simulation results show that the studied magnetic case is characterized by a heterogeneous magnetic field distribution. This observation is relevant to the analysis of mixed convection in ferronanofluid flow under the influence of a magnetic field, as presented in the following sections.

6.3 Heat transfer calculations

Main set of equations used in heat transfer calculation procedure:

Local Nusselt number:

$$\text{Nu}_i = \frac{h_i \cdot d_{in}}{k_{fli}} \quad (6.1)$$

Where d_{in} is an inner diameter of the test section tube, k_{fli} a thermal conductivity of the ferronanofluid at the position of a thermocouple.

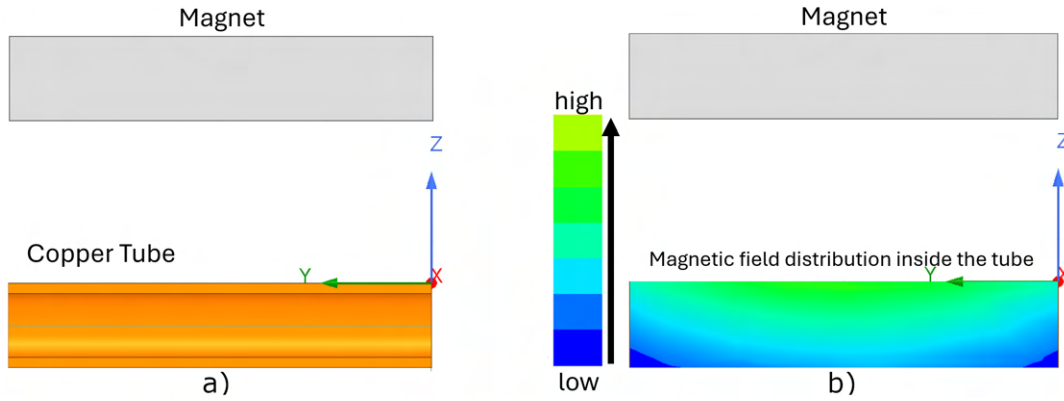


FIGURE 6.5: Geometry of the test section a). Results obtained with a numerical simulation b). The magnetic field strength distribution is depicted by colours in the image.

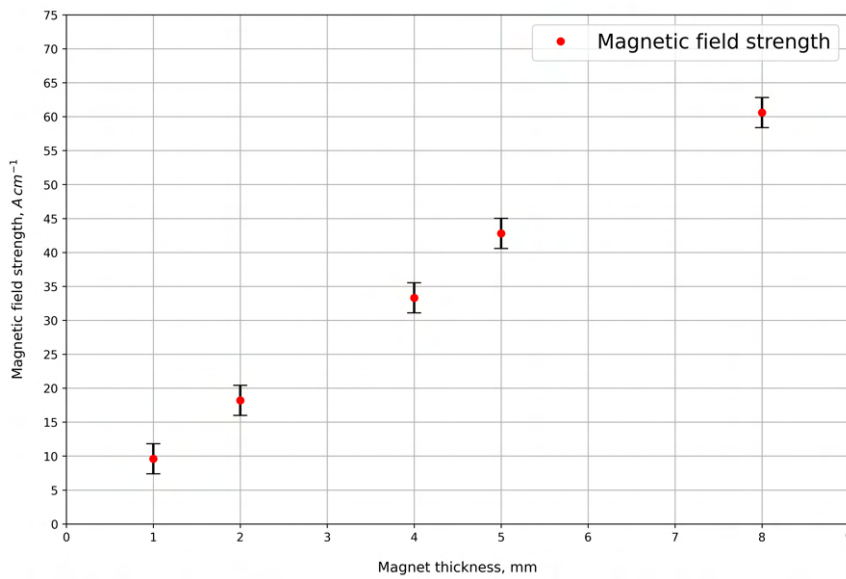


FIGURE 6.6: Spot measurements of the magnetic field strength inside the test section for the magnets used.

Local heat transfer coefficient:

$$h_i = \frac{q}{T_{walli} - T_{fli}} \quad (6.2)$$

Where q is a heat flux, T_{walli} a temperature of the inner wall at the position of a thermocouple, T_{fli} a calculated fluid temperature at the position of a thermocouple.

Calculation of the inner wall temperature for one-dimensional, steady-state conduction in a tube:

$$T_{walli} = T_{tci} - \frac{q \cdot d_{in} \cdot \log\left(\frac{d_{out}}{d_{in}}\right)}{2 \cdot k_{Cu}} \quad (6.3)$$

Where T_{tci} is a temperature of the outer wall measured by a thermocouple, d_{out} an outer tube diameter.

Calculation of the bulk fluid temperature at the thermocouple position:

$$T_{fli} = T_{in} + \frac{q \cdot \pi \cdot d_{in} \cdot x_i}{m_{fl} \cdot c_{pfl}} \quad (6.4)$$

Where x_i is a thermocouple position, m_{fl} a ferronano fluid mass flow, c_{pfl} a specific heat capacity of the fluid.

Nusselt number change for horizontal flow:

$$Nu_{\%} = \frac{Nu_{mf} - Nu_{base}}{Nu_{base}} \cdot 100\% \quad (6.5)$$

Where Nu_{mf} is calculated Nusselt number for ferronano fluid flow under the influence of a magnetic field, Nu_{base} a calculated Nusselt number for ferronano fluid flow without magnetic field presence.

Dimensionless axial distance x^+ [143]:

$$x^+ = \frac{x_i}{d_{in} \cdot Re \cdot Pr} \quad (6.6)$$

To provide a complete description of the flow taking into account the presence of a magnetic field, two additional force relations characterizing the flow are introduced. To define the relationship between magnetic and inertial forces in the flow, the magnetic number Mn is used [144]:

$$Mn = \frac{\text{magnetic force}}{\text{inertia force}} = \frac{\mu_0 \cdot \chi \cdot H^2}{\rho \cdot u^2} \quad (6.7)$$

Where μ_0 is vacuum magnetic permeability, χ a magnetic susceptibility, H a magnetic field strength, u a fluid velocity, and μ a dynamic viscosity of the fluid.

To complete all the dominant force relations in the investigated case, it is necessary to introduce the magnetic and viscous force relation $MnRe$ [23, 145]:

$$MnRe = \frac{\text{magnetic force}}{\text{viscous force}} = \frac{\mu_0 \cdot \chi \cdot H^2 \cdot \rho \cdot d_{in}^2}{\mu^2} \quad (6.8)$$

Errors are calculated using propagation of uncertainty, and presented in a form of error bars in the figs. The set of equations used to calculate local Nu number error:

$$u_c(Nu_i) = \sqrt{\left(\frac{\partial Nu_i}{\partial h_i}\right)^2 \cdot u_c^2(h_i) + \left(\frac{\partial Nu_i}{\partial d_{in}}\right)^2 \cdot u_c^2(d_{in}) + \left(\frac{\partial Nu_i}{\partial k_{fli}}\right)^2 \cdot u_c^2(k_{fli})} \quad (6.9)$$

$$u_c(h_i) = \sqrt{\left(\frac{\partial h_i}{\partial q}\right)^2 \cdot u_c^2(q) + \left(\frac{\partial h_i}{\partial T_{walli}}\right)^2 \cdot u_c^2(T_{walli}) + \left(\frac{\partial h_i}{\partial T_{fli}}\right)^2 \cdot u_c^2(T_{fli})} \quad (6.10)$$

$$u_c(T_{walli}) = \sqrt{\left(\frac{\partial T_{walli}}{\partial T_{ici}}\right)^2 \cdot u_c^2(T_{ici}) + \left(\frac{\partial T_{walli}}{\partial q}\right)^2 \cdot u_c^2(q) + \left(\frac{\partial T_{walli}}{\partial d_{in}}\right)^2 \cdot u_c^2(d_{in}) + \left(\frac{\partial T_{walli}}{\partial d_{out}}\right)^2 \cdot u_c^2(d_{out}) + \left(\frac{\partial T_{walli}}{\partial k_{Cu}}\right)^2 \cdot u_c^2(k_{Cu})} \quad (6.11)$$

$$u_c(T_{fli}) = \sqrt{\left(\frac{\partial T_{fli}}{\partial T_{in}}\right)^2 \cdot u_c^2(T_{in}) + \left(\frac{\partial T_{fli}}{\partial q}\right)^2 \cdot u_c^2(q) + \left(\frac{\partial T_{fli}}{\partial d_{in}}\right)^2 \cdot u_c^2(d_{in}) + \left(\frac{\partial T_{fli}}{\partial x_i}\right)^2 \cdot u_c^2(x_i) + \left(\frac{\partial T_{fli}}{\partial m_{fl}}\right)^2 \cdot u_c^2(m_{fl}) + \left(\frac{\partial T_{fli}}{\partial c_{pfl}}\right)^2 \cdot u_c^2(c_{pfl})} \quad (6.12)$$

6.4 Mixed convection

When analyzing the heat transfer impact of the magnetic field discussed in this study, it is crucial to consider the concurrent occurrence of secondary motions. Secondary motions of a fluid arise due to radial density gradients caused by heating. Emerging buoyancy forces cause fluid circulation presented in the Fig. 6.7. This mass transfer is characterized by counter-rotating vortex structures divided into two segments: the weaker segment directed toward the top of the tube, and the stronger, central segment, directing flow toward the bottom of the tube [83, 107, 108].

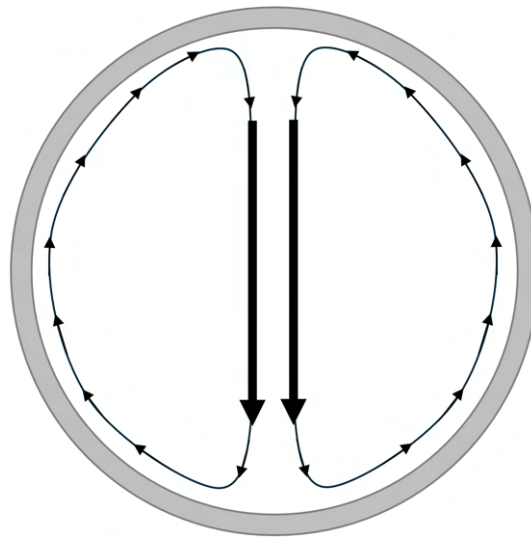


FIGURE 6.7: Mass transfer in mixed convection. The figure shows a plane perpendicular to the flow in a tube. The arrows represent the circulation of the liquid.

The progression of heat transfer along the test section can be divided into four regions, each characterized by a specific force balance [107]:

- R1 – Forced convection caused by the pump is dominating, buoyancy forces are negligible.
- R2 – Buoyancy forces due to the temperature gradient cause fluid circulation, resulting in an increase of the Nusselt number.
- R3 – As a result of circulation and thus equalization of the temperature of the flowing fluid, secondary motions disappear, the Nusselt number does not increase further.
- R4 - Forced convection caused by the pump is again dominating.

The existence of secondary motions in MSG-W10 was confirmed by experiments on fluid flow without influence of a magnetic field for each Reynolds number investigated. Fig. 6.8 illustrates the values of the local Nusselt number in relation to the dimensionless axial distance x^+ . At the first four thermocouple positions, the Nusselt number values are typical of laminar flow (region R1). Upon passing the fifth

thermocouple position, the Nusselt number value increases due to secondary motions (region R2). Further downstream, the increase stops (region R3) and eventually the Nusselt number decreases, as in the pre-secondary motion region (region R4).

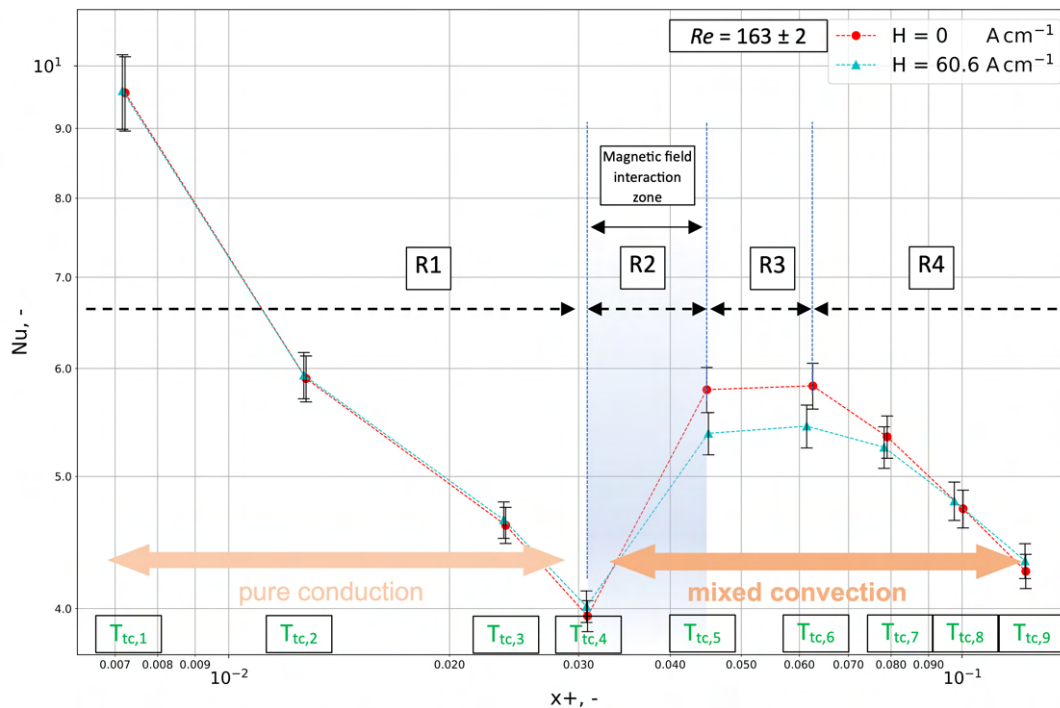


FIGURE 6.8: Development of the local Nusselt number along the tube in relation to dimensionless axial distance x^+ for $Re = 163$ in a horizontal flow. Red dots represent results for a non-magnetic field case, and cyan triangles case of 60.6 A cm^{-1} magnetic field strength with the magnet placed above the tube [142].

Under conditions of laminar flow, a colder liquid from the flow core migrates towards the tube wall. This process increases the temperature difference between the wall and the fluid, ultimately leading to improved heat transfer. The introduction of a magnetic field interferes this process. The magnetic field acting on ferronanoparticles produces a force that acts toward the direction of the permanent magnet, affecting mass transfer within the liquid and subsequently influencing heat transfer [23]. Fig. 6.8 presents the influence of a magnetic field on ferronanofluid flow for $Re = 163$. Red dots present the data for the ferronanofluid flow without a magnetic field, cyan triangles show the data for the flow influenced by a permanent magnet situated above the test section. Here, the magnetic force opposes the secondary motions leading to a noticeable deterioration in heat transfer, as evidenced by the reduced values of the local Nusselt number.

6.5 Impact of a static magnet located above the tube

Fig. 6.9 presents an analysis of the results in a horizontal flow. Fig. 6.9a, 6.9b, 6.9c correspond to the successive Reynolds numbers tested for a magnet located above the tube. At the lowest magnetic field strength of 9.6 A cm^{-1} , the magnetic field's

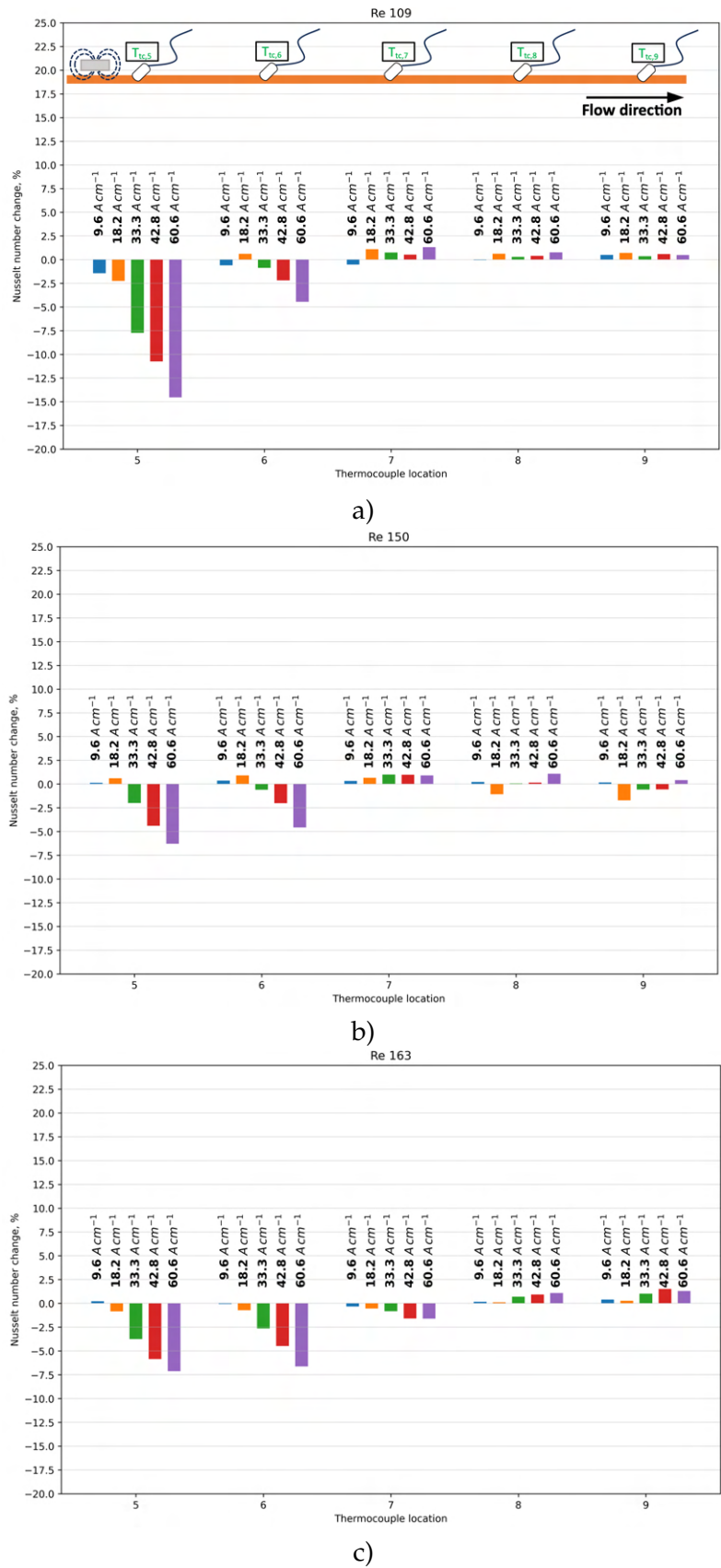


FIGURE 6.9: Change of the local Nusselt number for examined Reynolds values and magnetic field strengths along the test section for a magnet located above the test tube in a horizontal flow [142].

influence does not exceed 2.5% along the tube's length in any of the Reynolds number cases. For the analyzed range of Reynolds number values, this magnitude of magnetic field strength is insufficient to induce an impact on the heat transfer parameters.

For a magnetic field strength of 18.2 A cm^{-1} , the impact of the magnetic field on the Nusselt number along the length of the tube remains below 2.5%, mirroring the scenario observed with the previous magnetic field strength. For $Re = 109$, a deterioration is evident at the fifth thermocouple position. Still, the effect does not exceed 2.5%, preventing to draw meaningful conclusions.

For a magnetic field strength of 33.3 A cm^{-1} , each of the tested flows showed some deterioration of heat transfer directly behind the magnet position, indicating its interaction with the fluid. The magnet attracts ferronanoparticles in the direction opposite to the direction of secondary motion flow inside the tube, diminishing it and thus deteriorating heat transfer. The most substantial negative effect occurs for $Re = 109$ amounting to -7.7 %, which subsequently decreases at $Re = 150$, only to rise again at $Re = 163$.

At the next thermocouple position, the negative effect of magnet presence is noticeable only at $Re = 163$. In all other instances, it dissipates. This observation suggests that the higher velocity of the flowing medium enables the magnetic field's induced effects to be transported further, extending their influence on heat transfer along the test section.

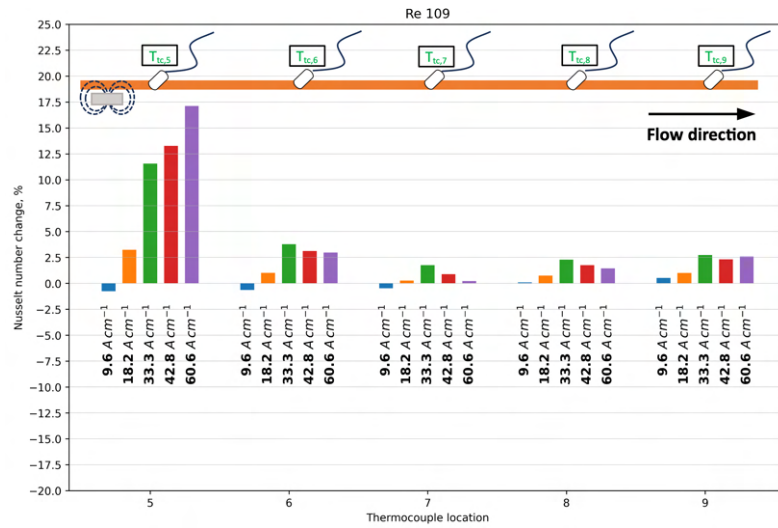
For a magnetic field strength of 42.8 A cm^{-1} , the influence is further intensified. the maximum reduction in the heat transfer parameters occurs for $Re = 109$, with a value of -10.7%, and the effect softens at $Re = 150$, again exceeding -5% for $Re = 163$. The results at subsequent positions exhibit similar tendencies to those observed at a field strength of 33.3 A cm^{-1} , with relaxation occurring after the seventh thermocouple.

At the highest evaluated magnetic field strength of 60.6 A cm^{-1} , the negative impact on heat transfer was maximized, reaching -14.5% for $Re = 109$. Notably, at this magnetic field intensity, the heat transfer effects at the sixth thermocouple were observable in all instances, indicating its potency in influencing mass transfer, even at the lowest flow velocities.

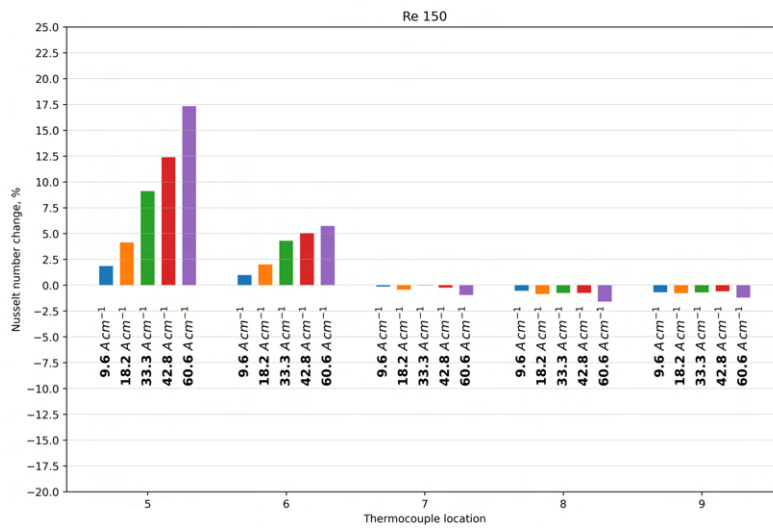
6.6 Impact of a static magnet located under the tube

Fig. 6.10 presents an analysis of the results in a horizontal flow. Fig. 6.10a, 6.10b, 6.10c correspond to the successive Reynolds numbers tested for a magnet located below the tube. At the lowest magnetic field strength of 9.6 A cm^{-1} , the outcome is similar to that of the configuration with a magnet positioned above the tube. At the magnet vicinity such low strength has no discernible impact on flow dynamics or heat transfer at any position of the test section.

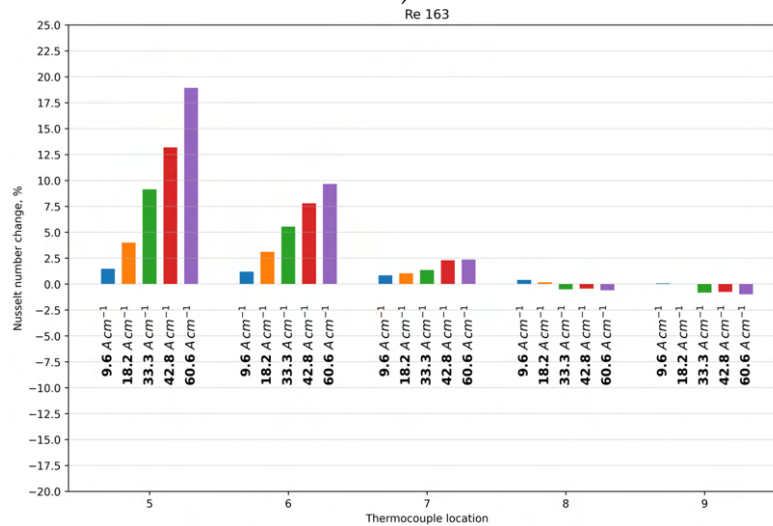
Increase of the magnetic field strength to 18.2 A cm^{-1} leads to an increase of the Nusselt number for every value of Reynolds number, exceeding the value of



a)



b)



c)

FIGURE 6.10: Change of the local Nusselt number for examined Reynolds values and magnetic field strengths along the test section for a magnet located below the test tube in a horizontal flow [142]

2.5%, and reaching more than 4% for $Re = 150$. The impact is also noticeable at the sixth position of the thermocouple for $Re = 163$. In other cases, the distance between measurement positions was sufficient for the Nusselt number change to drop below 2.5%. With the higher velocity of the medium, the effect can be transported over a greater distance of the section. For lower Re values, the movement of the ferronanoparticles is restricted to shorter distances due to viscosity effects.

For a magnetic field of 33.3 A cm^{-1} a noticeable effect on the improvement of heat transfer is present. Past the magnet, the enhancement for $Re = 163$ and $Re = 150$ is around 9.1% and 11.5% for $Re = 109$. The increased magnetic field strength also improves heat transfer at the sixth thermocouple position, with values exceeding 2.5% for all Reynolds number values, and 5% for $Re = 163$. For 18.2 A cm^{-1} only the highest Reynolds number allowed the magnetic field effect to become apparent at the sixth position, while here the impact of magnetic field on mass transfer is sufficient to project it by heat transfer improvement for every Reynolds number at the sixth position.

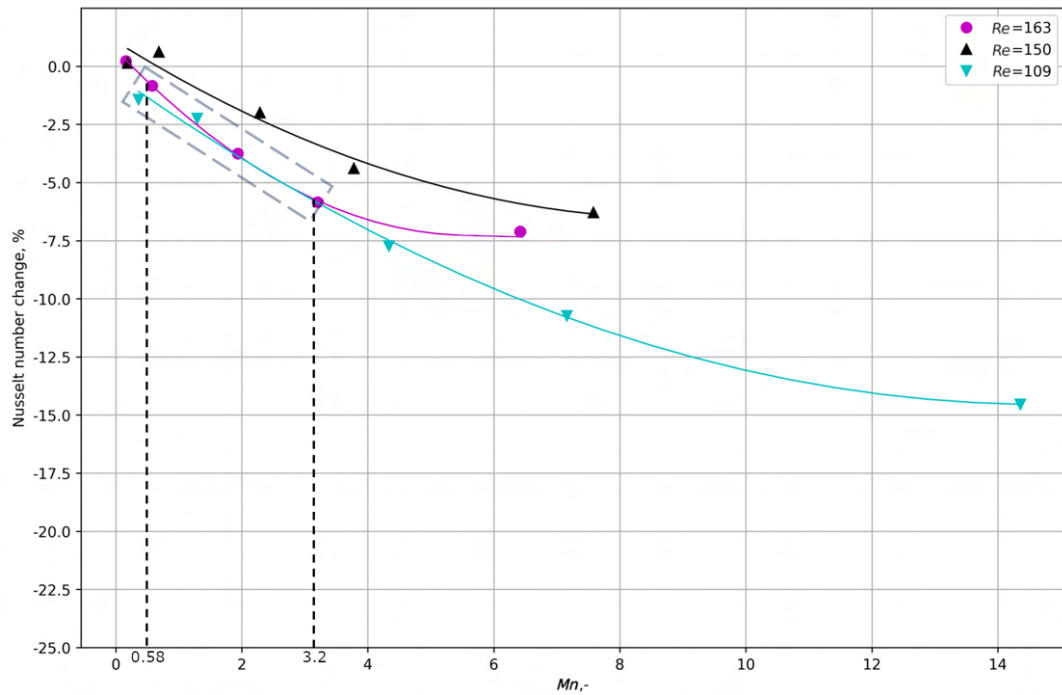
A further increase of the magnetic field strength to 42.8 A cm^{-1} brings a consequent enhancement of heat transfer for every Reynolds number case, reaching values close to 12.5% in the magnet vicinity. At the sixth thermocouple position, for Reynolds numbers of 150 and 163 the effect of interaction is less pronounced, but the trend preserves. At $Re = 109$ the improvement value does not exceed that of the previous strength.

The highest magnetic field strength of 60.6 A cm^{-1} provides further increase of Nusselt number. The greatest enhancement in heat transfer is achieved close to the magnet, at the fifth thermocouple position. At the sixth thermocouple position, this improvement for $Re = 150$ and $Re = 163$ also reaches the greatest values, while for $Re = 109$ there is no further increase.

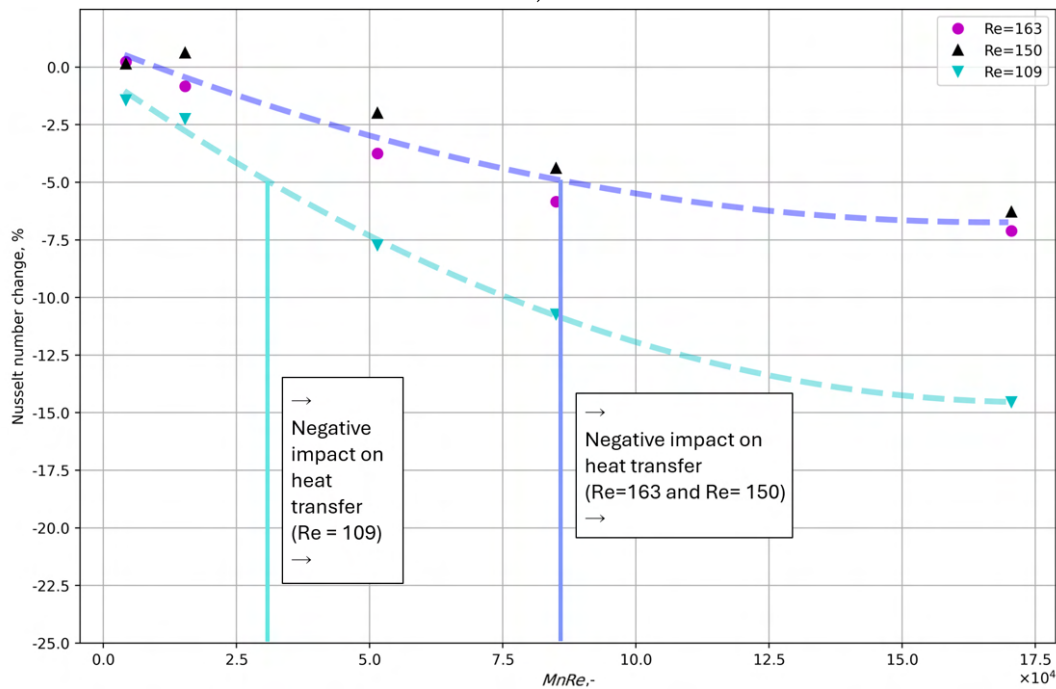
6.7 Effect of flow conditions on heat transfer

Figure 6.11a illustrates the relationship between change in the Nusselt number and the Mn number (which reflects the ratio of magnetic forces to inertia forces) at the position of the fifth thermocouple in a flow affected by a magnet placed above the test tube. The low-velocity flow at $Re = 109$ exhibits the most significant change in the Nusselt number, with twice the deterioration of heat transfer compared to the other two flow conditions. The changes in the Nusselt number for $Re = 109$ and $Re = 163$ are similar within the range of Mn number of 0.58 to 3.2. For this range, Nusselt number change can be estimated using Mn number. However, that is not true for the higher values of the Mn number. The Nusselt number change for $Re = 109$ decreases more than for $Re = 163$.

This difference is better pronounced in fig. 6.11b, that shows the relationship between change in the Nusselt number and the $MnRe$ number (representing the ratio of magnetic forces to viscosity forces). For $Re = 163$ and 150 there is a small difference

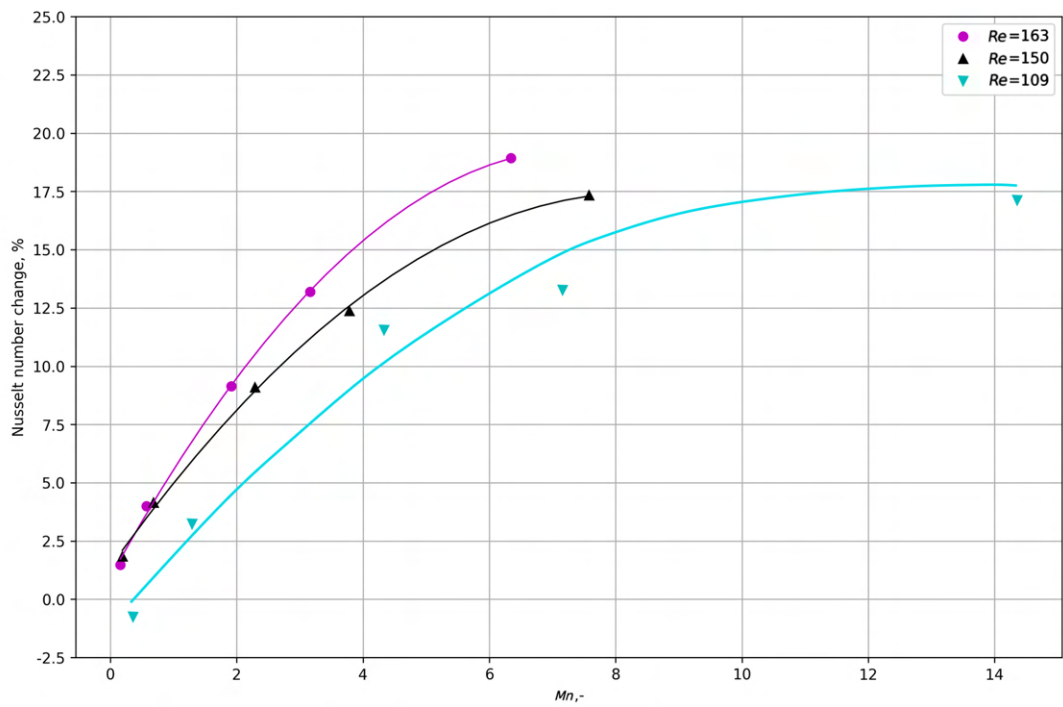


a)

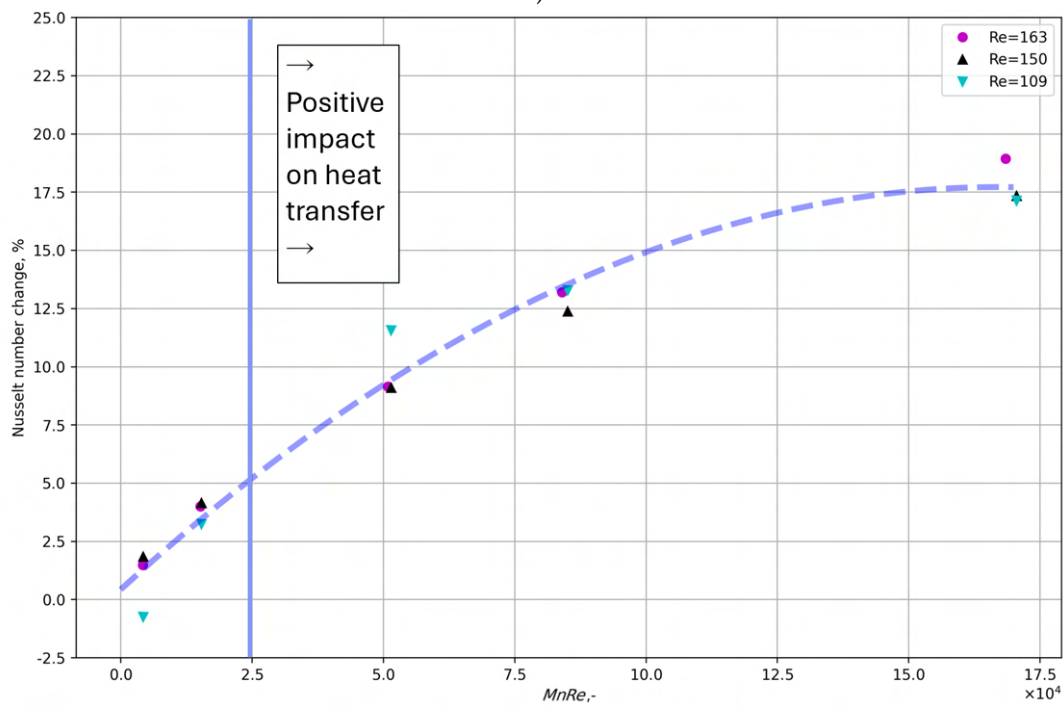


b)

FIGURE 6.11: Relations between dominant forces and Nusselt number change in a ferrofluid flow affected by a magnet placed above the test tube. Graph a) presents the relation between Nusselt number change and Mn , graph b) the relation between Nusselt number change and $MnRe$. Cyan, downward pointing triangles denote flow for $Re = 109$, black, upward pointing triangles for $Re = 150$ and magenta dots for $Re = 163$ [142]



a)



b)

FIGURE 6.12: Relations between dominant forces and Nusselt number change in a ferrofluid flow affected by a magnet placed under the test tube. Graph a) presents the relation between Nusselt number change and $Mn,-$, graph b) the relation between Nusselt number change and $MnRe,-$. Cyan, downward pointing triangles denote flow for $Re = 109$, black, upward pointing triangles for $Re = 150$ and magenta dots for $Re = 163$ [142].

in the Nusselt number change in the $MnRe$ range investigated. For the $Re = 109$, the combination of high magnetic field strength and low medium velocity provides two times higher Nusselt number decrease. This analysis does not indicate that the flows are similar in the Mn number range of 0.58 to 3.2. It is hypothesized that for the flow at $Re = 109$, a different interaction mechanism between the magnetic field and ferronanoparticles occurred. That is projected by much higher heat transfer deterioration for high Mn number values. The critical values at which the Nusselt number change exceeds 5% are $MnRe = 32,000$ for $Re = 109$ and $MnRe = 88,000$ for $Re = 150$ and 163.

Fig. 6.12 a) presents the relationship between the Nusselt number change and the Mn number at the position of the fifth thermocouple in a flow affected by a magnet placed under the test tube. The increase of the Nusselt number in this configuration is unaffected by the fluid velocity within the investigated Reynolds number range. It is important to note that viscosity through the experiments remained similar, due to the consistent use of the same ferronanofluid. For the flow affected by a magnet placed under the tube, the calculation of the Mn number alone does not allow to describe the change of the Nusselt number. The determination of the critical Mn value for which the heat transfer is affected is also not possible.

The $MnRe$ number (Fig. 6.12b) enables such determination. The measured values collapse on a single curve, meaning that the Nusselt number change can be determined independently from the Re number. Only the magnetic field strength influences the heat transfer. The critical value above which the heat transfer improves by 5% is $MnRe = 24,000$. In comparison to the results obtained for the magnet above the test section, there is no change in the mechanism of magnetic field interaction with the ferronanofluid.

6.8 Chapter summary

The key findings for a horizontal laminar flow of ferronanofluid follow:

- The effect of the magnetic field orientation in relation to gravity in a temperature gradient induced secondary motions defines the change of the heat transfer. Positioning the magnet under the test tube leads only to an increase in the Nusselt number, while above, only to a decrease. A magnetic field of 60 A cm^{-1} generated by a magnet positioned above the test section reduces the local Nusselt number by 15%. A magnet positioned under the test section increases the local Nusselt number by 17.5%. This is a result of magnetic force, which, when acting in the same direction as the stronger mass transfer component of vortex in the secondary motion, amplifies the motion and increases the flow of colder fluid from the flow core. A magnet located above the tube attracts ferronanoparticles in the opposite direction to that component, and therefore worsens the heat transfer.

- The influence of a magnetic field interaction with the ferronanofluid on heat transfer is most prominent in the closest vicinity of the magnet, and the effect intensifies with increasing magnetic field strength. Using the introduced similarity numbers, the critical values below which the effect on heat transfer is negligible were identified. It was found that these values depend on the orientation of the magnetic field and the mechanism of interaction between the magnetic field and the ferronanofluid. Taking the 5% Nusselt number change as the threshold, the critical value for the orientation of magnet above the tube is $MnRe = 24,000$, while for the configuration with the magnet below the tube are $MnRe = 32,000$ for $Re = 109$ and $MnRe = 88,000$ for $Re = 150$ and 163 .
- The magnetic field interaction effect dissipates in the flow, causing the Nusselt number to return to the initial value. That is caused by viscous dissipation and superparamagnetism of ferronanoparticles. Increase of the Re number extends the distance of magnetic field interaction effect.
- At the lowest investigated $Re = 109$ and the highest tested magnetic field strength of 60 A cm^{-1} acting against the secondary motion, the reduction in the local Nusselt number is shifted relative to cases with $Re = 150$ and 163 . This is due to a change in the mechanism of interaction of the magnetic field and ferronanoparticles.

Chapter 7

Effect of inclination on heat transfer

This chapter presents the investigation of the impact of flow inclination and the influence of a magnetic field on heat transfer. The experiments were conducted at four Reynolds number values of 106, 185, 264, and 397 and inclination angles of 30°, 60°, and 90°. That was performed in two experimental series. The first series examined heat transfer in an upward flow, analyzing how changes in flow direction relative to gravity influence mixed convection. The second series investigated the potential to modify heat transfer using a static magnet installed on the test section in configurations above and below the test tube.

7.1 Experimental setup and methods

The setup used for this experiment is identical to that employed in the investigation of horizontal ferronanofluid flow. The device is constructed to allow inclination of the main test section, as depicted in the Fig. 7.1. It utilizes flexible Teflon hoses connecting the test section with stationary hardware, allowing the test tube to be mounted on a rail that can be rotated from a horizontal to a vertical position.

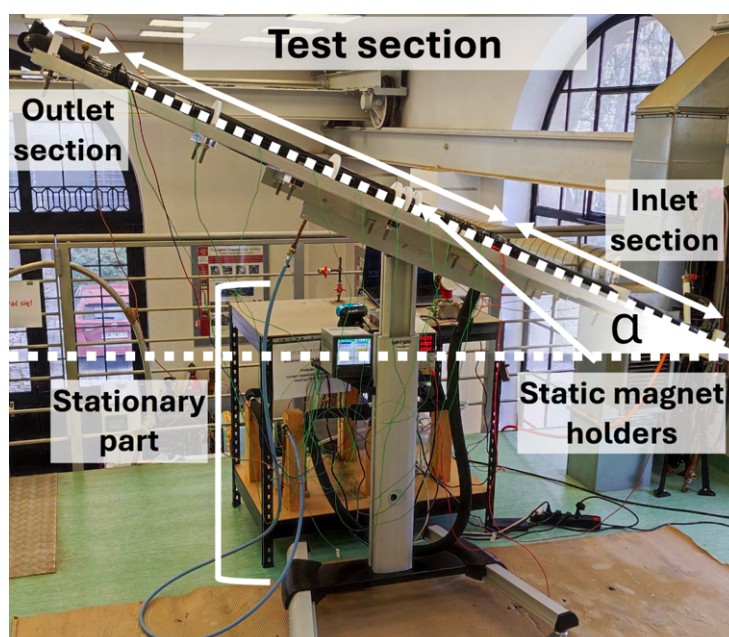


FIGURE 7.1: Photo of experimental setup for inclined configurations [146].

The method used to calculate the local Nusselt number is identical to that used for horizontal flow in the previous chapter. However, the description of Nusselt number change was adjusted:

$$Nu_{\%} = \frac{Nu_{inf} - Nu_{base}}{Nu_{base}} \cdot 100\% \quad (7.1)$$

Where Nu_{inf} is the calculated Nusselt number for inclined ferronanofluid flow with a magnetic field, Nu_{base} is the calculated Nusselt number for inclined ferronanofluid flow without a magnetic field.

To analyze the effect of inclination on the Nusselt number, fitting functions were used to approximate the data. To minimize the mean square error, the data was divided into two groups, corresponding to the different physical phenomena occurring in the flow (Fig. 7.2., part one - conduction, part two - mixed convection). An exponential function was used for the conduction part, while a third-degree polynomial was applied to the mixed convection part. The average Nusselt number value over the corresponding intervals was calculated using the following equation:

$$f_{avg} = \frac{1}{b-a} \int_a^b f(x) dx \quad (7.2)$$

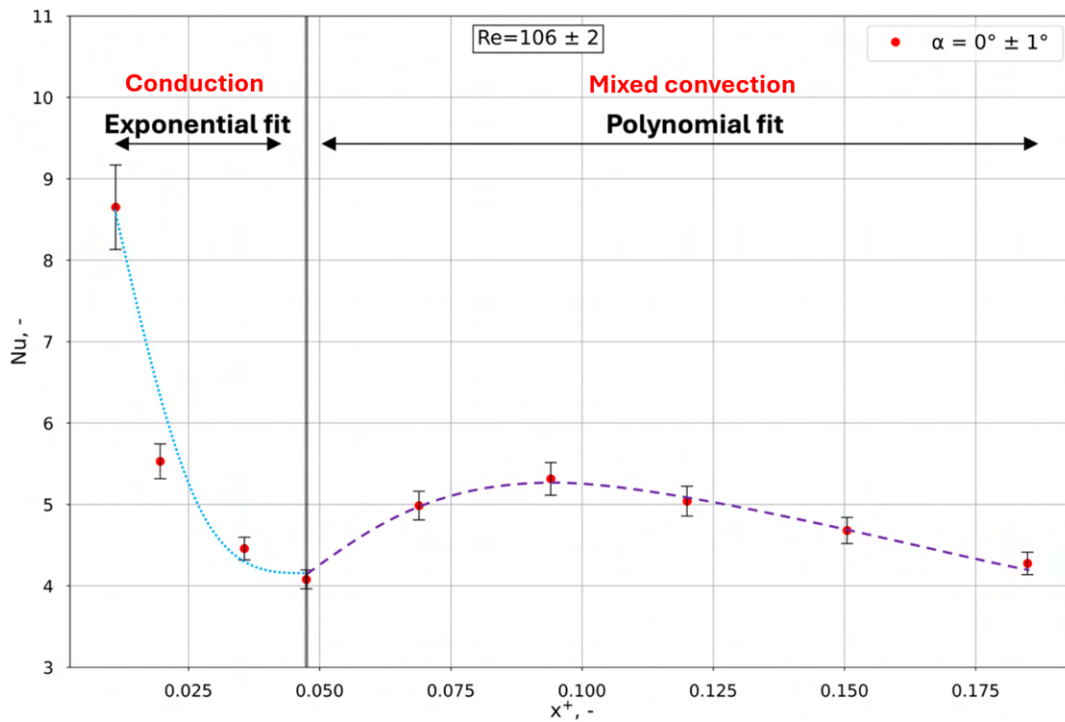


FIGURE 7.2: Example fits of the experimental data. The exponential fit is used in the pure conduction part. The polynomial fit is used in the part where mixed convection is involved [146].

7.2 Mixed convection in inclined flow

The emergence of mixed convection depends on the contribution of the temperature gradient. To determine its occurrence, flow maps determining the convection regime were established in the past [104, 105]. Figs. 7.3 and 7.4 show the position of the studied ferrofluid flows within the maps. The blue dots represent data points recorded at the 4th thermocouple position, just prior to the onset of mixed convection. These data are representative for both flows investigated, with and without the presence of a magnetic field.

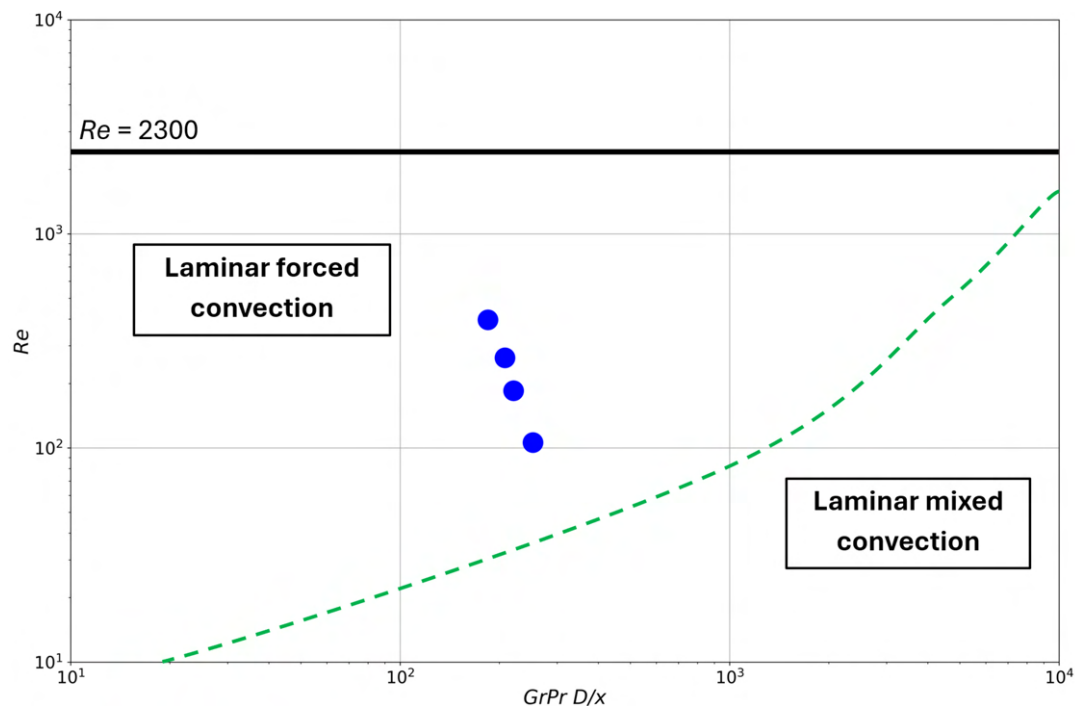


FIGURE 7.3: The position of the experimental data on the flow maps created by Metz and Eckert [104] for horizontal flow. The blue points represent the flows considered in this study, green dashed lines represent expected boundaries between flow regimes [146].

The data points in the graphs indicate the regime of forced convection for each investigated Reynolds number, well below the natural transition to the turbulent regime. Similar conclusions can be drawn from the investigation of Ghajar and Tam [105], who presented updated flow maps for the uniform wall heat flux condition based on their earlier research [106]. In this case, the results also fall within the forced convection regime. This may be due to the range of flow conditions used to derive the equation separating forced and mixed convection regimes ($Re = 280 - 49000$, $Pr = 4 - 158$, $Gr = 1000 - 2.5 \cdot 10^5$). The Grashof number values investigated in this study are outside this range and only one value of the Reynolds number is within it (Tab. 7.1). However, the authors noted that in each of the cases where mixed convection took place, it became apparent at distances of $20 < x/d_{in} < 70$ (x is the distance from the inlet to the test section, d_{in} is the inner diameter of the tube). This is consistent with the results presented here (Fig. 7.5, $x/d_{in} = 41$). Rudl et al. [83] also observed mixed

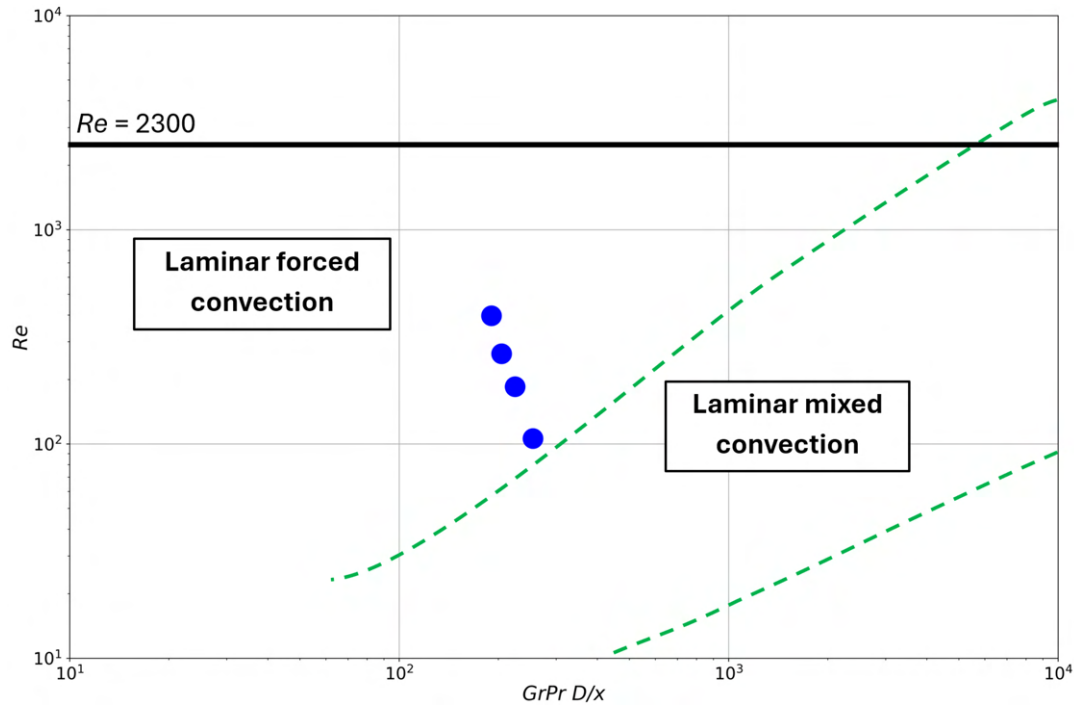


FIGURE 7.4: The position of the experimental data on the flow maps created by Metais and Eckert [104] for vertical flow. The blue points represent the flows considered in this study, green dashed lines represent expected boundaries between flow regimes [146].

convection in ferronanofluid flow under similar conditions (horizontal ferronanofluid flow, $Re = 126.4$, $Gr = 603$, $GrPr = 8100$).

Re	Angle	Pr	Gr	$GrPr$
106	0°	16.2	636	10,300
	90°	16.3	639	10,400
185	0°	16.9	533	9,000
	90°	16.9	544	9,190
264	0°	17.2	494	8,500
	90°	17.2	484	8,320
397	0°	17.4	433	7,530
	90°	17.4	447	7,780

TABLE 7.1: The calculated values of Prandtl number (Pr), Grashof number (Gr), and their product ($GrPr$) for different Reynolds numbers (Re) and inclination angles (0° and 90°). These parameters were evaluated at the 4th thermocouple position in the test section. The green color indicates values that fall within the range used to create the map presented in [105], the red color signifies values outside this range.

Everts et al. [147] compared their measurements with the flow regime map by Metais and Eckert [104]. Although the Nusselt number values suggested the presence of free convection effects, all the data fell within the forced convection zone. A similar situation was observed with a map developed by Tam et al. [148]. Based on this, the authors concluded that existing flow regime maps are insufficient to describe low Prandtl number flows in tubes with small diameters. As a result, they generated new flow maps for developed and developing flows within the following parameter

ranges: $Re = 502 - 2936$, $Pr = 3 - 139.5$, $Gz = 2.7 - 1241$, $Gr = 106 - 4.2 \cdot 10^5$, $Gr^* = 596 - 7.0 \cdot 10^6$. Unfortunately, the Reynolds number range in this study falls below the range for which Everts et al. generated the new maps, making it impossible to unequivocally confirm mixed convection based on their findings. However, the high Nusselt number values observed clearly indicate the presence of mixed convection, highlighting the need to update the maps with a new data.

Current flow regime maps do not adequately describe flows under low Reynolds number conditions. More experimental data are needed to identify the new critical conditions for regime transitions. Additionally, for nanofluids, the analysis is further complicated by the presence of solid particles. Colla et al. [107] observed that for TiO_2 water-based nanofluid, the deviation from the analytical solution occurs farther along the flow than for water, and the heat transfer impact of mixed convection is significantly weaker. The authors attributed this effect to Brownian motion and thermophoresis, which cause local fluid temperature equalization, and concluded that single-phase models are insufficient to describe the convection process in nanofluids. These results contradict the findings of Utomo et al. [108], who observed that the results for alumina and titania nanofluids were similar to those obtained for water, suggesting that the single-phase model is sufficient to predict the thermal performance of nanofluids.

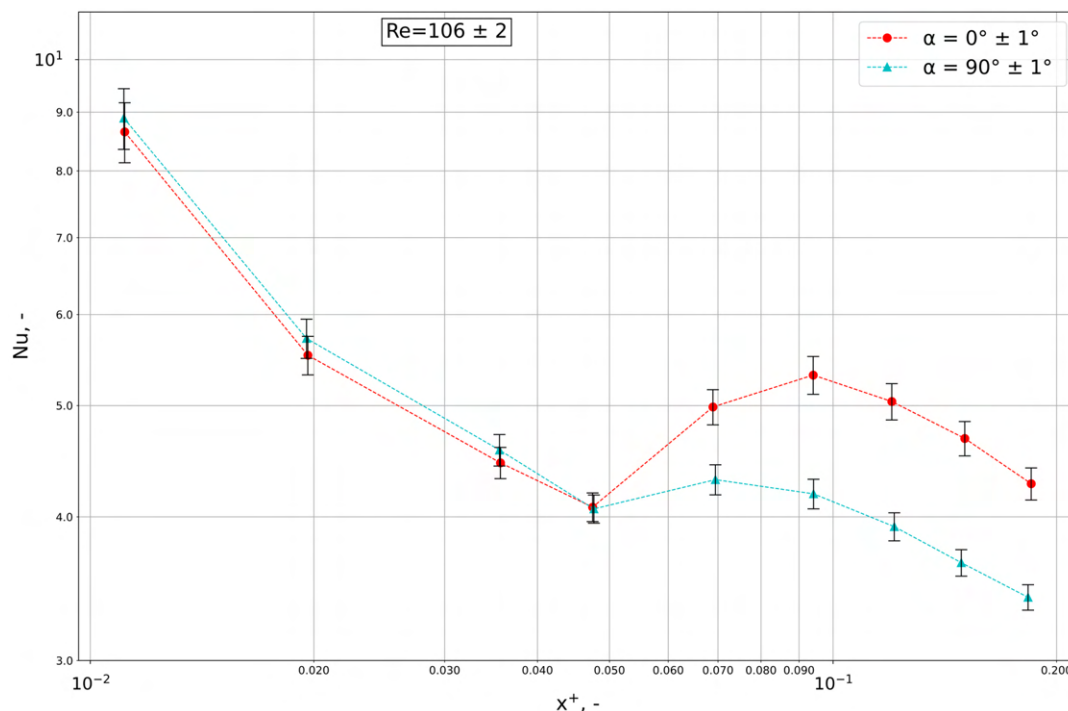


FIGURE 7.5: Development of the local Nusselt number along the test section relative to the dimensionless axial distance x^+ . Red dots represent the horizontal flow for $Re = 106$ without the presence of a magnetic field. Cyan triangles represent the vertical flow for $Re = 106$ without the presence of a magnetic field [146].

Fig. 7.5 compares the change in the local value of the Nusselt number for two orientations of the test tube, horizontal ($\alpha=0^\circ$), and vertical ($\alpha=90^\circ$) with upward flow.

The curves represent the aggregated data shown in Fig. 7.6. The values of the Nusselt number in the R1 region for both configurations are similar, within the measurement error. In the mixed convection region, there is a decrease in the Nusselt number for the vertical orientation. Although the vertical position results in reduced heat transfer compared to horizontal flow, a noticeable change in the Nusselt number occurs. This shift requires an alternative explanation, as the configuration of the flow and gravity differs from the horizontal case.

In non-vertical flows with mixed convection, lower-temperature fluid is expected to move toward the region near the wall, increasing the temperature gradient and enhancing heat transfer. In the ideal vertical orientation of the flow, the direction of the buoyancy force is in line with the fluid flow, making mixed convection unlikely. Nevertheless, heat transfer enhancement is evident.

This can be attributed to the fact that the buoyancy force remains present and increases the velocity of the fluid near the wall [114]. The other reason can be the formation of flow profile distortions caused by fluid heating, as shown in [112]. In this study, every effort was made to ensure that the tested inclination accurately represents the angle between the flow vector and gravity. However, factors such as measurement inaccuracies, test tube curvature, or deflection could lead to a mismatch between these vectors, promoting fluid circulation instead of a simple increase in fluid velocity near the wall. For the vertical position, the increase in the Nusselt number may also result from mass transfer. The analysis of the Nusselt number variation along the test section (Fig. 7.5) revealed that the curve's shape is flattened but remained similar to that of the horizontal configuration. While flow instabilities may have occurred in the tested case, the radial mixing component is significantly weaker than in horizontal flow.

Fig. 7.6 presents the change in the averaged value of the Nusselt for the investigated inclinations and Reynolds number values. For the lowest Reynolds number values, $Re = 106$ and $Re = 185$, the contribution of mixed convection to the averaged Nusselt number is the highest. Increased inclination weakens the mixing process, causing the Nusselt number to drop. As the Reynolds number increases, this negative effect diminishes and disappears entirely for Reynolds numbers above 264.

7.3 Magnetic field effect on inclined flow heat transfer

Fig. 7.7 illustrates the impact of a permanent magnet on the local Nusselt number in vertical upward flow. The distribution confirms the localized nature of the interaction between the permanent magnet and the flowing medium, as evidenced by changes in the Nusselt number at the 5th and 6th thermocouple positions. Heat transfer improves for both magnet configurations, whether placed above or below the test section. These findings indicate that conclusions from horizontal flow studies in the previous chapter and in [83] are not directly applicable to vertical flow. In vertical flow, heat transfer enhancement occurs with both magnet configurations. In horizontal

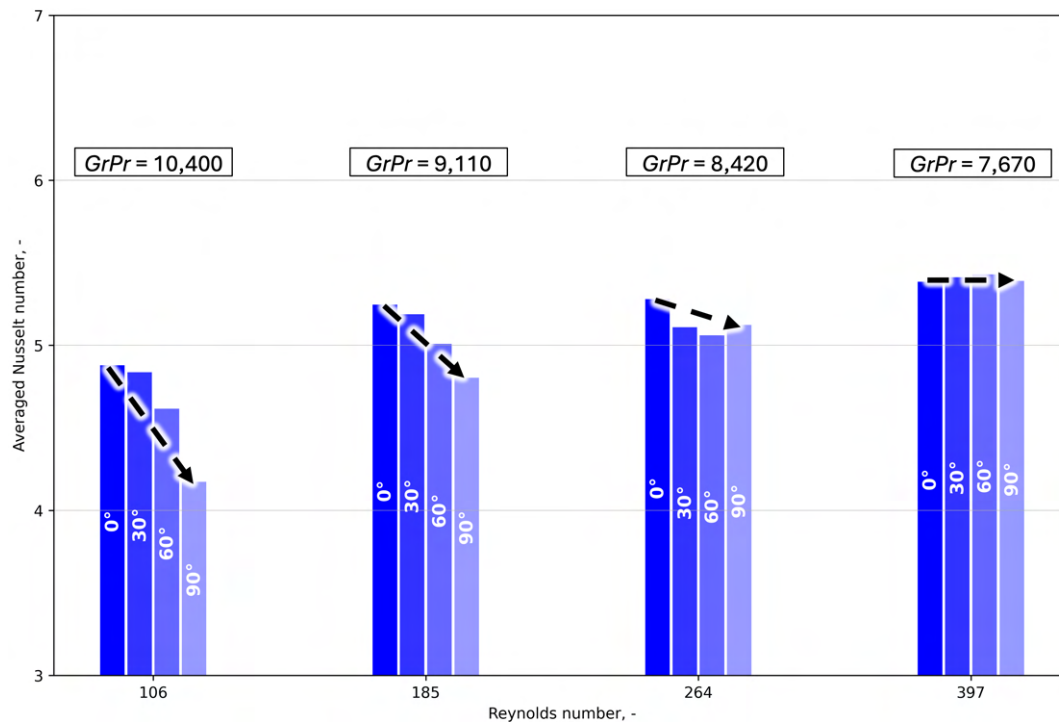


FIGURE 7.6: The averaged Nusselt number for the entire test section as a function of both Reynolds number and inclination angle. Inclination of (0°) represents horizontal flow, (90°) vertical upward flow [146].

flow, this holds true only when a magnet is placed under the test tube, as it intensifies mixed convection. By analogy, the enhanced heat transfer in vertical flow must be caused by improved mass transfer for both magnet configurations. This indicates that vertical mass transfer in mixed convection is symmetrical and that the flow disturbances observed in [112] are less affected by the magnetic field orientation.

Orfi et al. [149] in their study on laminar mixed convection in inclined tubes, provided insights into the development of secondary flow structures and the potential formation of two- and four-vortex patterns. The authors noted that the circumferentially averaged Nusselt number is insensitive to vortex patterns in mixed convection, making it nearly impossible to deduce flow patterns based solely on the Nusselt number. Above a certain critical inclination angle, a two-vortex structure is a stable solution. The analysis indicated that as the inclination increases, the vortex center moves upward, and the flow field became nearly symmetrical at the highest investigated angle of 80° .

This study's results and methods do not allow for determining which vortex structure was present at each tested inclination, even though this is crucial for explaining the changes in the magnetic field's effect on heat transfer. It is hypothesized that between angles of 60° and 90° , the flow structure changed or the vortices shifted to positions where the magnet orientations produced similar effects on the averaged Nusselt number.

Figs. 7.8, 7.9, 7.10 illustrate the effects of permanent magnet positions on the averaged Nusselt number in the mixed convection zone for the tested inclinations.

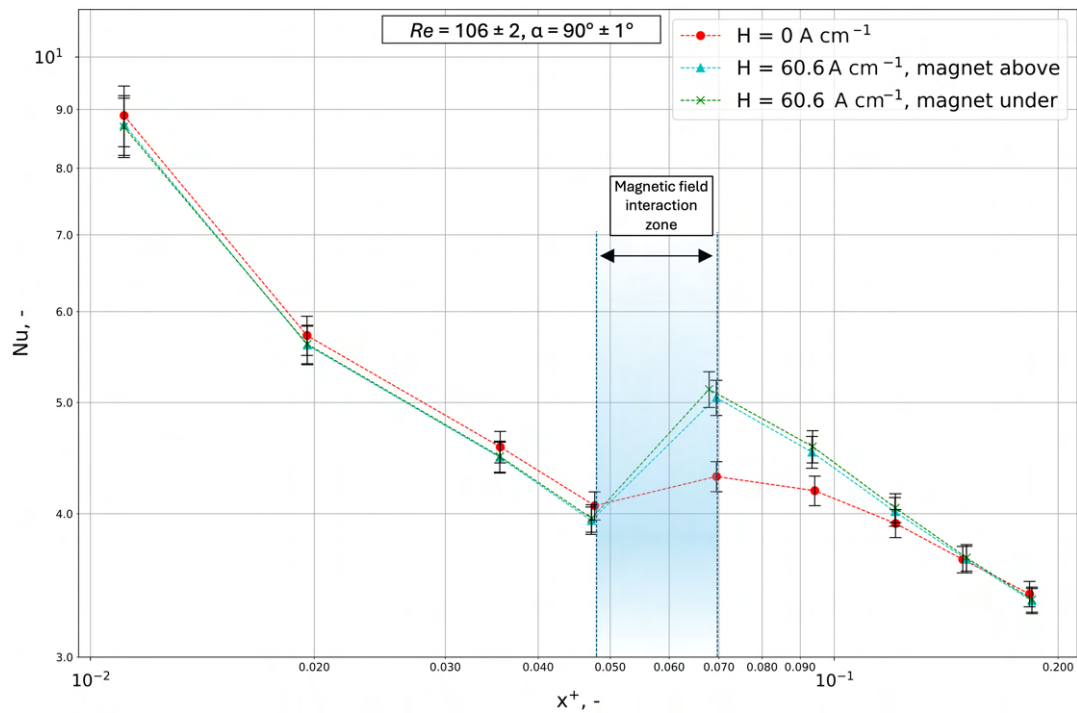


FIGURE 7.7: Development of the local Nusselt number along the test section relative to the dimensionless axial distance x^+ . Red dots represent the vertical flow for $Re = 106$ without the presence of a magnetic field. Cyan triangles represent the vertical flow for $Re = 106$ with a static magnet placed above the test tube (in relation to horizontal position of the test tube). Green crosses represent the vertical flow for $Re = 106$ with a static magnet placed under the test tube (in relation to horizontal position of the test tube) [146].

These figures include a horizontal dashed line marking a 2.5% threshold to exclude negligible magnet effects on heat transfer.

At 30° (Fig. 7.8), none of the magnet configurations produced a significant positive effect on heat transfer across the entire Reynolds number range studied. For Reynolds number of 185, when the magnet is positioned above the tube, heat transfer deteriorated, although this effect decreased as Re increased. However, as shown in Fig. 7.6, an inclination of 30° did not introduce a significant deterioration in heat transfer. Based on the observed magnetic field effect, it is not recommended to use magnets in order to enhance heat transfer.

The increase of inclination to 60° (Fig. 7.9) yielded results similar to those at 30° . For a magnet placed above the tube, the greatest deterioration in heat transfer occurred for $Re = 185$ and decreased with increasing Re . A magnet placed under the tube had no effect on the averaged heat transfer for Reynolds numbers ranging from 185 to 397. For $Re = 106$, the situation differed from that at 30° and aligned with the findings from the horizontal flow investigation. It should be noted that the relationship between the flow direction and gravity changed, resulting in a different mass transfer pattern in mixed convection. However, the result obtained for 60° inclination, combined with the simulation results of mixed convection reported by Utomo et al. [108] and the analysis presented in the investigation on the horizontal

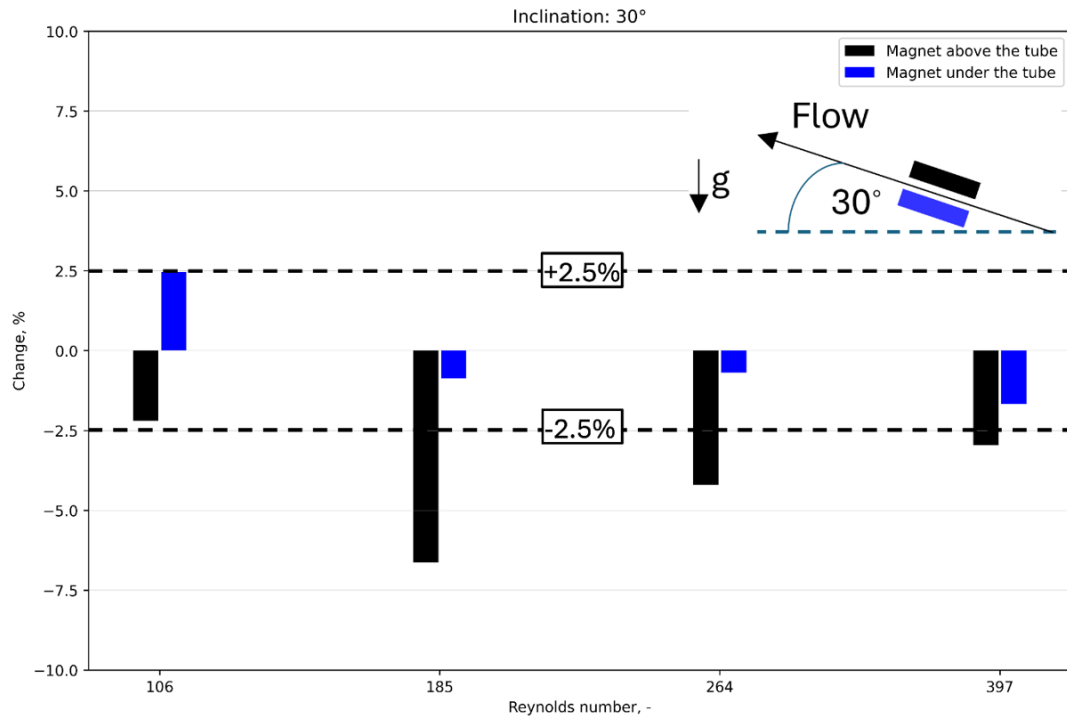


FIGURE 7.8: Change of the averaged Nusselt number for the test section inclined at 30° under the influence of a magnetic field [146].

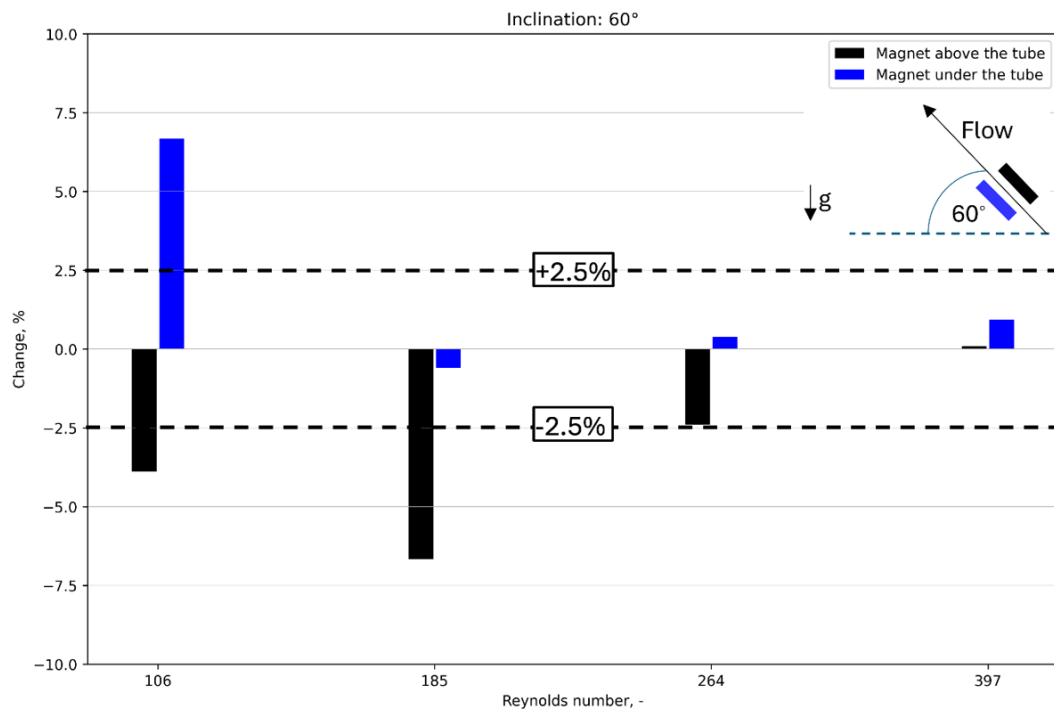


FIGURE 7.9: Change of the averaged Nusselt number for the part of the test section inclined at 60° under the influence of a magnetic field [146].

flow, indicate that the magnetic field counteracted or assisted the mass transfer that occurred in the flow.

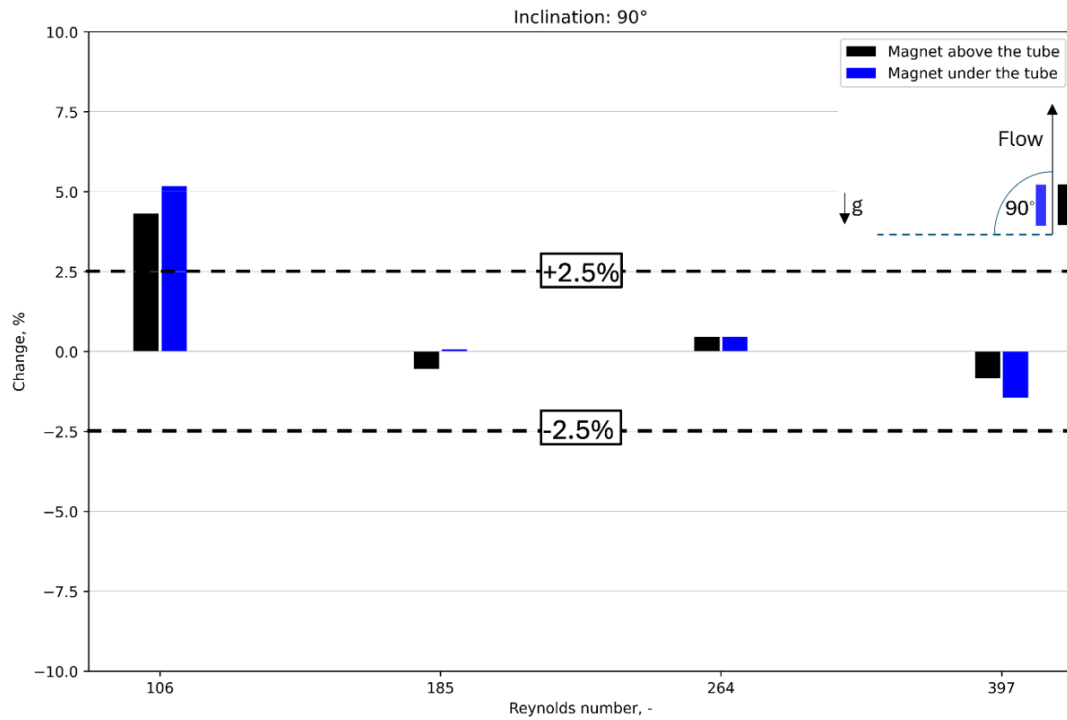


FIGURE 7.10: Change of the averaged Nusselt number for the part of the test section inclined at 90° under the influence of a magnetic field [146].

The effect of the magnetic field on vertical flow (Fig. 7.10), regardless of the permanent magnet's position, has no significant effect on flows with Reynolds numbers ranging from 185 to 397. It neither enhanced heat transfer performance in upward flows for $Re \geq 264$ nor mitigated the deterioration observed at $Re = 185$ (Fig. 7.6). For flow characterized by $Re = 106$, the situation differed, also from horizontal flow studies. Both magnet configurations resulted in a comparable 5% increase in the average Nusselt number.

7.4 Chapter summary

Key findings regarding inclined laminar ferronano fluid flow:

- Mixed convection occurred in the ferronano fluid flow under all investigated conditions, as evidenced by the increase in the local Nusselt number. These results do not align with the flow regime maps available in the literature, which indicate a different flow regime. Therefore, the maps should be updated with additional measurement data to enhance their applicability.
- The flow inclination for $Re = 106$ and 185 leads to a deterioration of heat transfer. For the vertical flow, averaged Nusselt number is decreased by 14% for $Re = 106$ and 7% for $Re = 185$. This is due to the weakening of secondary motion, reaching a minimum in a vertical position. The negative effect of inclination decreases with increasing Reynolds number, and from $Re = 264$ it is marginal.
- The possibility of improving heat transfer in an inclined flow with a permanent magnet is limited. The maximum achieved change of the averaged Nusselt number is 7%. In addition, the choice of magnetic configuration requires the knowledge of mass transfer in mixed convection for a given spatial orientation.
- Mixed convection's influence on heat transfer is present in vertical flow, despite the alignment of flow and gravity vectors. The cause is the fluid velocity increase at the wall, rather than the transport of the medium from the flow core to near the exchanger wall, as in horizontal flow.
- The vertical flow is symmetrical, the change in heat transfer is independent of the position of the magnet, unlike other inclinations and the horizontal orientation of the test section.

Chapter 8

Conclusions

This dissertation explores the application of ferronanofluids in convective heat transfer. The introduction underscores the necessity for novel solutions to improve heat exchange efficiency and why the use of nanofluids is a promising direction. The literature review reveals that the underlying reasons for the enhanced heat transfer performance of nanofluids remain unclear. This ambiguity is undoubtedly due to the wide variety of nanoparticle types. The next section features studies employing nanofluids in heat transfer scenarios. The section highlights the key challenges hindering their application and widespread use. In addition to sharing the general properties of nanofluids, ferronanofluids are uniquely responsive to magnetic fields. This allows to influence mass and heat transfer. However, the additional magnetic force introduces complexities in analyzing the flow dynamics. The third chapter presents a literature review on ferronanofluid flows in the presence of a magnetic field. Three interaction mechanisms between the magnetic field and ferronanoparticles are identified: wall aggregation, chain formation, and secondary motions. The influence of three forces: inertia, magnetic, and viscous, complicates the explicit determination of the interaction mechanism and requires systematization using similarity numbers. Mixed convection flows deserve special attention, as the current state of knowledge does not provide answers regarding this phenomenon for low Reynolds and Grashof numbers. Despite the common occurrence of inclined flow in real-world applications, the current knowledge on inclined nanofluid flows is limited, and the impact of flow inclination on heat transfer remains unclear.

To address these issues, three experimental series are conducted, presented in chapters 5 to 7. The first series involves experiments defining the influence of the magnetic field on the dynamics of the ferronanofluid droplet and ferronanoparticle distribution under a magnetic field. This is done using a contact angle measurement setup equipped with coils providing a magnetic field. The main conclusions from these experiments are as follows:

- Two instantaneous regimes of a magnetic field and the ferronanofluid droplet interaction are found. Both depend on the strength of the magnetic field. For a magnetic Bond number $Bo_m < 2.5$, the pinning-fixed regime is present. Here, the contact angle increases, but the droplet radius remains unchanged. For $Bo_m > 2.5$, the droplet enters a metastable state where an additional de-pinning

regime occurs. This regime is characterized by a decrease in the contact angle and a stretch of the droplet in the direction of the coils. In addition the droplet's transition from the pinning-fixed regime into the de-pinning regime over time is possible.

- The influence of the magnetic field during the drying process of the drops is reflected by the final crack pattern. In magnetic field free environments, cracks form due to elastic stresses. The application of a magnetic field introduces additional magnetic stress. The latter can order the magnetite particles and therefore lead to development of cracks that follow the direction of a magnetic field. The effect of an elongated droplet shape changes in crack alignment is negligible.
- The correlation of increasing pad size with increasing magnetic field strength is noted. The number of circumferential cracks caused by the radial stress component decreases under the magnetic field. The cause for this is seen in the ferronanoparticle ordering, which increases the critical stress required for a crack to develop.

The sixth chapter presents results concerning the laminar horizontal flow of ferronanofluid under the influence of a magnetic field. The experiments are conducted using an experimental setup that allows the magnetic field interaction with the flowing ferronanofluid. The conclusions from the experiments are as follows:

- The effect of the magnetic field orientation in relation to gravity defines the change of the heat transfer. Locating the magnet under the test tube can only lead to an increase of a Nusselt number, while above, only to a decrease. A magnetic field of 60 A cm^{-1} generated by a magnet positioned above the test section reduces the local Nusselt number by 15%. A magnet positioned under the test section increases the local Nusselt number by 17.5%.
- Based on the introduced similarity numbers, the critical values below which the effect on heat transfer is negligible were identified. For the magnet placed under the test section, this value is $MnRe = 25,000$. For the configuration with the magnet placed above the section, it is $MnRe = 32,000$ for $Re = 109$, and $MnRe = 88,000$ for $Re = 150$ and 163 . It was found that these values depend on the orientation of the magnetic field and the mechanism of interaction between the magnetic field and the ferronanofluid.
- The magnetic field interaction effect dissipates in the flow, causing the Nusselt number to return to the initial value. That is caused by viscous dissipation and superparamagnetism of ferronanoparticles. Increase of the Re number extends the distance of magnetic field interaction effect.
- At the lowest investigated $Re = 109$ and the highest tested magnetic field strength of 60 A cm^{-1} acting against the secondary motion, the reduction

in the local Nusselt number is shifted relative to cases with $Re = 150$ and 163 . This is due to a change in the mechanism of interaction of the magnetic field and ferronanoparticles.

The third series of measurements concerns inclined flow. The experiments are conducted on the same setup as experiments on horizontal flow, as it was designed to allow the test section rotation. The conclusions drawn from these studies:

- Mixed convection occurred in the ferronanofluid flow under all investigated conditions, as evidenced by the increase in the local Nusselt number. These results do not align with the flow regime maps available in the literature, which indicate a different flow regime. Therefore, the maps should be updated with additional measurement data to enhance their applicability.
- The flow inclination for $Re = 106$ and 185 leads to a deterioration of heat transfer. For the vertical flow, averaged Nusselt number is decreased by 14% for $Re = 106$ and 7% for $Re = 185$. This is due to the weakening of secondary motion, reaching a minimum in a vertical position. The negative effect of inclination decreases with increasing Reynolds number, and from $Re = 264$ it is marginal.
- The possibility of improving heat transfer in an inclined flow with a permanent magnet is limited. The maximum achieved change of the averaged Nusselt number is 7%. In addition, the choice of magnetic configuration requires knowledge of mass transfer in mixed convection for a given spatial orientation.
- Mixed convection's influence on heat transfer is present in vertical flow, despite the alignment of flow and gravity vectors. The cause is the fluid velocity increase at the wall, rather than the transport of the medium from the flow core to near the exchanger wall, as in horizontal flow.
- The vertical flow is symmetrical, the change in heat transfer is independent of the position of the magnet, unlike other inclinations and the horizontal orientation of the test section.

The experimental research conducted in this dissertation has verified the stated theses, offering both qualitative and quantitative insights into the complex interplay of forces influencing heat transfer in ferronanofluid flows:

- **Understanding the relationships between viscous, inertial, magnetic, and gravitational forces is crucial for assessing ferronanofluids' impact on convective heat transfer. These relationships can be described by appropriate similarity numbers that express the ratio of forces that affect the flow of ferronanofluids.**

The analysis demonstrated that the determination of the force balance can be used to predict heat transfer in ferronanofluid flow. The systematization of forces can be done using similarity numbers, as shown with the introduced Mn

number, which relates magnetic forces to inertial forces, and $MnRe$ number, which relates magnetic to viscous forces.

- **For any ferronanofluid, certain critical value of introduced similarity number reflects the potential to affect heat transfer.**

Critical values of the $MnRe$ number were identified beyond which magnetic fields noticeably influence heat transfer. These values depend on the orientation of the magnetic field and the mechanism of interaction between the magnetic field and the ferronanofluid.

- **The mutual orientation of gravity and the flow direction of ferronanofluid in various spatial configurations influences the development of secondary motions, which can either enhance or reduce heat transfer.**

It was shown that flow inclination affects secondary motions and, consequently, heat transfer. The flow inclination led to a deterioration in heat transfer for $Re = 106$ and 185 due to weakened secondary motions. The negative effect diminished at higher Reynolds numbers. Mixed convection was present in vertical flow conditions, highlighting the significance of flow orientation in determining heat transfer performance.

- **The external magnetic field intensifies or suppresses secondary motions in various spatial configurations, and thus allows to actively influence heat transfer.**

The experiments demonstrated that magnetic fields can both enhance and suppress heat transfer, depending on the flow orientation. The possibility of improving heat transfer in an inclined flow with a permanent magnet is limited. The choice of magnetic configuration to achieve desired effect requires knowledge of mass transfer in mixed convection for a given spatial orientation.

In summary, the experimental results substantiate the dissertation's hypotheses, providing a deeper understanding of the force interactions in ferronanofluid flows and highlighting practical pathways for optimizing heat and mass transfer using controlled magnetic fields.

An outline for future scientific efforts on ferronanofluid heat transfer experiments emerges from the conclusions of this dissertation. The research should prioritize the exploration of dynamically controlled magnetic fields to enable continuous control over the transfer of ferronanoparticles with respect to mixed convection. Comprehensive studies are essential to understand the interaction between the magnetic field and ferronanofluid flow, aiming to establish magnetic-flow maps and identify critical similarity numbers where the interaction mechanisms change. Integrating these data with heat transfer and pressure drop analyses will enable the identification of optimal flow conditions.

The interplay between the magnetic field and inclined mixed convection flow influences heat transfer. However, determination of the impact on heat transfer

requires insights into the mass transfer induced by free convection. To effectively control heat transfer in ferronanofluid inclined flow, further investigations are required. The research should target the mass transfer in inclined flows of ferronanofluids to determine the optimal magnetic field for heat transfer. Further experiments need to employ dynamically controlled magnetic fields of varying intensities and orientations. Nevertheless, the process of mixed convection in nanofluids is complex and necessitates deeper investigation, particularly at low Reynolds number values, to accurately determine flow regimes.

Bibliography

- [1] Warren M.. Rohsenow, J. P. Hartnett, and Young I.. Cho. *Handbook of heat transfer*. McGraw-Hill, 1998. ISBN: 9780070535558.
- [2] Elsevier B.V. *Search engine results from the website <https://www.sciencedirect.com/>*. Oct. 2024.
- [3] Stephen U.S. Choi and Jeffrey A. Eastman. "Enhancing thermal conductivity of fluids with nanoparticles". In: *American Society of Mechanical Engineers, Fluids Engineering Division (Publication) FED 231* (1995), pp. 99–105.
- [4] Sarit K. Das, Stephen U. S. Choi, Wenhua Yu, and T. Pradeep. *Nanofluids*. Wiley, July 2007, pp. 1–397. ISBN: 9780470074732. DOI: [10.1002/9780470180693](https://doi.org/10.1002/9780470180693). URL: <https://onlinelibrary.wiley.com/doi/book/10.1002/9780470180693>.
- [5] Gianluca Puliti, Samuel Paolucci, and Mihir Sen. "Thermodynamic properties of gold-water nanolayer mixtures using molecular dynamics". In: *Journal of Nanoparticle Research* 13.9 (2011), pp. 4277–4293. ISSN: 1572896X. DOI: [10.1007/s11051-011-0373-4](https://doi.org/10.1007/s11051-011-0373-4).
- [6] Vincenzo Bianco, Oronzio Manca, Sergio Nardini, and Kambiz Vafai. *Heat Transfer Enhancement with Nanofluids*. Ed. by Vincenzo Bianco, Oronzio Manca, Sergio Nardini, and Kambiz Vafai. CRC Press, Apr. 2015, pp. 341–364. ISBN: 9780429171833. URL: <https://www.taylorfrancis.com/books/9781482254020>.
- [7] Hendrik Boertz, Albert Baars, Janusz T. Cieśliński, and Sławomir Smoleń. "Turbulence Model Evaluation for Numerical Modelling of Turbulent Flow and Heat Transfer of Nanofluids". In: *Applied Mechanics and Materials* 831. April (2016), pp. 165–180. DOI: [10.4028/www.scientific.net/amm.831.165](https://doi.org/10.4028/www.scientific.net/amm.831.165).
- [8] Gawęł Żyła. "Viscosity and thermal conductivity of MgO–EG nanofluids: Experimental results and theoretical models predictions". In: *Journal of Thermal Analysis and Calorimetry* 129.1 (2017), pp. 171–180. ISSN: 15882926. DOI: [10.1007/s10973-017-6130-x](https://doi.org/10.1007/s10973-017-6130-x).
- [9] A. Kujawska, B. Zajaczkowski, L. M. Wilde, and M. H. Buschmann. "Geyser boiling in a thermosyphon with nanofluids and surfactant solution". In: *International Journal of Thermal Sciences* 139 (2019), pp. 195–216. ISSN: 12900729. DOI: [10.1016/j.ijthermalsci.2019.02.001](https://doi.org/10.1016/j.ijthermalsci.2019.02.001).

- [10] David C. Venerus et al. "Viscosity measurements on colloidal dispersions (nanofluids) for heat transfer applications". In: *Applied Rheology* 20.4 (2010), p. 2. ISSN: 16178106. DOI: [10.3933/App1Rheol-20-44582](https://doi.org/10.3933/App1Rheol-20-44582).
- [11] Matthias H. Buschmann. "Thermal conductivity and heat transfer of ceramic nanofluids". In: *International Journal of Thermal Sciences*. Vol. 62. 2012, pp. 19–28. DOI: [10.1016/j.ijthermalsci.2011.09.019](https://doi.org/10.1016/j.ijthermalsci.2011.09.019).
- [12] Rosa Mondragón et al. "Experimental characterization and modeling of thermophysical properties of nanofluids at high temperature conditions for heat transfer applications". In: *Powder Technology* 249 (2013), pp. 516–529. ISSN: 00325910. DOI: [10.1016/j.powtec.2013.08.035](https://doi.org/10.1016/j.powtec.2013.08.035). URL: <http://dx.doi.org/10.1016/j.powtec.2013.08.035>.
- [13] Dorota Sawicka, Janusz T. Cieśliński, and Slawomir Smolen. "A comparison of empirical correlations of viscosity and thermal conductivity of water-ethylene glycol-Al₂O₃ nanofluids". In: *Nanomaterials* 10.8 (2020), pp. 1–24. ISSN: 20794991. DOI: [10.3390/nano10081487](https://doi.org/10.3390/nano10081487).
- [14] R. Mulka et al. "Drying silica-nanofluid droplets". In: *Colloids and Surfaces A: Physicochemical and Engineering Aspects* 623 (Aug. 2021), p. 126730. ISSN: 18734359. DOI: [10.1016/j.colsurfa.2021.126730](https://doi.org/10.1016/j.colsurfa.2021.126730). URL: <https://linkinghub.elsevier.com/retrieve/pii/S0927775721005999>.
- [15] R. Mulka, B. Zajączkowski, E. Neuber, and M. H. Buschmann. "Contact angle of the ferronanofluid and influence of the magnetic field on the drying droplet". In: *International Journal of Thermofluids* 14.April (2022), p. 100152. ISSN: 26662027. DOI: [10.1016/j.ijft.2022.100152](https://doi.org/10.1016/j.ijft.2022.100152). URL: <https://linkinghub.elsevier.com/retrieve/pii/S2666202722000180>.
- [16] Patrice Estellé et al. "Current trends in surface tension and wetting behavior of nanofluids". In: *Renewable and Sustainable Energy Reviews* 94.July 2018 (2018), pp. 931–944. ISSN: 18790690. DOI: [10.1016/j.rser.2018.07.006](https://doi.org/10.1016/j.rser.2018.07.006).
- [17] M. H. Buschmann et al. "Correct interpretation of nanofluid convective heat transfer". In: *International Journal of Thermal Sciences* 129 (July 2018), pp. 504–531. ISSN: 12900729. DOI: [10.1016/j.ijthermalsci.2017.11.003](https://doi.org/10.1016/j.ijthermalsci.2017.11.003). URL: <https://linkinghub.elsevier.com/retrieve/pii/S1290072917310748>.
- [18] M. Hernaiz et al. "The contact angle of nanofluids as thermophysical property". In: *Journal of Colloid and Interface Science* 547 (July 2019), pp. 393–406. ISSN: 10957103. DOI: [10.1016/j.jcis.2019.04.007](https://doi.org/10.1016/j.jcis.2019.04.007). URL: <https://linkinghub.elsevier.com/retrieve/pii/S0021979719304229>.
- [19] Agnieszka Kujawska et al. "Impact of Silica Nanofluid Deposition on Thermosyphon Performance". In: *Heat Transfer Engineering* 42.19-20 (Nov. 2021), pp. 1702–1719. ISSN: 0145-7632. DOI: [10.1080/01457632.2020.1818413](https://doi.org/10.1080/01457632.2020.1818413). URL: <https://doi.org/10.1080/01457632.2020.1818413https://www.tandfonline.com/doi/full/10.1080/01457632.2020.1818413>.

- [20] W. C. Elmore. "The magnetization of ferromagnetic colloids". In: *Physical Review* 54.12 (1938), pp. 1092–1095. ISSN: 0031899X. DOI: [10.1103/PhysRev.54.1092](https://doi.org/10.1103/PhysRev.54.1092).
- [21] Papell Solomon Stephen. *US3215572A - Low viscosity magnetic fluid obtained by the colloidal suspension of magnetic particles*. 1963.
- [22] S. Stephen Papell and Otto C Faber. *On the influence of nonuniform magnetic fields on ferromagnetic colloidal sols*. Tech. rep. National Aeronautics and Space Administration.
- [23] Matthias H. Buschmann. "Critical review of heat transfer experiments in ferrohydrodynamic pipe flow utilising ferronanofluids". In: *International Journal of Thermal Sciences* 157.December 2019 (2020), p. 106426. ISSN: 12900729. DOI: [10.1016/j.ijthermalsci.2020.106426](https://doi.org/10.1016/j.ijthermalsci.2020.106426). URL: <https://doi.org/10.1016/j.ijthermalsci.2020.106426>.
- [24] William M. Haynes. *CRC Handbook of Chemistry and Physics*. Ed. by W. M. Haynes, David R. Lide, and Thomas J. Bruno. 97th ed. Vol. 18. 4. CRC Press, June 2016, pp. 115–115. ISBN: 9781315380476. DOI: [10.1201/9781315380476](https://doi.org/10.1201/9781315380476). URL: <https://www.taylorfrancis.com/books/9781498754293>.
- [25] J. Mølgaard and W. W. Smeltzer. "Thermal conductivity of magnetite and hematite". In: *Journal of Applied Physics* 42.9 (1971), pp. 3644–3647. ISSN: 00218979. DOI: [10.1063/1.1660785](https://doi.org/10.1063/1.1660785).
- [26] Xuemei Feng and Drew W. Johnson. "Mass transfer in SiO₂ nanofluids: A case against purported nanoparticle convection effects". In: *International Journal of Heat and Mass Transfer* 55.13-14 (2012), pp. 3447–3453. ISSN: 00179310. DOI: [10.1016/j.ijheatmasstransfer.2012.03.009](https://doi.org/10.1016/j.ijheatmasstransfer.2012.03.009).
- [27] Ismail Tavman et al. "Experimental study on thermal conductivity and viscosity of water-based nanofluids". In: *Heat Transfer Research* 41.3 (2010), pp. 339–351. ISSN: 10642285. DOI: [10.1615/HeatTransRes.v41.i3.100](https://doi.org/10.1615/HeatTransRes.v41.i3.100).
- [28] Jianhong Bao et al. "Viscosity of graphene in lubricating oil, ethylene glycol and glycerol". In: *Journal of Thermal Analysis and Calorimetry* 148.21 (Nov. 2023), pp. 11455–11465. ISSN: 15882926. DOI: [10.1007/s10973-023-12498-2](https://doi.org/10.1007/s10973-023-12498-2).
- [29] Pawel Keblinski, Jeffrey A. Eastman, and David G. Cahill. "Nanofluids for thermal transport". In: *Materials Today* 8.6 (2005), pp. 36–44. ISSN: 13697021. DOI: [10.1016/S1369-7021\(05\)70936-6](https://doi.org/10.1016/S1369-7021(05)70936-6).
- [30] Yongqing He, Qincheng Bi, and Tingkuan Chen. "Heat transfer of ferrofluids: A review". In: *Development of Research in Microscale and Nanoscale Thermal and Fluid Sciences* 5 (2016), pp. 129–152.

- [31] Aleksandra A. Bozhko and Sergey A. Suslov. *Convection in Ferro-Nanofluids: Experiments and Theory*. Vol. 40. Advances in Mechanics and Mathematics. Cham: Springer International Publishing, 2018. ISBN: 978-3-319-94426-5. DOI: [10.1007/978-3-319-94427-2](https://doi.org/10.1007/978-3-319-94427-2). URL: <http://link.springer.com/10.1007/978-3-319-94427-2>.
- [32] Seval Genc. "Heat Transfer of Ferrofluids". In: *Nanofluid Heat and Mass Transfer in Engineering Problems* March (2017). DOI: [10.5772/65912](https://doi.org/10.5772/65912).
- [33] Antonis Sergis and Yannis Hardalupas. "Anomalous heat transfer modes of nanofluids: A review based on statistical analysis". In: *Nanoscale Research Letters* 6 (2011), pp. 1–37. ISSN: 19317573. DOI: [10.1186/1556-276X-6-391](https://doi.org/10.1186/1556-276X-6-391).
- [34] Chu Nie, W. H. Marlow, and Y. A. Hassan. "Discussion of proposed mechanisms of thermal conductivity enhancement in nanofluids". In: *International Journal of Heat and Mass Transfer* 51.5-6 (2008), pp. 1342–1348. ISSN: 00179310. DOI: [10.1016/j.ijheatmasstransfer.2007.11.034](https://doi.org/10.1016/j.ijheatmasstransfer.2007.11.034).
- [35] K. S. Hong, Tae Keun Hong, and Ho Soon Yang. "Thermal conductivity of Fe nanofluids depending on the cluster size of nanoparticles". In: *Applied Physics Letters* 88.3 (2006), pp. 1–3. ISSN: 00036951. DOI: [10.1063/1.2166199](https://doi.org/10.1063/1.2166199).
- [36] Melanie Tetreault-Friend et al. "Critical heat flux maxima resulting from the controlled morphology of nanoporous hydrophilic surface layers". In: *Applied Physics Letters* 108.24 (2016). ISSN: 00036951. DOI: [10.1063/1.4954012](https://doi.org/10.1063/1.4954012). URL: <http://dx.doi.org/10.1063/1.4954012>.
- [37] Matthias H. Buschmann and Uwe Franzke. "Improvement of thermosyphon performance by employing nanofluid". In: *International Journal of Refrigeration* 40 (2014), pp. 416–428. ISSN: 01407007. DOI: [10.1016/j.ijrefrig.2013.11.022](https://doi.org/10.1016/j.ijrefrig.2013.11.022). URL: <http://dx.doi.org/10.1016/j.ijrefrig.2013.11.022>.
- [38] Bartosz Zajaczkowski and Robert Mulka. "Chapter 4 - Nanofluids for industrial heating and cooling". In: *Towards Nanofluids for Large-Scale Industrial Applications*. Ed. by Bharat A Bhanvase, Divya P Barai, Gawel Żyła, and Zafar Said. Elsevier, 2024, pp. 73–98. ISBN: 978-0-443-15483-6. DOI: <https://doi.org/10.1016/B978-0-443-15483-6.00007-X>. URL: <https://www.sciencedirect.com/science/article/pii/B978044315483600007X>.
- [39] T. D. Kolflat. "Cooling Tower Practices." In: *Power Engineering (Barrington, Illinois)* 78.1 (1974), pp. 32–39. ISSN: 00325961. DOI: [10.1016/b978-0-7506-1005-6.50006-x](https://doi.org/10.1016/b978-0-7506-1005-6.50006-x).
- [40] S. Askari et al. "A novel approach for energy and water conservation in wet cooling towers by using MWNTs and nanoporous graphene nanofluids". In: *Energy Conversion and Management* 109 (Feb. 2016), pp. 10–18. ISSN: 01968904. DOI: [10.1016/j.enconman.2015.11.053](https://doi.org/10.1016/j.enconman.2015.11.053).

- [41] Peyman Imani-Mofrad, Saeed Zeinali Heris, and Mehdi Shanbedi. "Experimental investigation of the effect of different nanofluids on the thermal performance of a wet cooling tower using a new method for equalization of ambient conditions". In: *Energy Conversion and Management* 158 (Feb. 2018), pp. 23–35. ISSN: 01968904. DOI: [10.1016/j.enconman.2017.12.056](https://doi.org/10.1016/j.enconman.2017.12.056).
- [42] Nazanin Karimi Bakhtiyar, Reza Javadpour, Saeed Zeinali Heris, and Mousa Mohammadpourfard. "Improving the thermal characteristics of a cooling tower by replacing the operating fluid with functionalized and non-functionalized aqueous MWCNT nanofluids". In: *Case Studies in Thermal Engineering* 39 (Nov. 2022), 1DUMMY. ISSN: 2214157X. DOI: [10.1016/j.csite.2022.102422](https://doi.org/10.1016/j.csite.2022.102422). URL: <https://linkinghub.elsevier.com/retrieve/pii/S2214157X2200658X>.
- [43] Ashraf Mimi Elsaid. "A novel approach for energy and mass transfer characteristics in wet cooling towers associated with vapor-compression air conditioning system by using MgO and TiO₂ based H₂O nanofluids". In: *Energy Conversion and Management* 204 (Jan. 2020). ISSN: 01968904. DOI: [10.1016/j.enconman.2019.112289](https://doi.org/10.1016/j.enconman.2019.112289).
- [44] Mehdi Rahmati. "Effects of ZnO/water nanofluid on the thermal performance of wet cooling towers". In: *International Journal of Refrigeration* 131 (Nov. 2021), pp. 526–534. ISSN: 01407007. DOI: [10.1016/j.ijrefrig.2021.03.017](https://doi.org/10.1016/j.ijrefrig.2021.03.017).
- [45] Xiaocui Xie et al. "Bench-Scale Experimental Study on the Heat Transfer Intensification of a Closed Wet Cooling Tower Using Aluminum Oxide Nanofluids". In: *Industrial and Engineering Chemistry Research* 56.20 (May 2017), pp. 6022–6034. ISSN: 15205045. DOI: [10.1021/acs.iecr.7b00724](https://doi.org/10.1021/acs.iecr.7b00724).
- [46] Saman Rashidi, Omid Mahian, and Ehsan Mohseni Languri. *Applications of nanofluids in condensing and evaporating systems: A review*. Mar. 2018. DOI: [10.1007/s10973-017-6773-7](https://doi.org/10.1007/s10973-017-6773-7).
- [47] L. Doretto et al. "Nanoparticle Deposition during Cu-Water Nanofluid Pool Boiling". In: *Journal of Physics: Conference Series* 923.1 (Nov. 2017), p. 012004. ISSN: 17426596. DOI: [10.1088/1742-6596/923/1/012004](https://doi.org/10.1088/1742-6596/923/1/012004). URL: <https://iopscience.iop.org/article/10.1088/1742-6596/923/1/012004>.
- [48] Sauchung Fu, Chiyan Tso, Yicksau Fong, and Christopher Y.H. Chao. "Evaporation of Al₂O₃-water nanofluids in an externally micro-grooved evaporator". In: *Science and Technology for the Built Environment* 23.2 (2017), pp. 345–354. ISSN: 2374474X. DOI: [10.1080/23744731.2016.1250562](https://doi.org/10.1080/23744731.2016.1250562).
- [49] Roger R. Riehl. "Thermal enhancement using nanofluids on high heat dissipation electronic components". In: *Journal of Nanofluids* 8.1 (Jan. 2019), pp. 30–40. ISSN: 2169432X. DOI: [10.1166/jon.2019.1563](https://doi.org/10.1166/jon.2019.1563).
- [50] Advanced Micro Devices Inc. *Epyc 9004 series processors data sheet*. Tech. rep. Advanced Micro Devices, Inc., 2022.

- [51] NVIDIA Corporation. *GeForce RTX 4090 User Guide*. Tech. rep. NVIDIA Corporation, 2022.
- [52] Jesús Esarte et al. “Nanofluid as Advanced Cooling Technology. Success Stories”. In: *Heat Transfer - Design, Experimentation and Applications*. IntechOpen, Sept. 2021. DOI: [10.5772/intechopen.96247](https://doi.org/10.5772/intechopen.96247). URL: <https://www.intechopen.com/books/heat-transfer-design-experimentation-and-applications/nanofluid-as-advanced-cooling-technology-success-stories>.
- [53] Roger R. Riehl and S. M. Sohel Murshed. “Life Time Expectancy Prediction and Ageing Process of Heat Pipes Using Nanofluids”. In: *Heat Transfer Engineering* 42.19-20 (2021), pp. 1755–1764. ISSN: 15210537. DOI: [10.1080/01457632.2020.1818423](https://doi.org/10.1080/01457632.2020.1818423).
- [54] Anton Firth, Bo Zhang, and Aidong Yang. “Quantification of global waste heat and its environmental effects”. In: *Applied Energy* 235.November 2018 (2019), pp. 1314–1334. ISSN: 03062619. DOI: [10.1016/j.apenergy.2018.10.102](https://doi.org/10.1016/j.apenergy.2018.10.102).
- [55] G. Cavazzini et al. “Contribution of Metal-Organic-Heat Carrier nanoparticles in a R245fa low-grade heat recovery Organic Rankine Cycle”. In: *Energy Conversion and Management* 199 (Nov. 2019). ISSN: 01968904. DOI: [10.1016/j.enconman.2019.111960](https://doi.org/10.1016/j.enconman.2019.111960).
- [56] Dhruv Raj Karana and Rashmi Rekha Sahoo. “Performance effect on the TEG system for waste heat recovery in automobiles using ZnO and SiO₂ nanofluid coolants”. In: *Heat Transfer - Asian Research* 48.1 (Jan. 2019), pp. 216–232. ISSN: 15231496. DOI: [10.1002/htj.21379](https://doi.org/10.1002/htj.21379).
- [57] Zhi Li, Wenhao Li, and Zhen Chen. “Performance analysis of thermoelectric based automotivewaste heat recovery system with nanofluid coolant”. In: *Energies* 10.10 (Oct. 2017). ISSN: 19961073. DOI: [10.3390/en10101489](https://doi.org/10.3390/en10101489).
- [58] Samuel Sami. “Analysis of nanofluids behavior in a pv-thermal-driven organic rankine cycle with cooling capability”. In: *Applied System Innovation* 3.1 (Mar. 2020), pp. 1–21. ISSN: 25715577. DOI: [10.3390/asi3010012](https://doi.org/10.3390/asi3010012).
- [59] Shohreh Soltani, Alibakhsh Kasaeian, Hamid Sarrafha, and Dongsheng Wen. “An experimental investigation of a hybrid photovoltaic / thermoelectric system with nanofluid application”. In: *Solar Energy* 155 (2017), pp. 1033–1043. ISSN: 0038092X. DOI: [10.1016/j.solener.2017.06.069](https://doi.org/10.1016/j.solener.2017.06.069).
- [60] S. M.Sohel Murshed and Patrice Estellé. “A state of the art review on viscosity of nanofluids”. In: *Renewable and Sustainable Energy Reviews* 76 (2017), pp. 1134–1152. ISSN: 18790690. DOI: [10.1016/j.rser.2017.03.113](https://doi.org/10.1016/j.rser.2017.03.113).
- [61] Zhengguang Liu, Gaoyang Hou, and Hessam Taherian. “Techno-economic analysis of Al₂O₃/CuO nanofluid applied in various horizontal ground heat exchangers”. In: *International Journal of Energy Research* 46.15 (Sept. 2022), pp. 22894–22912. ISSN: 1099114X. DOI: [10.1002/er.8593](https://doi.org/10.1002/er.8593). URL: <https://onlinelibrary.wiley.com/doi/10.1002/er.8593>.

- [62] Venkateswara R. Kode et al. "Techno-Economic Analysis of Atmospheric Water Generation by Hybrid Nanofluids to Mitigate Global Water Scarcity". In: *Liquids* 2.3 (Aug. 2022), pp. 183–195. DOI: [10.3390/liquids2030012](https://doi.org/10.3390/liquids2030012).
- [63] Mehdi Mehrpooya, Meqdad Dehqani, Seyed Ali Mousavi, and SM Ali Moosavian. "Heat transfer and economic analyses of using various nanofluids in shell and tube heat exchangers for the cogeneration and solar-driven organic Rankine cycle systems". In: *International Journal of Low-Carbon Technologies* 17 (2022), pp. 11–22. ISSN: 17481325. DOI: [10.1093/ijlct/ctab075](https://doi.org/10.1093/ijlct/ctab075).
- [64] Peyman Taheri and Ali Reza Zahedi. "Techno-economic analysis of a renewable quadruple hybrid system for efficient water/biofuel production". In: *Solar Energy* 211 (Nov. 2020), pp. 1053–1069. ISSN: 0038092X. DOI: [10.1016/j.solener.2020.10.040](https://doi.org/10.1016/j.solener.2020.10.040).
- [65] Amir Beheshti, Mehdi Shanbedi, and Saeed Zeinali Heris. "Heat transfer and rheological properties of transformer oil-oxidized MWCNT nanofluid". In: *Journal of Thermal Analysis and Calorimetry* 118.3 (2014), pp. 1451–1460. ISSN: 15882926. DOI: [10.1007/s10973-014-4048-0](https://doi.org/10.1007/s10973-014-4048-0).
- [66] Michal Rajňák et al. "Effect of ferrofluid magnetization on transformer temperature rise". In: *Journal of Physics D: Applied Physics* 55.34 (Aug. 2022). ISSN: 13616463. DOI: [10.1088/1361-6463/ac7425](https://doi.org/10.1088/1361-6463/ac7425).
- [67] Juraj Kurimsky et al. "Electrical discharges in ferrofluids based on mineral oil and novel gas-to-liquid oil". In: *Journal of Molecular Liquids* 325 (Mar. 2021), p. 115244. ISSN: 01677322. DOI: [10.1016/j.molliq.2020.115244](https://doi.org/10.1016/j.molliq.2020.115244). URL: <https://linkinghub.elsevier.com/retrieve/pii/S0167732220374869>.
- [68] Nazanin Karimi Bakhtiyar, Reza Javadpour, Saeed Zeinali Heris, and Mousa Mohammadpourfard. "Improving the thermal characteristics of a cooling tower by replacing the operating fluid with functionalized and non-functionalized aqueous MWCNT nanofluids". In: *Case Studies in Thermal Engineering* 39 (Nov. 2022), 1DUMMY. ISSN: 2214157X. DOI: [10.1016/j.csite.2022.102422](https://doi.org/10.1016/j.csite.2022.102422). URL: <https://linkinghub.elsevier.com/retrieve/pii/S2214157X2200658X>.
- [69] M. Salem Ahmed, Mohamed R. Abdel Hady, and G. Abdallah. "Experimental investigation on the performance of chilled-water air conditioning unit using alumina nanofluids". In: *Thermal Science and Engineering Progress* 5 (Mar. 2018), pp. 589–596. ISSN: 24519049. DOI: [10.1016/j.tsep.2017.07.002](https://doi.org/10.1016/j.tsep.2017.07.002).
- [70] Marthe Braut et al. "Experimental investigation of erosion due to nanofluids". In: *Wear* 502-503 (Aug. 2022). ISSN: 00431648. DOI: [10.1016/j.wear.2022.204378](https://doi.org/10.1016/j.wear.2022.204378).

- [71] Karen Cacua et al. "Nanofluids' stability effects on the thermal performance of heat pipes: A critical review". In: *Journal of Thermal Analysis and Calorimetry* 136.4 (2019), pp. 1597–1614. ISSN: 15882926. DOI: [10.1007/s10973-018-7787-5](https://doi.org/10.1007/s10973-018-7787-5).
- [72] Mohammad Amini, Masoud Zareh, and Saeid Maleki. "Thermal performance analysis of mechanical draft cooling tower filled with rotational splash type packing by using nanofluids". In: *Applied Thermal Engineering* 175 (July 2020). ISSN: 13594311. DOI: [10.1016/j.applthermaleng.2020.115268](https://doi.org/10.1016/j.applthermaleng.2020.115268).
- [73] M. Z. Sharif et al. "Analyse de la performance du nanolubrifiant SiO₂/PAG dans un système de conditionnement d'air automobile". In: *International Journal of Refrigeration* 75 (2017), pp. 204–216. ISSN: 01407007. DOI: [10.1016/j.ijrefrig.2017.01.004](https://doi.org/10.1016/j.ijrefrig.2017.01.004). URL: <http://dx.doi.org/10.1016/j.ijrefrig.2017.01.004>.
- [74] Maria José Lourenço et al. "The balance between energy, environmental security, and technical performance: the regulatory challenge of nanofluids". In: *Nanomaterials* 11.8 (2021). ISSN: 20794991. DOI: [10.3390/nano11081871](https://doi.org/10.3390/nano11081871).
- [75] R. Azizian et al. "Effect of magnetic field on laminar convective heat transfer of magnetite nanofluids". In: *International Journal of Heat and Mass Transfer* 68 (2014), pp. 94–109. ISSN: 00179310. DOI: [10.1016/j.ijheatmasstransfer.2013.09.011](https://doi.org/10.1016/j.ijheatmasstransfer.2013.09.011).
- [76] Mohammed Asfer et al. "Effect of magnetic field on laminar convective heat transfer characteristics of ferrofluid flowing through a circular stainless steel tube". In: *International Journal of Heat and Fluid Flow* 59 (2016), pp. 74–86. ISSN: 0142727X. DOI: [10.1016/j.ijheatfluidflow.2016.01.009](https://doi.org/10.1016/j.ijheatfluidflow.2016.01.009).
- [77] Mahdim Hammodi Ali, Ahmed Hatf Kadhu, and Hussein AwadKurdi Saad. "Experimental Study of Forced Convection Heat Transfer Ferrofluid in Pipe Exposed to Magnetic Field". In: *International Journal of Innovative Research in Science, Engineering and Technology* 5.7 (July 2016), pp. 12008–12017. ISSN: 23476710. DOI: [10.15680/IJIRSET.2016.0507002](https://doi.org/10.15680/IJIRSET.2016.0507002). URL: http://ijirset.com/upload/2016/july/2A_Experimental.pdf.
- [78] Lei Shi, Yanwei Hu, and Yurong He. "Magnetocontrollable convective heat transfer of nanofluid through a straight tube". In: *Applied Thermal Engineering* 162.July (2019), p. 114220. ISSN: 13594311. DOI: [10.1016/j.applthermaleng.2019.114220](https://doi.org/10.1016/j.applthermaleng.2019.114220). URL: <https://doi.org/10.1016/j.applthermaleng.2019.114220>.
- [79] Jin Wang et al. "Experimental investigation on convective heat transfer of ferrofluids inside a pipe under various magnet orientations". In: *International Journal of Heat and Mass Transfer* 132 (2019), pp. 407–419. ISSN: 00179310. DOI: [10.1016/j.ijheatmasstransfer.2018.12.023](https://doi.org/10.1016/j.ijheatmasstransfer.2018.12.023). URL: <https://doi.org/10.1016/j.ijheatmasstransfer.2018.12.023>.

- [80] Abderraouf Dahmani, José Muñoz-Cámara, Juan Pedro Solano, and Samir Laouedj. "Thermal-Hydraulic Analysis of Ferrofluid Laminar Flow in Tube Under Non-Uniform Magnetic Field Created By a Periodic Current-Carrying Wire". In: *Frontiers in Heat and Mass Transfer* 18 (2022). ISSN: 21518629. DOI: [10.5098/hmt.18.42](https://doi.org/10.5098/hmt.18.42).
- [81] A. Shahsavari, M. Saghafian, M. R. Salimpour, and M. B. Shafii. "Experimental investigation on laminar forced convective heat transfer of ferrofluid loaded with carbon nanotubes under constant and alternating magnetic fields". In: *Experimental Thermal and Fluid Science* 76 (2016), pp. 1–11. ISSN: 08941777. DOI: [10.1016/j.expthermflusci.2016.03.010](https://doi.org/10.1016/j.expthermflusci.2016.03.010). URL: <http://dx.doi.org/10.1016/j.expthermflusci.2016.03.010>.
- [82] Sajjad Ahangar Zonouzi et al. "Experimental investigation of the flow and heat transfer of magnetic nanofluid in a vertical tube in the presence of magnetic quadrupole field". In: *Experimental Thermal and Fluid Science* 91.October 2017 (2018), pp. 155–165. ISSN: 08941777. DOI: [10.1016/j.expthermflusci.2017.10.013](https://doi.org/10.1016/j.expthermflusci.2017.10.013).
- [83] Johannes Rudl et al. "Laminar pipe flow with mixed convection under the influence of magnetic field". In: *Nanomaterials* 11.3 (2021). ISSN: 20794991. DOI: [10.3390/nano11030824](https://doi.org/10.3390/nano11030824).
- [84] Bin Sun, Yongjian Guo, Di Yang, and Hongwei Li. "The effect of constant magnetic field on convective heat transfer of Fe₃O₄/water magnetic nanofluid in horizontal circular tubes". In: *Applied Thermal Engineering* 171.December 2019 (2020), p. 114920. ISSN: 13594311. DOI: [10.1016/j.applthermaleng.2020.114920](https://doi.org/10.1016/j.applthermaleng.2020.114920). URL: <https://doi.org/10.1016/j.applthermaleng.2020.114920>.
- [85] Maryam Dinarvand, Mahdiah Abolhasani, Faramarz Hormozi, and Zohreh Bahrami. "Experimental investigation and performance comparison of Fe₃O₄/water and CoFe₂O₄/ water ferrofluids in presence of a magnetic field in a cooling system". In: *Journal of the Taiwan Institute of Chemical Engineers* 148.April (2023), p. 104927. ISSN: 18761070. DOI: [10.1016/j.jtice.2023.104927](https://doi.org/10.1016/j.jtice.2023.104927). URL: <https://doi.org/10.1016/j.jtice.2023.104927>.
- [86] Yaghoub Mohammadfam and Saeed Zeinali Heris. "An experimental study of the influence of Fe₃O₄, MWCNT-Fe₃O₄, and Fe₃O₄@MWCNT nanoparticles on the thermophysical characteristics and laminar convective heat transfer of nanofluids: A comparative study". In: *Surfaces and Interfaces* 43.PB (2023), p. 103506. ISSN: 24680230. DOI: [10.1016/j.surfin.2023.103506](https://doi.org/10.1016/j.surfin.2023.103506). URL: <https://doi.org/10.1016/j.surfin.2023.103506>.
- [87] Sudip Shyam, Balkrishna Mehta, Pranab K. Mondal, and Somchai Wongwises. "Investigation into the thermo-hydrodynamics of ferrofluid flow under the influence of constant and alternating magnetic field by InfraRed Thermography". In: *International Journal of Heat and Mass Transfer* 135 (2019), pp. 1233–

1247. ISSN: 00179310. DOI: [10.1016/j.ijheatmasstransfer.2019.02.050](https://doi.org/10.1016/j.ijheatmasstransfer.2019.02.050). URL: <https://doi.org/10.1016/j.ijheatmasstransfer.2019.02.050>.
- [88] Mohammad Goharkhah, Armia Salarian, Mehdi Ashjaee, and Mahmoud Shahabadi. "Convective heat transfer characteristics of magnetite nanofluid under the influence of constant and alternating magnetic field". In: *Powder Technology* 274 (2015), pp. 258–267. ISSN: 1873328X. DOI: [10.1016/j.powtec.2015.01.031](https://doi.org/10.1016/j.powtec.2015.01.031).
- [89] Mehmet Gürdal et al. "Implementation of hybrid nanofluid flowing in dimpled tube subjected to magnetic field". In: *International Communications in Heat and Mass Transfer* 134 (2022). ISSN: 07351933. DOI: [10.1016/j.icheatmasstransfer.2022.106032](https://doi.org/10.1016/j.icheatmasstransfer.2022.106032).
- [90] Mehmet Gürdal et al. "An innovative approach of alternating magnetic field diversified with different wave types and magnet positions for ferrofluid flow in dimpled tube". In: *Journal of Magnetism and Magnetic Materials* 581. April (2023), p. 170975. ISSN: 03048853. DOI: [10.1016/j.jmmm.2023.170975](https://doi.org/10.1016/j.jmmm.2023.170975).
- [91] Mutlu Tekir et al. "Hydrothermal behavior of hybrid magnetite nanofluid flowing in a pipe under bi-directional magnetic field with different wave types". In: *Thermal Science and Engineering Progress* 34. June (2022). ISSN: 24519049. DOI: [10.1016/j.tsep.2022.101399](https://doi.org/10.1016/j.tsep.2022.101399).
- [92] A. Ghofrani, M. H. Dibaei, A. Hakim Sima, and M. B. Shafii. "Experimental investigation on laminar forced convection heat transfer of ferrofluids under an alternating magnetic field". In: *Experimental Thermal and Fluid Science* 49 (2013), pp. 193–200. ISSN: 08941777. DOI: [10.1016/j.expthermflusci.2013.04.018](https://doi.org/10.1016/j.expthermflusci.2013.04.018). URL: <http://dx.doi.org/10.1016/j.expthermflusci.2013.04.018>.
- [93] M. Yarahmadi, H. Moazami Goudarzi, and M. B. Shafii. "Experimental investigation into laminar forced convective heat transfer of ferrofluids under constant and oscillating magnetic field with different magnetic field arrangements and oscillation modes". In: *Experimental Thermal and Fluid Science* 68 (2015), pp. 601–611. ISSN: 08941777. DOI: [10.1016/j.expthermflusci.2015.07.002](https://doi.org/10.1016/j.expthermflusci.2015.07.002). URL: <http://dx.doi.org/10.1016/j.expthermflusci.2015.07.002>.
- [94] Anumut Siricharoenpanitch et al. "Heat Transfer of Ferrofluid in Fluted Tubes with an Electromagnetic Field". In: *Heat Transfer Engineering* 44.5 (2023), pp. 426–441. ISSN: 15210537. DOI: [10.1080/01457632.2022.2068219](https://doi.org/10.1080/01457632.2022.2068219). URL: <https://doi.org/10.1080/01457632.2022.2068219>.
- [95] Xilong Zhang and Yongliang Zhang. "Experimental study on enhanced heat transfer and flow performance of magnetic nanofluids under alternating magnetic field". In: *International Journal of Thermal Sciences* 164. January (2021), p. 106897. ISSN: 12900729. DOI: [10.1016/j.ijthermalsci.2021.106897](https://doi.org/10.1016/j.ijthermalsci.2021.106897). URL: <https://doi.org/10.1016/j.ijthermalsci.2021.106897>.

- [96] D. V. Guzei, A. V. Minakov, and M. I. Pryazhnikov. "Experimental-calculated study of the forced convection magnetic nanofluids". In: *Journal of Physics: Conference Series* 925.1 (2017). ISSN: 17426596. DOI: [10.1088/1742-6596/925/1/012008](https://doi.org/10.1088/1742-6596/925/1/012008).
- [97] Abdulhassan A Karamallah, Laith Jaafer Habeeb, and Ali Habeeb Asker. "The Effect of magnetic field with nanofluid on heat Transfer in a horizontal pipe". In: *Al-Khwarizmi Engineering Journal* 12.3 (2016), pp. 99–109. URL: <https://alkej.uobaghdad.edu.iq/index.php/alkej/article/view/312>.
- [98] Maryamalsadat Lajvardi et al. "Experimental investigation for enhanced ferrofluid heat transfer under magnetic field effect". In: *Journal of Magnetism and Magnetic Materials* 322.21 (2010), pp. 3508–3513. ISSN: 03048853. DOI: [10.1016/j.jmmm.2010.06.054](https://doi.org/10.1016/j.jmmm.2010.06.054). URL: <http://dx.doi.org/10.1016/j.jmmm.2010.06.054>.
- [99] Lili Sha, Yonglin Ju, Hua Zhang, and Jingxin Wang. "Experimental investigation on the convective heat transfer of Fe₃O₄/water nanofluids under constant magnetic field". In: *Applied Thermal Engineering* 113 (2017), pp. 566–574. ISSN: 13594311. DOI: [10.1016/j.applthermaleng.2016.11.060](https://doi.org/10.1016/j.applthermaleng.2016.11.060). URL: <http://dx.doi.org/10.1016/j.applthermaleng.2016.11.060>.
- [100] Mohammadhosein Dibaei and Hadi Kargarsharifabad. "New Achievements in Fe₃O₄ Nanofluid Fully Developed Forced Convection Heat Transfer under the Effect of a Magnetic Field: An Experimental Study". In: *Journal of Heat and Mass Transfer Research(JHMTR)* 4 (2016), pp. 1–12. ISSN: 2345-508X. DOI: [10.22075/jhmtr.2016.486](https://doi.org/10.22075/jhmtr.2016.486). URL: http://jhmtr.journals.semnan.ac.ir/article_486.html.
- [101] N. Hatami, A. Kazemnejad Banari, A. Malekzadeh, and A. R. Pouranfard. "The effect of magnetic field on nanofluids heat transfer through a uniformly heated horizontal tube". In: *Physics Letters, Section A: General, Atomic and Solid State Physics* 381.5 (2017), pp. 510–515. ISSN: 03759601. DOI: [10.1016/j.physleta.2016.12.017](https://doi.org/10.1016/j.physleta.2016.12.017). URL: <http://dx.doi.org/10.1016/j.physleta.2016.12.017>.
- [102] Mohammad Hosein Dibaei Bonab, Mohammad Behshad Shafii, and Mohammad Hasan Nobakhti. "Experimental and numerical investigation of fully developed forced convection of water-based Fe₃O₄ nanofluid passing through a tube in the presence of an alternating magnetic field". In: *Advances in Mechanical Engineering* 7.2 (2015), pp. 1–9. ISSN: 16878140. DOI: [10.1177/1687814015571023](https://doi.org/10.1177/1687814015571023).
- [103] *Reprinted from International Journal of Heat and Fluid Flow, Vol. 59, Effect of magnetic field on laminar convective heat transfer characteristics of ferrofluid flowing through a circular stainless steel tube, Mohammed Asfer, Balkrishna Mehta, Arun Kumar, Sameer Khandekar, Pradipta Kumar Panigrahi, Pages No. 74–86, 2016, with permission of Elsevier.*

- [104] B. Metais and E. R. G. Eckert. "Forced, Mixed, and Free Convection Regimes". In: *Journal of Heat Transfer* 86.2 (May 1964), pp. 295–296. ISSN: 0022-1481. DOI: [10.1115/1.3687128](https://doi.org/10.1115/1.3687128). URL: <https://asmedigitalcollection.asme.org/heattransfer/article/86/2/295/414106/Forced-Mixed-and-Free-Convection-Regimes>.
- [105] Afshin J. Ghajar and Lap Mou Tam. "Flow regime map for a horizontal pipe with uniform wall heat flux and three inlet configurations". In: *Experimental Thermal and Fluid Science* 10.3 (1995), pp. 287–297. ISSN: 08941777. DOI: [10.1016/0894-1777\(94\)00107-J](https://doi.org/10.1016/0894-1777(94)00107-J).
- [106] Afshin J. Ghajar and Lap-Mou Tam. "Heat transfer measurements and correlations in the transition region for a circular tube with three different inlet configurations". In: *Experimental Thermal and Fluid Science* 8.1 (Jan. 1994), pp. 79–90. ISSN: 08941777. DOI: [10.1016/0894-1777\(94\)90075-2](https://doi.org/10.1016/0894-1777(94)90075-2). URL: <https://linkinghub.elsevier.com/retrieve/pii/0894177794900752>.
- [107] L. Colla, L. Fedele, and M. H. Buschmann. "Laminar mixed convection of TiO₂-water nanofluid in horizontal uniformly heated pipe flow". In: *International Journal of Thermal Sciences* 97 (2015), pp. 26–40. ISSN: 12900729. DOI: [10.1016/j.ijthermalsci.2015.06.013](https://doi.org/10.1016/j.ijthermalsci.2015.06.013).
- [108] Adi T. Utomo, Heiko Poth, Phillip T. Robbins, and Andrzej W. Pacek. "Experimental and theoretical studies of thermal conductivity, viscosity and heat transfer coefficient of titania and alumina nanofluids". In: *International Journal of Heat and Mass Transfer* 55.25-26 (Dec. 2012), pp. 7772–7781. ISSN: 00179310. DOI: [10.1016/j.ijheatmasstransfer.2012.08.003](https://doi.org/10.1016/j.ijheatmasstransfer.2012.08.003).
- [109] Theodore Morgan Hallman. "Combined forced and free convection in a vertical tube". PhD thesis. Purdue University, 1958.
- [110] J. D. Jackson, M. A. Cotton, and B. P. Axcell. "Studies of mixed convection in vertical tubes". In: *International Journal of Heat and Fluid Flow* 10.1 (1989), pp. 2–15. ISSN: 0142727X. DOI: [10.1016/0142-727X\(89\)90049-0](https://doi.org/10.1016/0142-727X(89)90049-0).
- [111] Nicolas Galanis and Amin Behzadmehr. "Mixed Convection in Vertical Ducts". In: *6th IASME/WSEAS International Conference on FLUID MECHANICS and AERODYNAMICS (FMA'08)*. Vol. 30. 1964. 2008, pp. 6–12. ISBN: 9789606766985.
- [112] George F. Scheele and Thomas J. Hanratty. "Effect of natural convection on stability of flow in a vertical pipe". In: *Journal of Fluid Mechanics* 14.2 (1962), pp. 244–256. ISSN: 14697645. DOI: [10.1017/S0022112062001226](https://doi.org/10.1017/S0022112062001226).
- [113] Giovanni S. Barozzi, Enzo Zanchini, and Marco Mariotti. "Experimental investigation of combined forced and free convection in horizontal and inclined tubes". In: *Meccanica* 20.1 (1985), pp. 18–27. ISSN: 00256455. DOI: [10.1007/BF02337057](https://doi.org/10.1007/BF02337057).

- [114] Marilize Everts, Suvanjan Bhattacharyya, Abubakar I. Bashir, and Josua P. Meyer. "Heat transfer characteristics of assisting and opposing laminar flow through a vertical circular tube at low Reynolds numbers". In: *Applied Thermal Engineering* 179. July (2020), p. 115696. ISSN: 13594311. DOI: [10.1016/j.applthermaleng.2020.115696](https://doi.org/10.1016/j.applthermaleng.2020.115696). URL: <https://doi.org/10.1016/j.applthermaleng.2020.115696>.
- [115] M. Akbari, A. Behzadmehr, and F. Shahraki. "Fully developed mixed convection in horizontal and inclined tubes with uniform heat flux using nanofluid". In: *International Journal of Heat and Fluid Flow* 29.2 (Apr. 2008), pp. 545–556. ISSN: 0142727X. DOI: [10.1016/j.ijheatfluidflow.2007.11.006](https://doi.org/10.1016/j.ijheatfluidflow.2007.11.006).
- [116] S. Mirmasoumi and A. Behzadmehr. "Effects of nanoparticles mean diameter on the particle migration and thermo-hydraulic behavior of laminar mixed convection of a nanofluid in an inclined tube". In: *Heat and Mass Transfer/Waerme- und Stoffuebertragung* 48.8 (Aug. 2012), pp. 1297–1308. ISSN: 09477411. DOI: [10.1007/s00231-012-0978-x](https://doi.org/10.1007/s00231-012-0978-x).
- [117] R. Ben Mansour, N. Galanis, and C. T. Nguyen. "Developing laminar mixed convection of nanofluids in an inclined tube with uniform wall heat flux". In: *International Journal of Numerical Methods for Heat and Fluid Flow* 19.2 (Mar. 2009), pp. 146–164. ISSN: 09615539. DOI: [10.1108/09615530910930946](https://doi.org/10.1108/09615530910930946).
- [118] R. Ben Mansour, N. Galanis, and C. T. Nguyen. "Experimental study of mixed convection with water-Al₂O₃ nanofluid in inclined tube with uniform wall heat flux". In: *International Journal of Thermal Sciences* 50.3 (2011), pp. 403–410. ISSN: 12900729. DOI: [10.1016/j.ijthermalsci.2010.03.016](https://doi.org/10.1016/j.ijthermalsci.2010.03.016).
- [119] FerroTec Corporation. *Safety Data Sheet MSG W Series Ferrofluid*. Santa Clara, CA, USA, 2022.
- [120] Ravi Prasher, David Song, Jinlin Wang, and Patrick Phelan. "Measurements of nanofluid viscosity and its implications for thermal applications". In: *Applied Physics Letters* 89.13 (2006), pp. 2004–2007. ISSN: 00036951. DOI: [10.1063/1.2356113](https://doi.org/10.1063/1.2356113).
- [121] Albert Einstein. "A new determination of molecular dimensions". In: *Annalen der Physik* 19.4 (1906), pp. 289–306.
- [122] Eni Generalic. "Ostwald's viscometer". In: *Croatian-English Chemistry Dictionary & Glossary*. 29 June 2022. KTF-Split. (Sept. 2024).
- [123] Ian H. Bell, Jorrit Wronski, Sylvain Quoilin, and Vincent Lemort. "Pure and pseudo-pure fluid thermophysical property evaluation and the open-source thermophysical property library coolprop". In: *Industrial and Engineering Chemistry Research* 53.6 (Feb. 2014), pp. 2498–2508. ISSN: 08885885. DOI: [10.1021/ie4033999](https://doi.org/10.1021/ie4033999).

- [124] Gerard Ferrer et al. "New proposed methodology for specific heat capacity determination of materials for thermal energy storage (TES) by DSC". In: *Journal of Energy Storage* 11 (2017), pp. 1–6. ISSN: 2352152X. DOI: [10.1016/j.est.2017.02.002](https://doi.org/10.1016/j.est.2017.02.002).
- [125] Angelika Ehle, Steffen Feja, and Matthias H. Buschmann. "Temperature Dependency of Ceramic Nanofluids Shows Classical Behavior". In: *Journal of Thermophysics and Heat Transfer* 25.3 (July 2011), pp. 378–385. ISSN: 0887-8722. DOI: [10.2514/1.T3634](https://doi.org/10.2514/1.T3634). URL: <https://arc.aiaa.org/doi/10.2514/1.T3634>.
- [126] *Used with permission of American Inst of Aeronautics & Astronautics (AIAA), from Temperature Dependency of Ceramic Nanofluids Shows Classical Behavior, Ehle, Angelika; Feja, Steffen; Buschmann, Matthias H., Journal of thermophysics and heat transfer, Issue 3, Volume 25, publication date 2011-07-01; permission conveyed through Copyright Clearance Center, Inc.*
- [127] Alexandra Gimeno-Furio et al. "Stabilization and characterization of a nanofluid based on a eutectic mixture of diphenyl and diphenyl oxide and carbon nanoparticles under high temperature conditions". In: *International Journal of Heat and Mass Transfer* 113 (2017), pp. 908–913. ISSN: 00179310. DOI: [10.1016/j.ijheatmasstransfer.2017.05.097](https://doi.org/10.1016/j.ijheatmasstransfer.2017.05.097).
- [128] Siddharth Mehta, K. Prashanth Chauhan, and S. Kanagaraj. "Modeling of thermal conductivity of nanofluids by modifying Maxwell's equation using cell model approach". In: *Journal of Nanoparticle Research* 13.7 (2011), pp. 2791–2798. ISSN: 13880764. DOI: [10.1007/s11051-010-0167-0](https://doi.org/10.1007/s11051-010-0167-0).
- [129] Yaroslav Grosu, Abdessamad Faik, Iñigo Ortega-Fernández, and Bruno D'Aguanno. "Natural Magnetite for thermal energy storage: Excellent thermophysical properties, reversible latent heat transition and controlled thermal conductivity". In: *Solar Energy Materials and Solar Cells* 161 (Mar. 2017), pp. 170–176. ISSN: 09270248. DOI: [10.1016/j.solmat.2016.12.006](https://doi.org/10.1016/j.solmat.2016.12.006).
- [130] *Private correspondence with PD Dr.-Ing. habil. Matthias H. Buschmann.*
- [131] A. F. Stalder et al. "A snake-based approach to accurate determination of both contact points and contact angles". In: *Colloids and Surfaces A: Physicochemical and Engineering Aspects* 286.1-3 (2006), pp. 92–103. ISSN: 09277757. DOI: [10.1016/j.colsurfa.2006.03.008](https://doi.org/10.1016/j.colsurfa.2006.03.008).
- [132] Jonathan M. Schuster, Carlos E. Schvezov, and Mario R. Rosenberger. "Influence of Experimental Variables on the Measure of Contact Angle in Metals Using the Sessile Drop Method". In: *Procedia Materials Science* 8.2009 (2015), pp. 742–751. ISSN: 22118128. DOI: [10.1016/j.mspro.2015.04.131](https://doi.org/10.1016/j.mspro.2015.04.131). URL: <http://dx.doi.org/10.1016/j.mspro.2015.04.131>.
- [133] David Meeker. *Finite Element Method Magnetics: Version 4.2 User Manual*. 2020. URL: <https://www.femm.info/wiki/Documentation/>.

- [134] Nur Çobanoğlu et al. "Volume-independent contact angle prediction". In: *High Temperatures - High Pressures* 50.6 (2021), pp. 437–450. ISSN: 14723441. DOI: [10.32908/HTHP.V50.1021](https://doi.org/10.32908/HTHP.V50.1021).
- [135] Gui Ping Zhu, Nam Trung Nguyen, R. V. Ramanujan, and Xiao Yang Huang. "Nonlinear deformation of a ferrofluid droplet in a uniform magnetic field". In: *Langmuir* 27.24 (2011), pp. 14834–14841. ISSN: 07437463. DOI: [10.1021/la203931q](https://doi.org/10.1021/la203931q).
- [136] Nan Gao et al. "How drops start sliding over solid surfaces". In: *Nature Physics* 14.2 (2018), pp. 191–196. ISSN: 17452481. DOI: [10.1038/nphys4305](https://doi.org/10.1038/nphys4305).
- [137] Saeid Vafaei. "3D nanoparticle tracking inside the silver nanofluid". In: *Nanomaterials* 10.2 (Feb. 2020), p. 397. ISSN: 20794991. DOI: [10.3390/nano10020397](https://doi.org/10.3390/nano10020397). URL: <https://www.mdpi.com/2079-4991/10/2/397>.
- [138] M. Shahrooz Amin et al. "Surface tension measurement techniques of magnetic fluids at an interface between different fluids using perpendicular field instability". In: *Journal of Applied Physics* 97.10 (2005), pp. 8–11. ISSN: 00218979. DOI: [10.1063/1.1861374](https://doi.org/10.1063/1.1861374).
- [139] L. Pauchard et al. "When a crack is oriented by a magnetic field". In: *Physical Review E - Statistical, Nonlinear, and Soft Matter Physics* 77.2 (2008). ISSN: 15393755. DOI: [10.1103/PhysRevE.77.021402](https://doi.org/10.1103/PhysRevE.77.021402).
- [140] A. Groisman and E. Kaplan. "An experimental study of cracking induced by desiccation". In: *Epl* 25.6 (1994), pp. 415–420. ISSN: 12864854. DOI: [10.1209/0295-5075/25/6/004](https://doi.org/10.1209/0295-5075/25/6/004).
- [141] Kelly A. Shorlin, John R. De Bruyn, Malcolm Graham, and Stephen W. Morris. "Development and geometry of isotropic and directional shrinkage-crack patterns". In: *Physical Review E - Statistical Physics, Plasmas, Fluids, and Related Interdisciplinary Topics* 61.6 B (2000), pp. 6950–6957. ISSN: 1063651X. DOI: [10.1103/PhysRevE.61.6950](https://doi.org/10.1103/PhysRevE.61.6950).
- [142] Robert Mulka, Gabriela Beben, Bartosz Zajęzkowski, and Matthias H. Buschmann. "Magnetic field impact on ferronano fluid laminar flow". In: *International Journal of Thermal Sciences* 203 (Sept. 2024), p. 109108. ISSN: 12900729. DOI: [10.1016/j.ijthermalsci.2024.109108](https://doi.org/10.1016/j.ijthermalsci.2024.109108). URL: <https://linkinghub.elsevier.com/retrieve/pii/S1290072924002308>.
- [143] R.K. Shah and A.L. London. "Dimensionless Groups and Generalized Solutions". In: *Laminar Flow Forced Convection in Ducts*. Elsevier, 1978, pp. 37–60. DOI: [10.1016/b978-0-12-020051-1.50008-5](https://doi.org/10.1016/b978-0-12-020051-1.50008-5). URL: <https://linkinghub.elsevier.com/retrieve/pii/B9780120200511500085>.
- [144] E. E. Tzirtzilakis and M. A. Xenos. "Biomagnetic fluid flow in a driven cavity". In: *Meccanica* 48.1 (2013), pp. 187–200. ISSN: 00256455. DOI: [10.1007/s11012-012-9593-7](https://doi.org/10.1007/s11012-012-9593-7).

- [145] Yousef Haik and Ching-Jen Chen. "Development and mathematical modeling of biomagnetic fluid dynamics". English. PhD thesis. United States – Florida, 1997, p. 359. ISBN: 978-0-591-89620-6. URL: <https://www.proquest.com/dissertations-theses/development-mathematical-modeling-biomagnetic/docview/304350213/se-2?accountid=46407>.
- [146] Robert Mulka, Gabriela Beben, Bartosz Zajączkowski, and Matthias H. Buschmann. "Magnetic field influence on heat transfer in inclined laminar ferrofluid flow". In: *International Journal of Thermal Sciences* 205 (Nov. 2024), p. 109312. ISSN: 12900729. DOI: [10.1016/j.ijthermalsci.2024.109312](https://doi.org/10.1016/j.ijthermalsci.2024.109312). URL: <https://linkinghub.elsevier.com/retrieve/pii/S1290072924004344>.
- [147] M. Everts and J. P. Meyer. "Flow regime maps for smooth horizontal tubes at a constant heat flux". In: *International Journal of Heat and Mass Transfer* 117 (2018), pp. 1274–1290. ISSN: 00179310. DOI: [10.1016/j.ijheatmasstransfer.2017.10.073](https://doi.org/10.1016/j.ijheatmasstransfer.2017.10.073). URL: <https://doi.org/10.1016/j.ijheatmasstransfer.2017.10.073>.
- [148] H K Tam, L M Tam, A J Ghajar, and C W Cheong. "Development of A Unified Flow Regime Map for A Horizontal Pipe with The Support Vector Machines". In: *AIP Conference Proceedings* 1233.1 (May 2010), pp. 608–613. ISSN: 0094-243X. DOI: [10.1063/1.3452244](https://doi.org/10.1063/1.3452244). URL: <https://doi.org/10.1063/1.3452244>.
- [149] J. Orfi, N. Galanis, and C. T. Nguyen. "Bifurcation in steady laminar mixed convection flow in uniformly heated inclined tubes". In: *International Journal of Numerical Methods for Heat and Fluid Flow* 9.5 (1999), pp. 543–567. ISSN: 09615539. DOI: [10.1108/09615539910276845](https://doi.org/10.1108/09615539910276845).